Rare and Semileptonic decays at LHCb

LA THUILE 2024 - Les Rencontres de Physique de la Vallée d'Aoste

3rd-9th March 2024

Irene Bachiller on behalf of the LHCb Collaboration

LAPP, CNRS, France

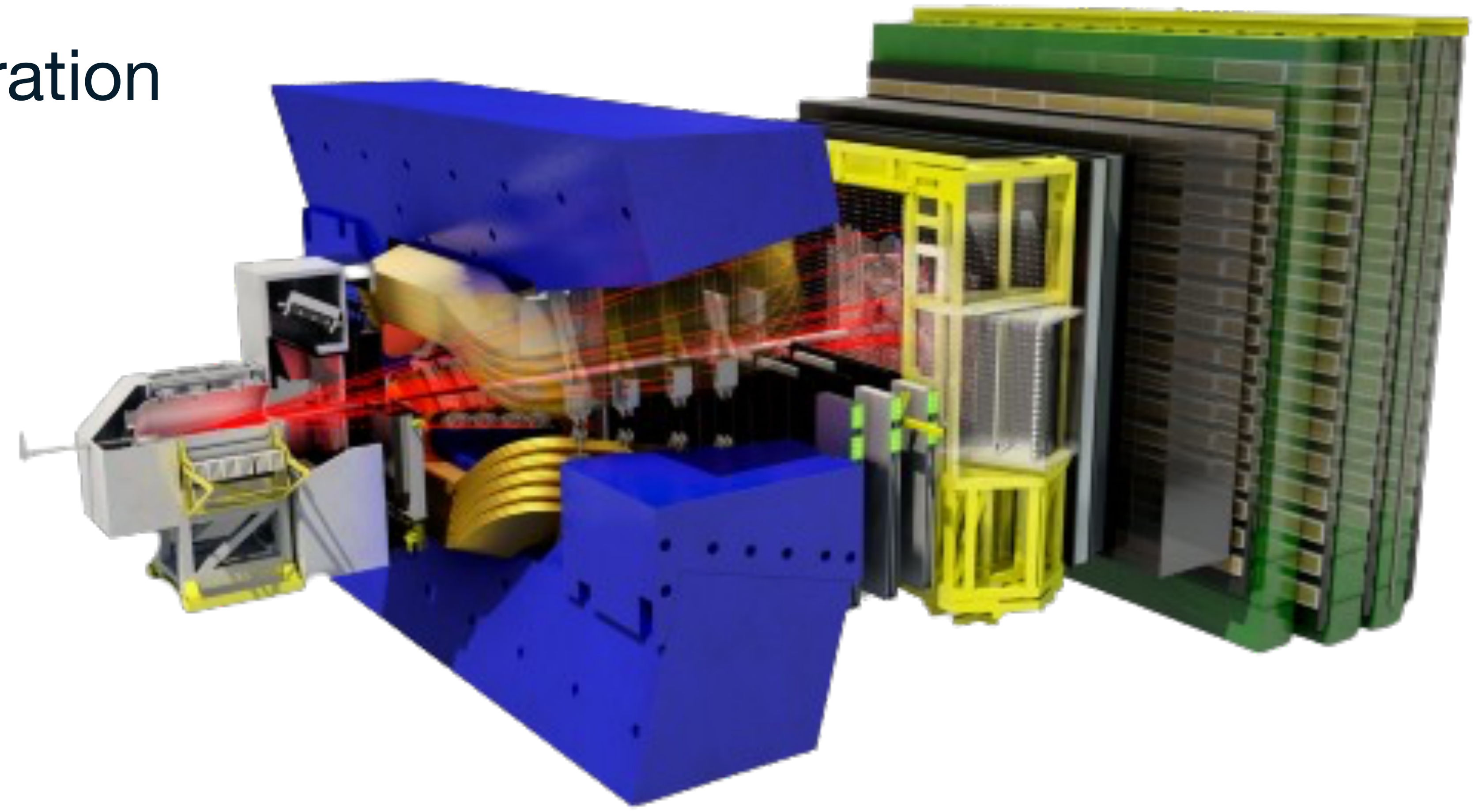

Laboratoire d'Annecy de Physique des Particules

Rare and Semileptonic *b*-hadron decays

Rare

Highly suppressed or forbidden in the SM:

- Higher orders diagrams: FCNC, box, penguin
- LFU tests
- Lepton flavour and baryon number violation
- Limited data samples
- E.g. $b \to sll$

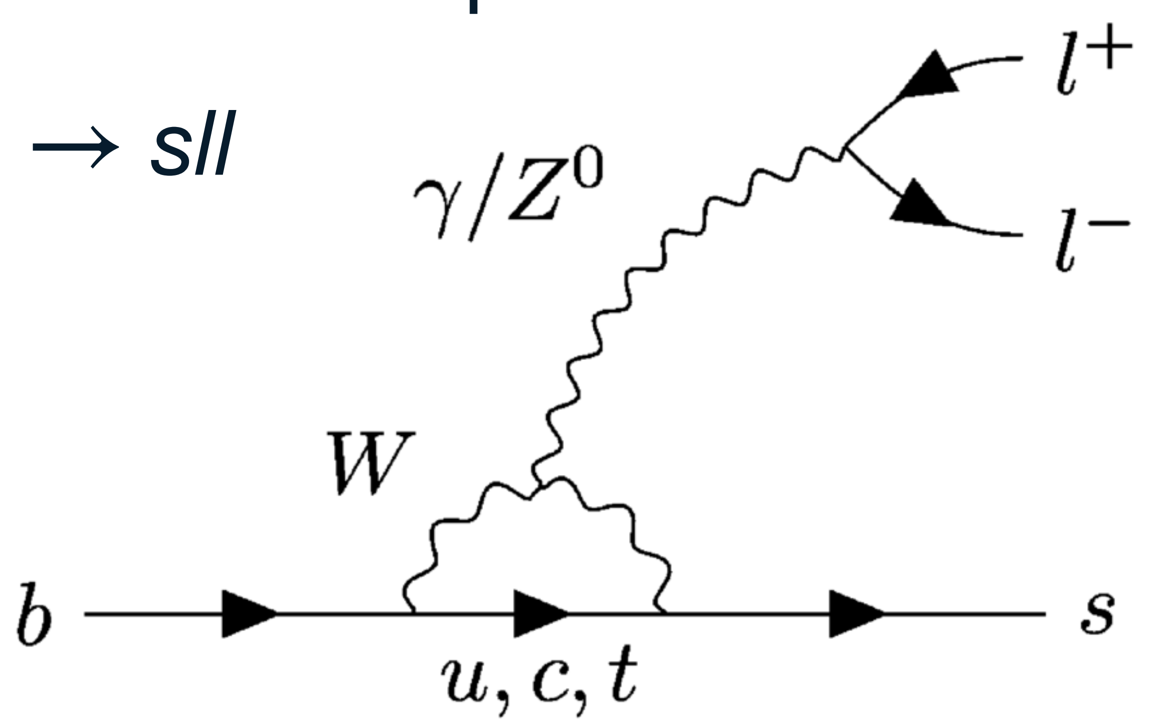

Semileptonic

Sensitive to hadronic and leptonic effects:

- Probe for $|V_{ub}|$ and $|V_{cb}|$
- LFU tests
- Possible 3rd generation enhanced coupling
- Large data samples
- E.g. $b \to cl\nu$

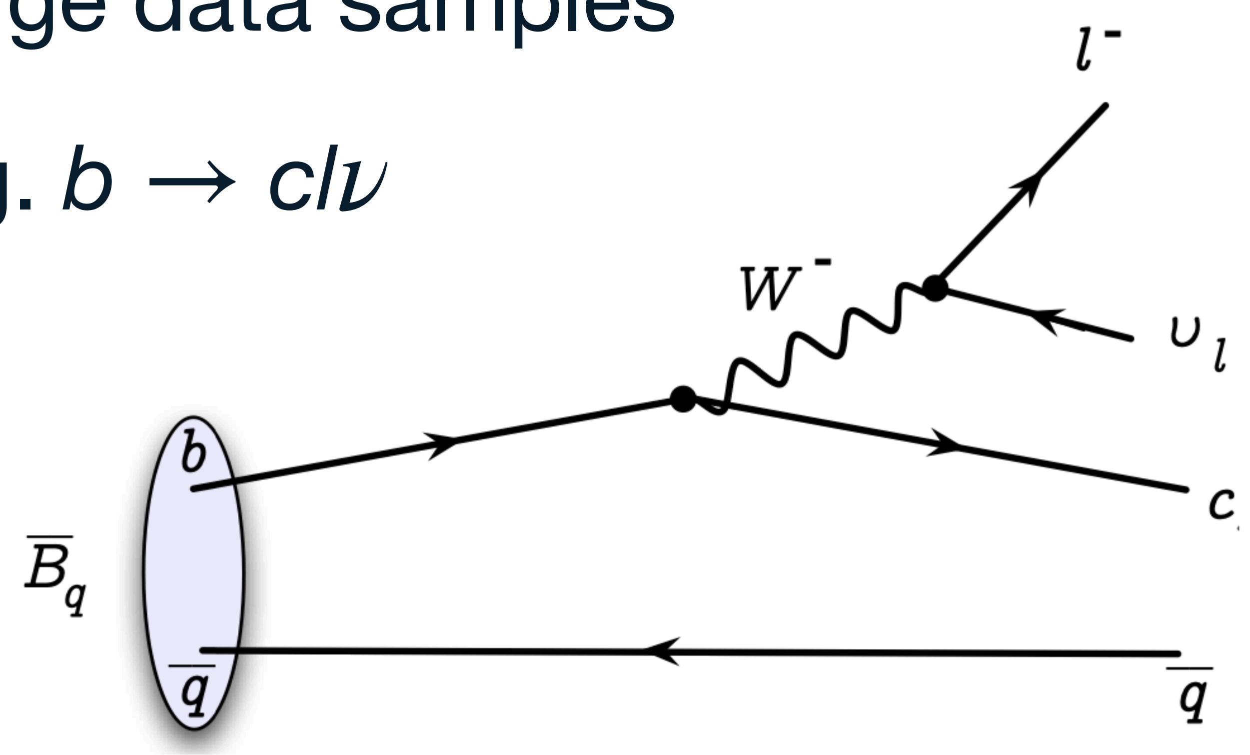

More about rare decays in presentation by M.Reboud.

More about semileptonic in presentation by M.Bordone.

LHCb detector for b-hadron decays

- The LHC has a large cross section of b and c hadrons:
  $\sigma(b\bar{b})_{7\ TeV} = 295\ \mu b$
  $\sigma(b\bar{b})_{13\ TeV} = 590\ \mu b$

- LHCb designed as forward spectrometer to focus on $b\bar{b}$ production:

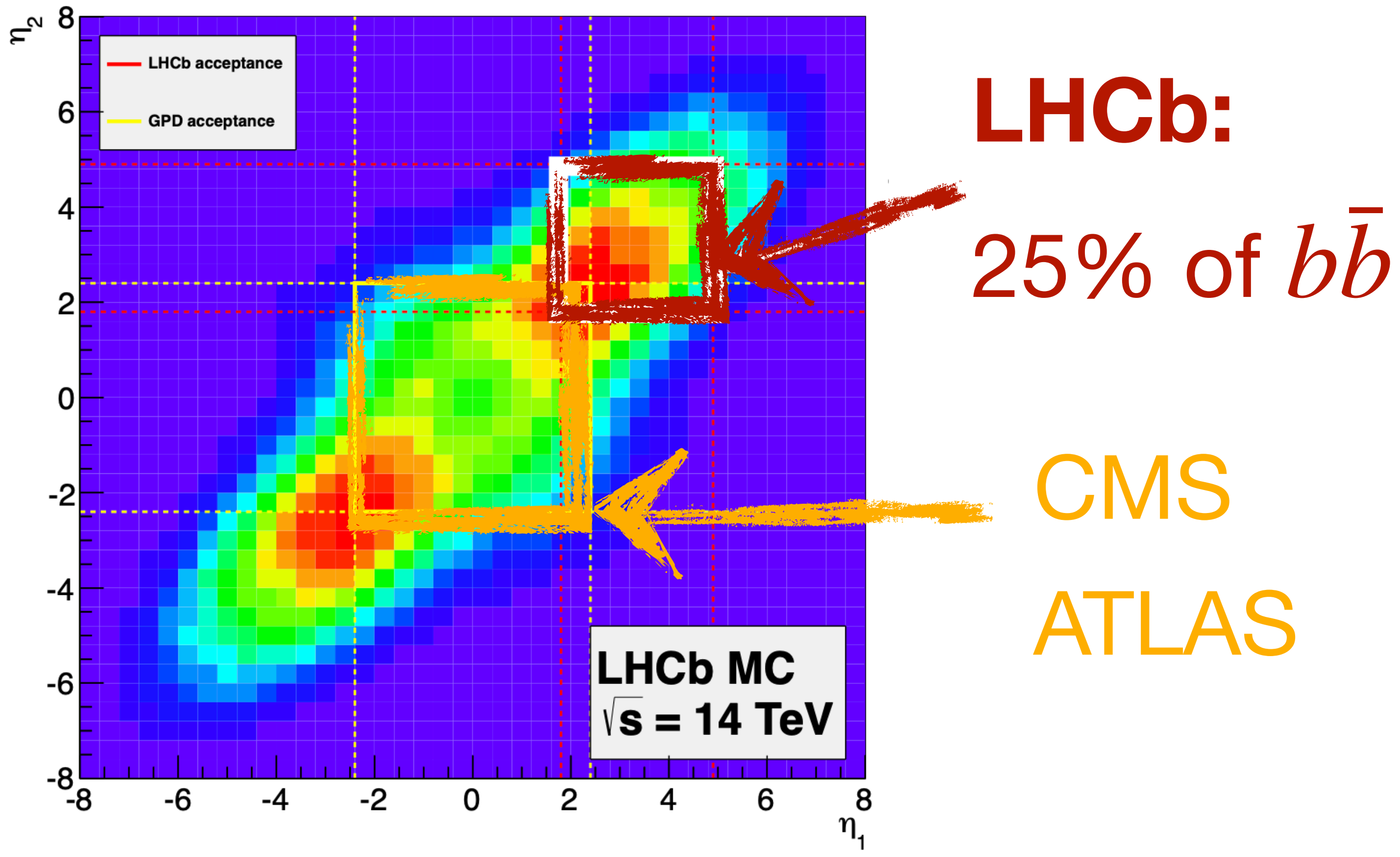

Phys.Rev.Lett.**118**(2017)052002

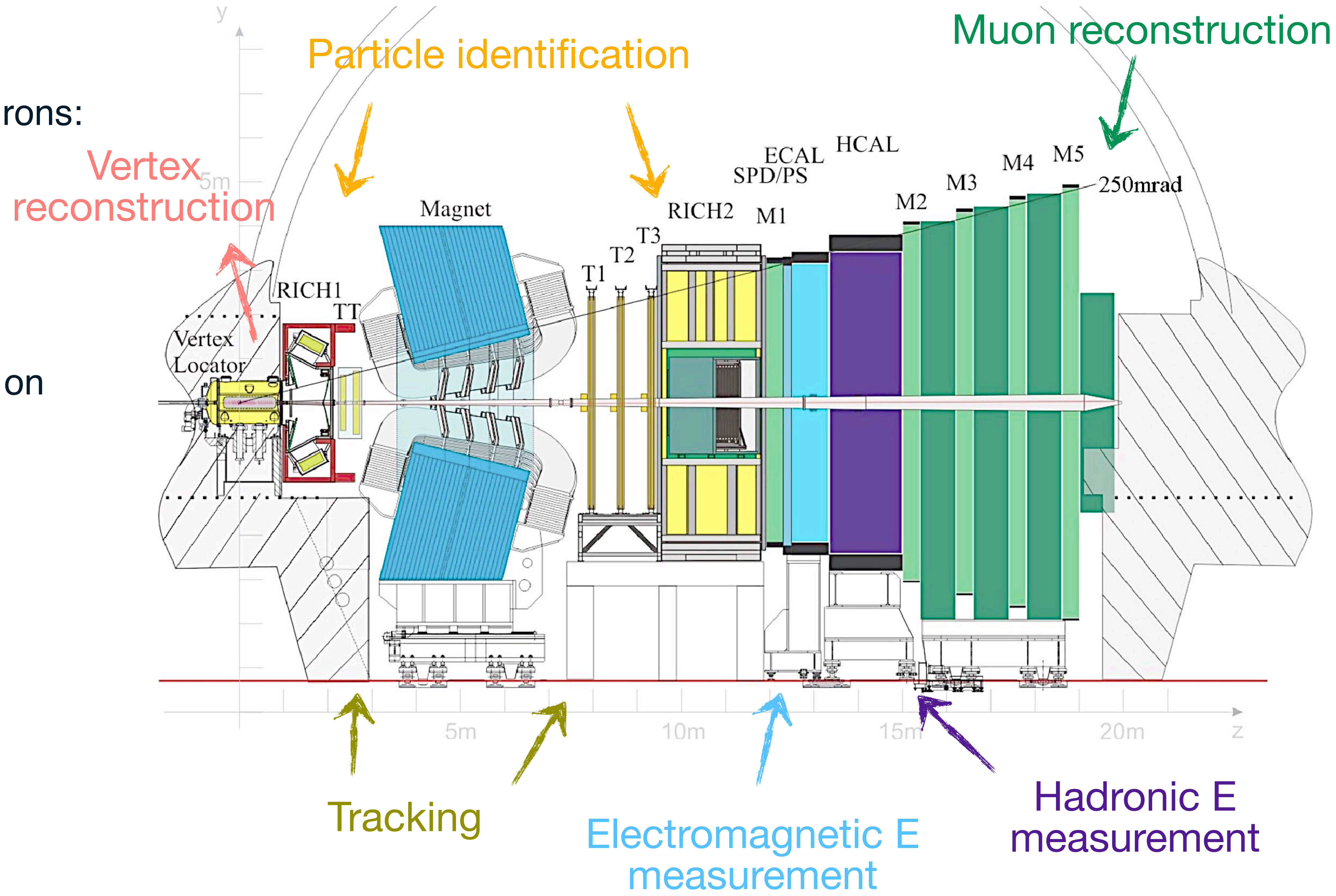

Int.J.Mod.Phys.**A30**,1530022(2015)
CERN-LHCC-2003-030

Amplitude analysis of the $B^0 \to K^{*0}\mu^+\mu^-$ decay

LHCb-PAPER-2023-033
arXiv 2312.09115

$B^0 \to K^{*0}\mu^+\mu^-$

LHCb-PAPER-2023-033
arXiv 2312.09115

CERN Seminar

Motivation: to determine the hadronic contributions in $B^0 \to K^{*0}\mu^+\mu^-$ decays.

Crucial for a final understanding of the $b \to s\mu^+\mu^-$ anomalies.

Goal: perform a model dependent amplitude analysis.

Strategy: fit the full 5D differential decay rate unbinned in q^2.

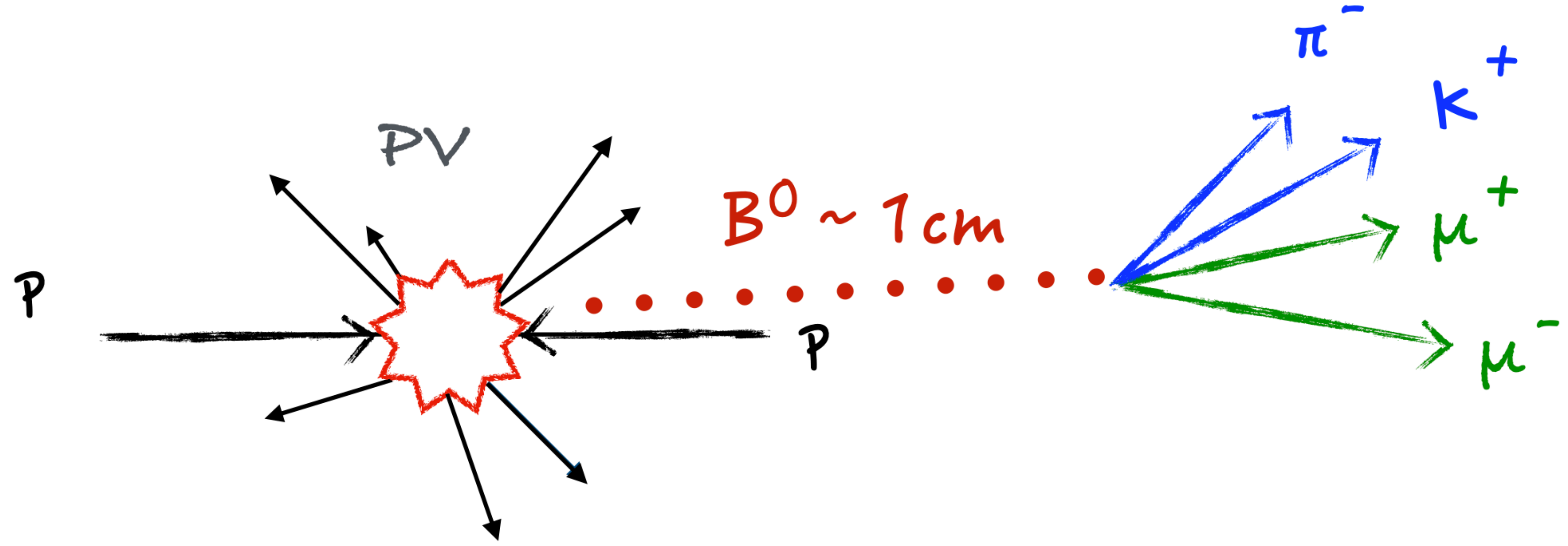

Decay amplitudes: choice of parametrisation introduces a model dependence.

Local form factors (FFs) constrained to:

Gubernari, Reboud, vanDyk, Virto [arXiv:2305.06301]

Non-local hadronic terms based on the param. from:

Bobeth, Chrzaszcz, vanDyk, Virto [EPJC **78** (2018) 451]
Gubernari, vanDyk, Virto [JHEP **02** (2021) 088]
Gubernari, Reboud, vanDyk, Virto [JHEP **09** (2022) 133]

non-local hadronic matrix elements "charm-loop"

$$\mathcal{A}_\lambda^{L,R} = \mathcal{N}_\lambda \left\{ \left[(\mathcal{C}_9 \pm \mathcal{C}_9') \mp (\mathcal{C}_{10} \pm \mathcal{C}_{10}') \right] \mathcal{F}_\lambda(q^2) + \frac{2 m_b M_B}{q^2} \left[(\mathcal{C}_7 \pm \mathcal{C}_7') \mathcal{F}_\lambda^T(q^2) - 16\pi^2 \frac{M_B}{m_b} \mathcal{H}_\lambda(q^2) \right] \right\}$$

Wilson coeff.

Form Factors

$B^0 \to K^{*0}\mu^+\mu^-$

LHCb-PAPER-2023-033
arXiv 2312.09115

- Differential decay rate can only access the relative size of the Wilson coefficients.
- Scale of Wilson coefficients set by branching ratio.
- Extended fit allows to link the observed yield to the signal branching fraction.

Greljo, Salko, Smolkovic, Stangl [JHEP05 (2023) 087]

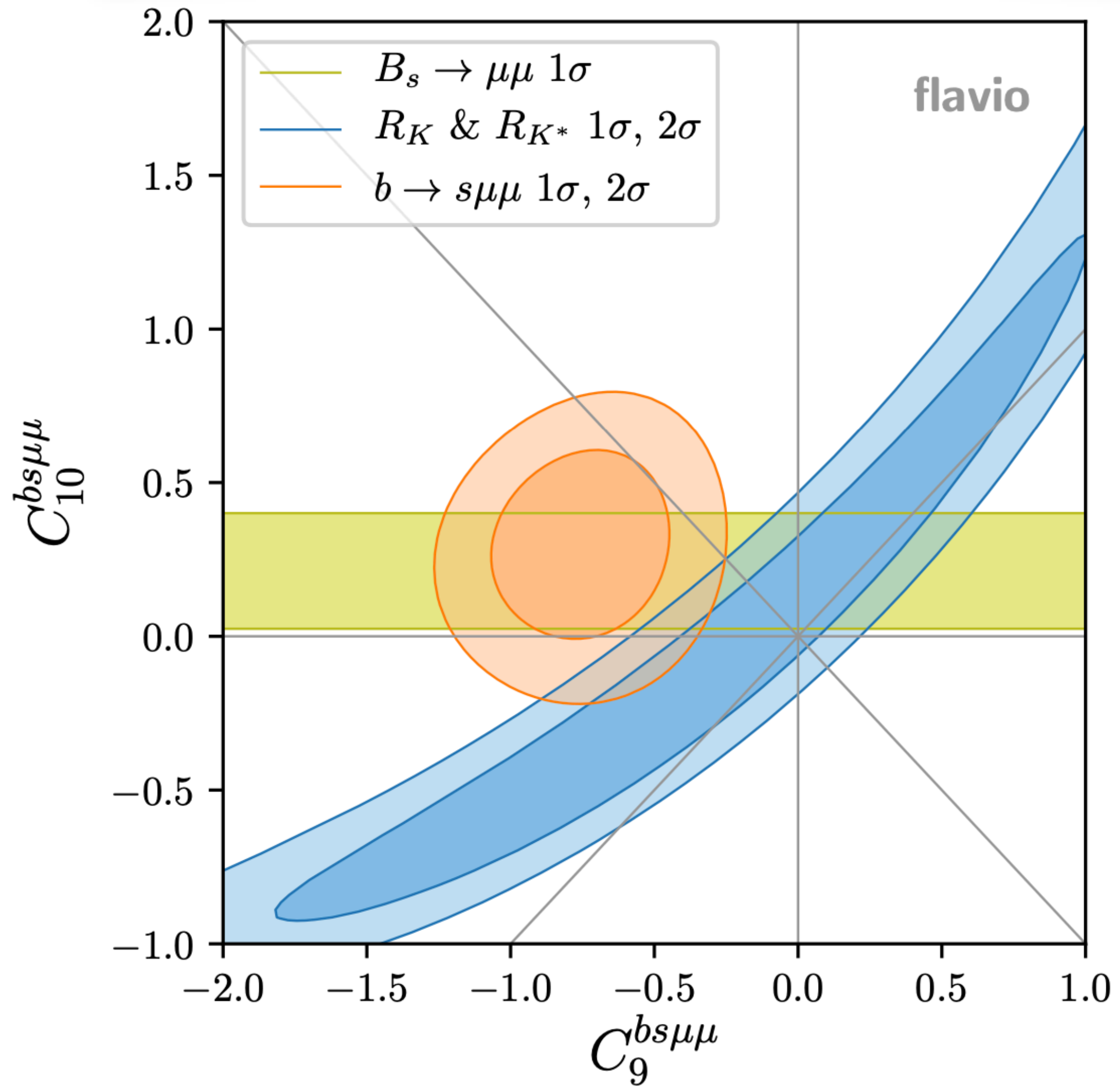

Normalised to $B^0 \to J/\psi K^+\pi^-$ control channel to reduce systematics.

$$\mathcal{B}(B^0 \to K^{*0}\mu^+\mu^-) = \frac{\tau_B}{\hbar}\int_{q^2_{\min}}^{q^2_{\max}}\int_{k^2_{\min}}^{k^2_{\max}} \frac{d^2\Gamma}{dq^2 dk^2} dq^2 dk^2$$

$$N_{sig} = N_{J/\psi K\pi} \times \frac{\mathcal{B}(B^0 \to K^{*0}\mu^+\mu^-) \times \frac{2}{3}}{\mathcal{B}(B^0 \to J/\psi K^+\pi^-) \times f^{J/\psi K\pi}_{\pm 100\text{MeV}} \times \mathcal{B}(J/\psi \to \mu^+\mu^-)} \times R_\varepsilon$$

$K^{*0} \to K^+\pi^-$

Wilson coefficients enter here

from mass fit to control channel (include exotica contribution)

from Belle dedicated $B^0 \to J/\psi K^+\pi^-$ amplitude analysis

[Phys.Rev.D90 (2014) 1122009]

PDG

Ratio of efficiency: from simulations

$B^0 \to K^{*0}\mu^+\mu^-$

P_5' angular observable: from the fit result, the classic binned observables can be reproduced. Impact of $c\bar{c}$ on *P'* found to be consistent with predictions.

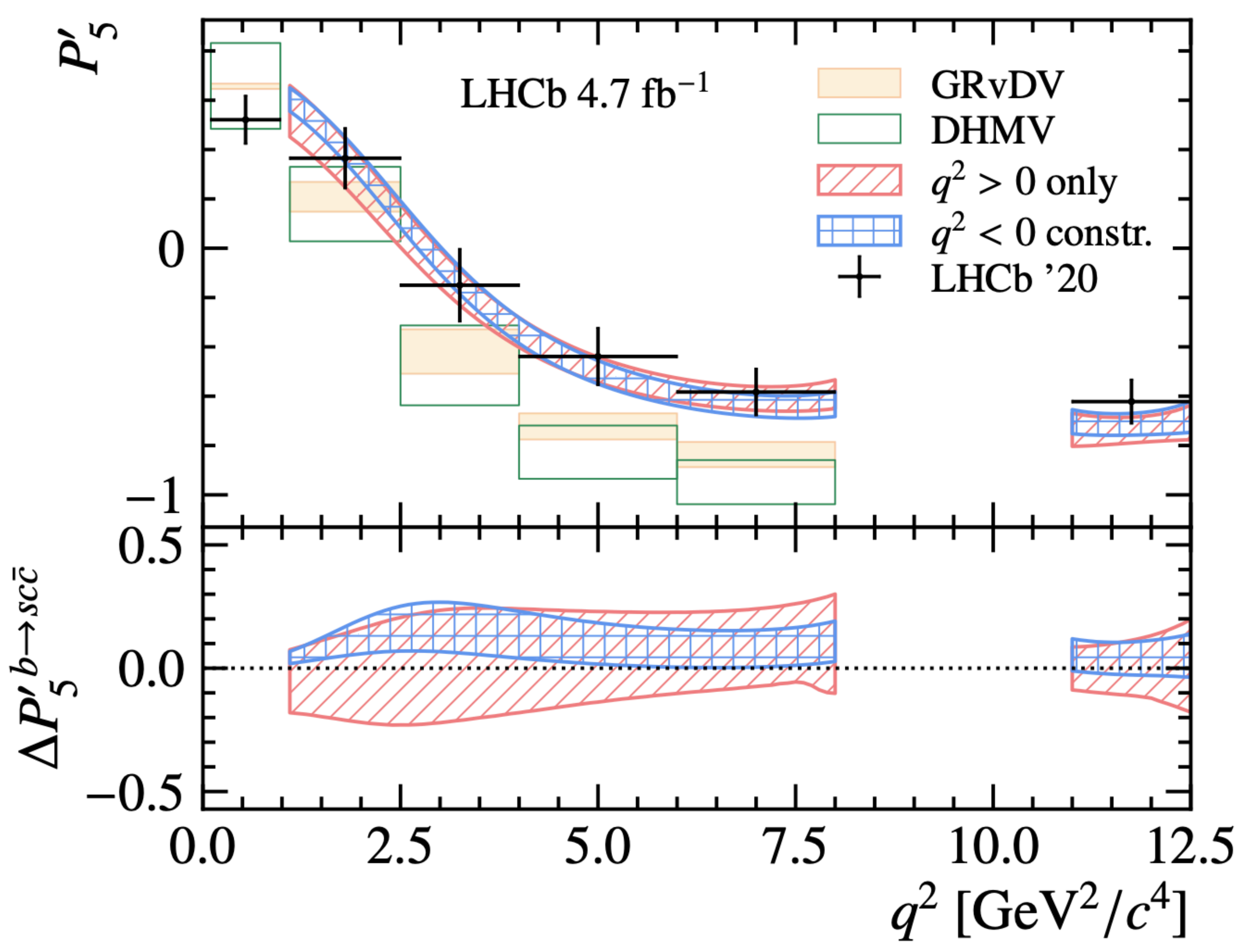

Wilson coefficients: consistent with global analyses of $b \to s\mu^+\mu^-$ decays.

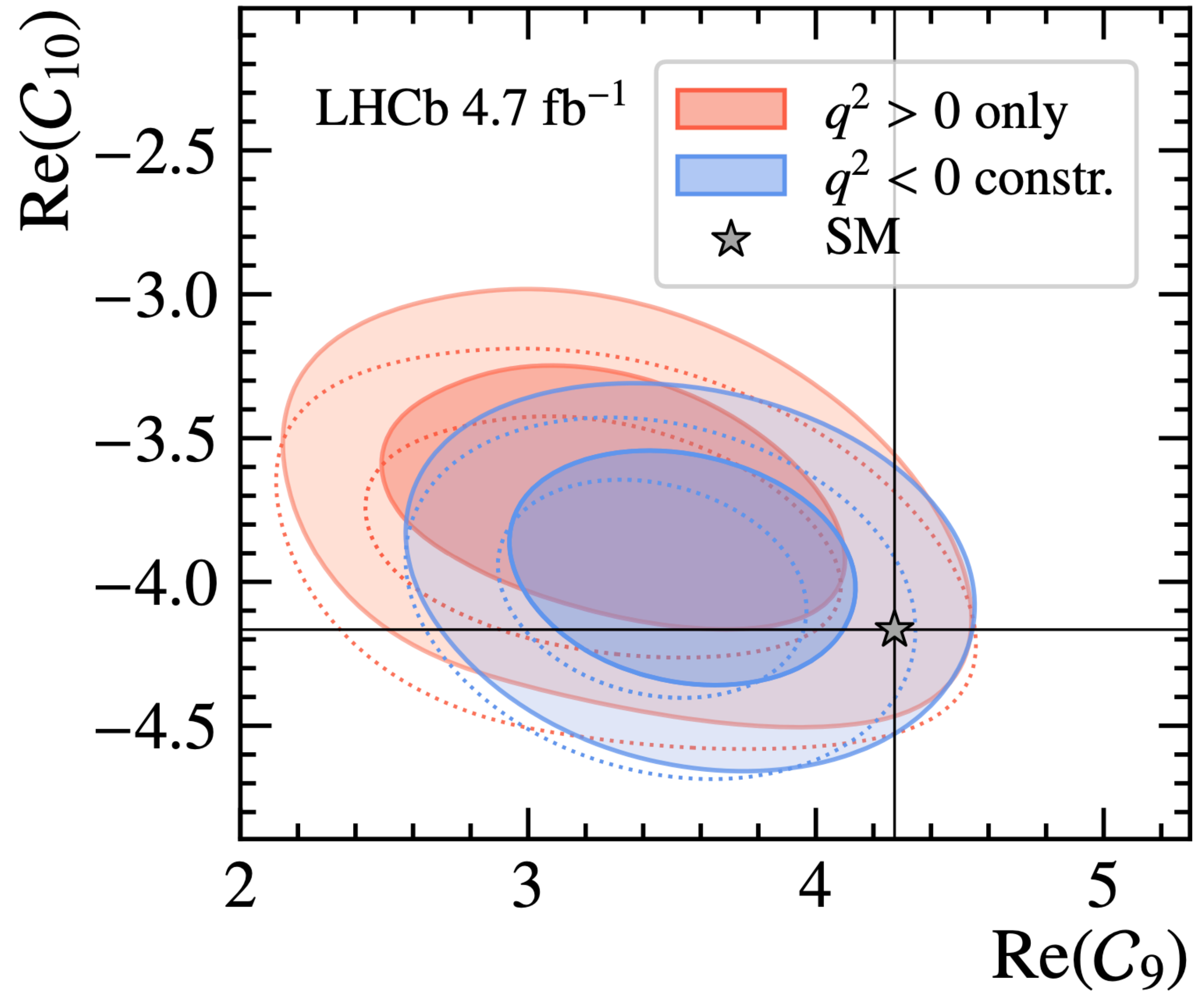

New analysis method to determine hadronic contributions in $B^0 \to K^{*0}\mu^+\mu^-$ decays.

$\mathcal{B}(\phi \to \mu^+\mu^-)/\mathcal{B}(\phi \to e^+e^-)$ with charm meson decays

LHCb-PAPER-2023-038
arXiv 2402.01336

$\mathcal{B}(\phi \to \mu^+\mu^-)/\mathcal{B}(\phi \to e^+e^-)$

LHCb-PAPER-2023-038
arXiv 2402.01336

- Electrons and muons exploit different subdetectors.
  ↓
- Bremmstrahlung energy loss is greater for electrons.
  ↓
- Worse resolution and lower reconstruction efficiency.
  ↓
- Hard to control their relative efficiency in LFU observables.
  ↓
- **Double ratios** to cancel out common syst. uncertainties between rare and control modes.

The R_H observables, theoretically clean:

$q^2 \equiv$ momentum transfer to the pair of leptons

$$R_{H_s} = \frac{\int_{q^2_{\min}}^{q^2_{\max}} \frac{d\mathcal{B}(B\to H_s \mu^+\mu^-)}{dq^2} dq^2}{\int_{q^2_{\min}}^{q^2_{\max}} \frac{d\mathcal{B}(B\to H_s e^+e^-)}{dq^2} dq^2} \overset{\text{SM}}{=} 1 \pm \mathcal{O}(10^{-2})$$

QED

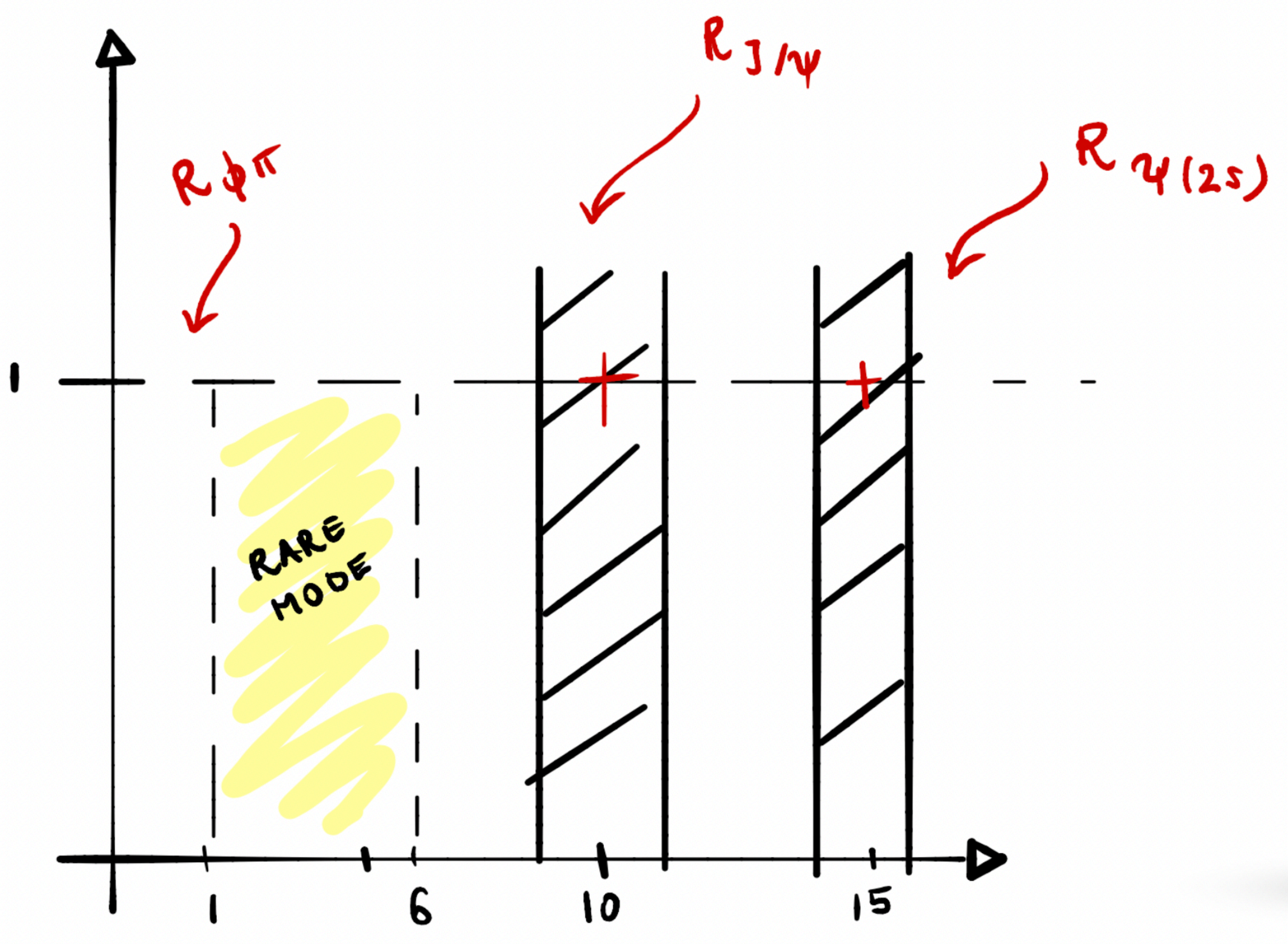

The resonant $D^+_{(s)} \to \phi(l^+l^-)\pi^+$ are ideal control channels in the **low q²** region.

The q² region lower than where most precise LFU measurements are done.

Clear detector signature and a high BF ⇒ allow to verify with precision the $h \to e$ data driven estimation strategy.

D. **Lancierini**
Joint SPS-APS Annual Meeting

First control mode at low q² (ϕ mass).

$\phi \equiv \phi(1020)$

$\mathcal{B}(\phi \to \mu^+\mu^-)/\mathcal{B}(\phi \to e^+e^-)$

LHCb-PAPER-2023-038
arXiv 2402.01336

Strategy

Signal yield extraction: maximum likelihood fits

Efficiency calculation: simulation and data samples.

$$R_{\phi\pi}^{d(s)} = \beta \cdot \frac{N(D^+_{(s)} \to \phi(\mu\mu)\pi^+)}{N(D^+_{(s)} \to \phi(ee)\pi^+)} \cdot \frac{\varepsilon(D^+_{(s)} \to \phi(ee)\pi^+)}{\varepsilon(D^+_{(s)} \to \phi(\mu\mu)\pi^+)} \Big/ r_{J/\psi}$$

$$r_{J/\psi} = \mathcal{B}(B^+ \to H_s J/\psi(\to \mu^+\mu^-))/\mathcal{B}(B^+ \to H_s J/\psi(\to e^+e^-))$$

As ϕ and J/ψ decays are dominated by photon exchange, LFU is expected to hold in this process.

Measurement of $R^d_{\phi\pi}$ and $R^s_{\phi\pi}$ done integrated.

Additionally, differential measurement provided:

- **Angle** between the leptons: $\alpha(l^+l^-)$
- The **maximum p$_T$** of the leptons: $\max(p_T(l^+), p_T(l^-))$

$\mathcal{B}(\phi \to \mu^+\mu^-)/\mathcal{B}(\phi \to e^+e^-)$

LHCb-PAPER-2023-038
arXiv 2402.01336

Normalisation channel mass fits:

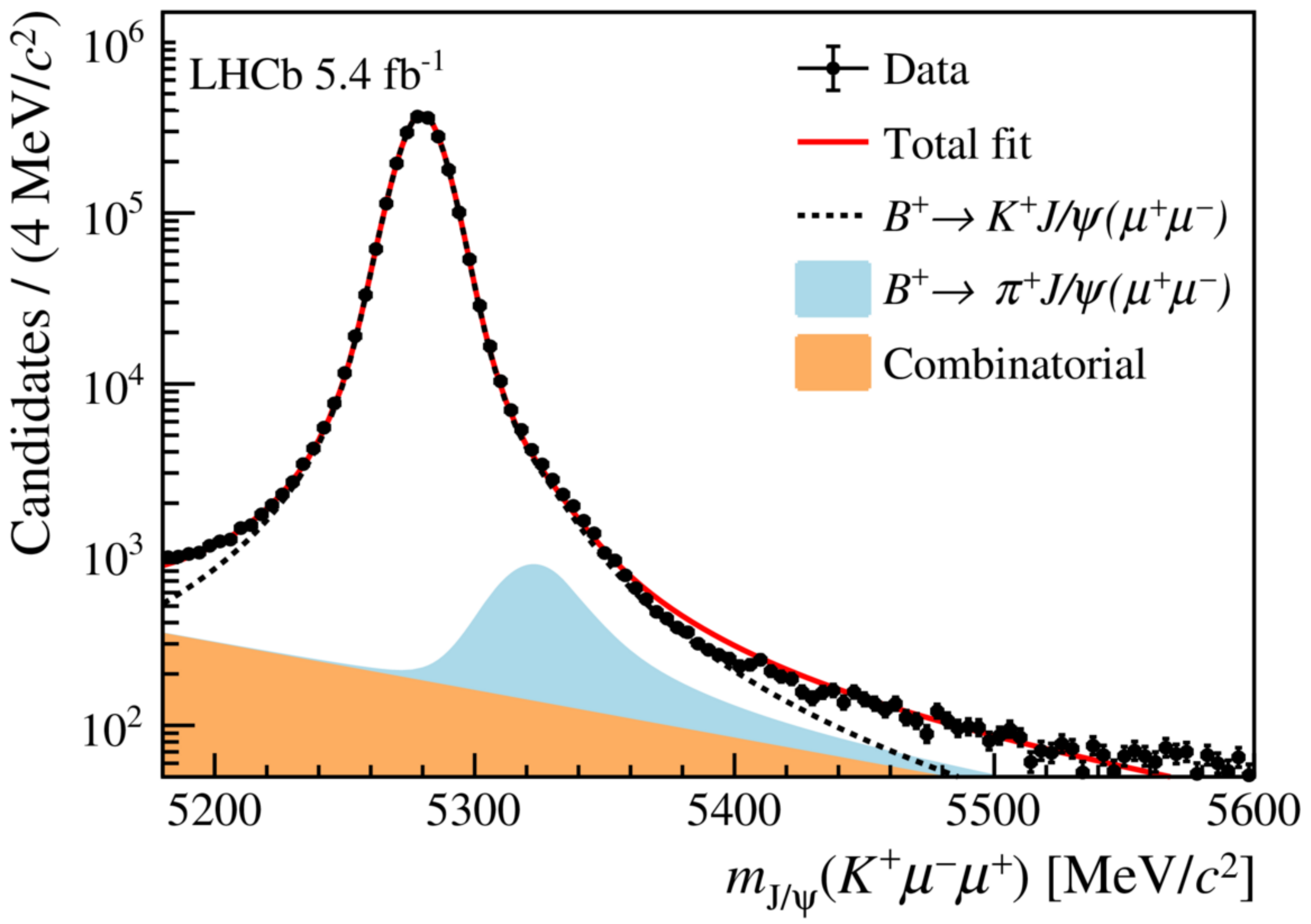

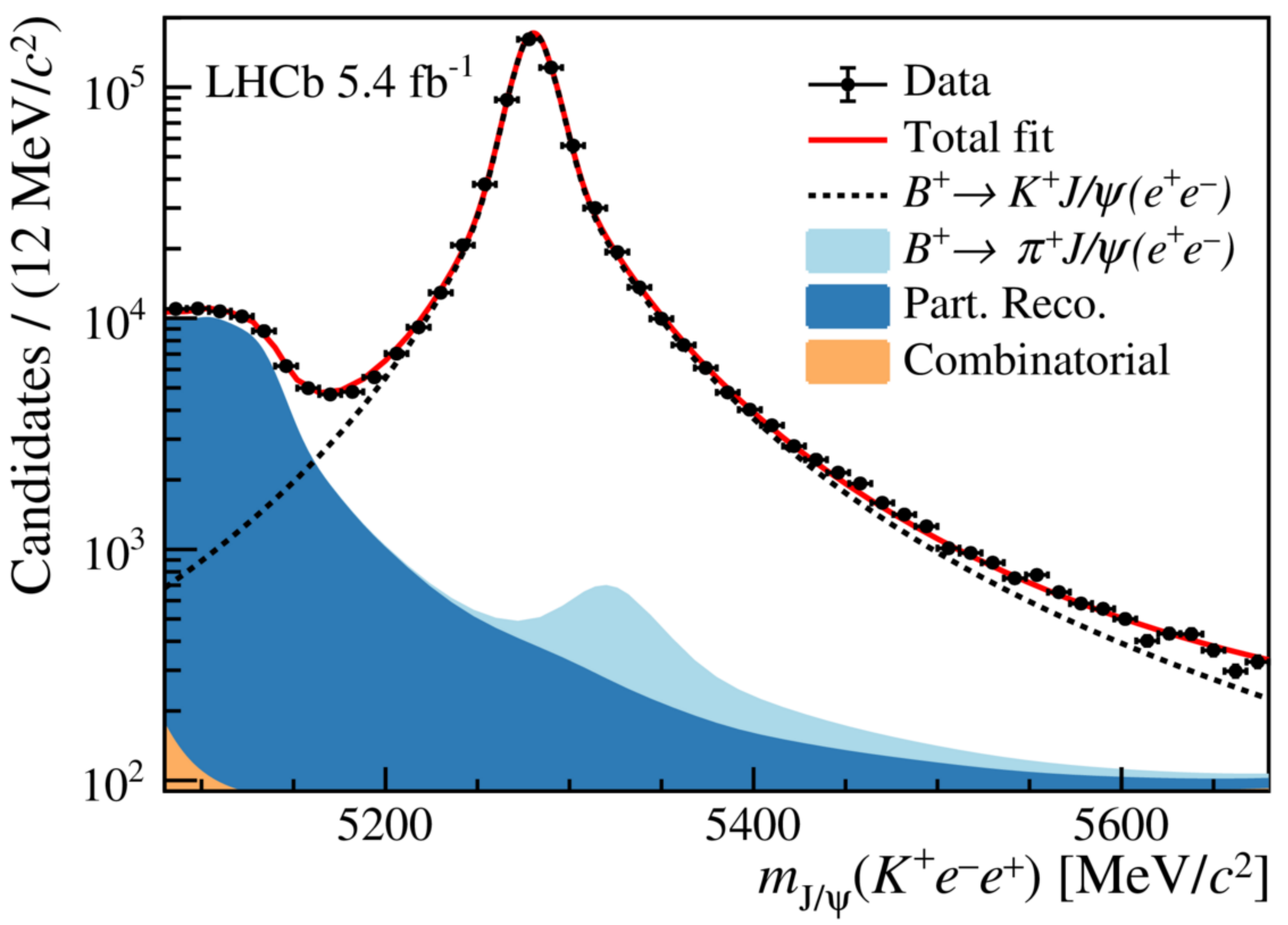

Final fits

Both masses constrain the intermediate resonance to the J/ψ / ϕ mass in the track fit.

Normalisation: B^+ mass from $B^+ \to K^+J/\psi(\to l^+l^-)$ decay. Assuming that LFU holds in J/ψ decays.

Signal: D^+ and D_s^+ mass from $D_{(s)}^+ \to \phi(l^+l^-)\pi^+$ decays with ϕ constraint.

Reconstructed $D_{(s)}^+$ mass:

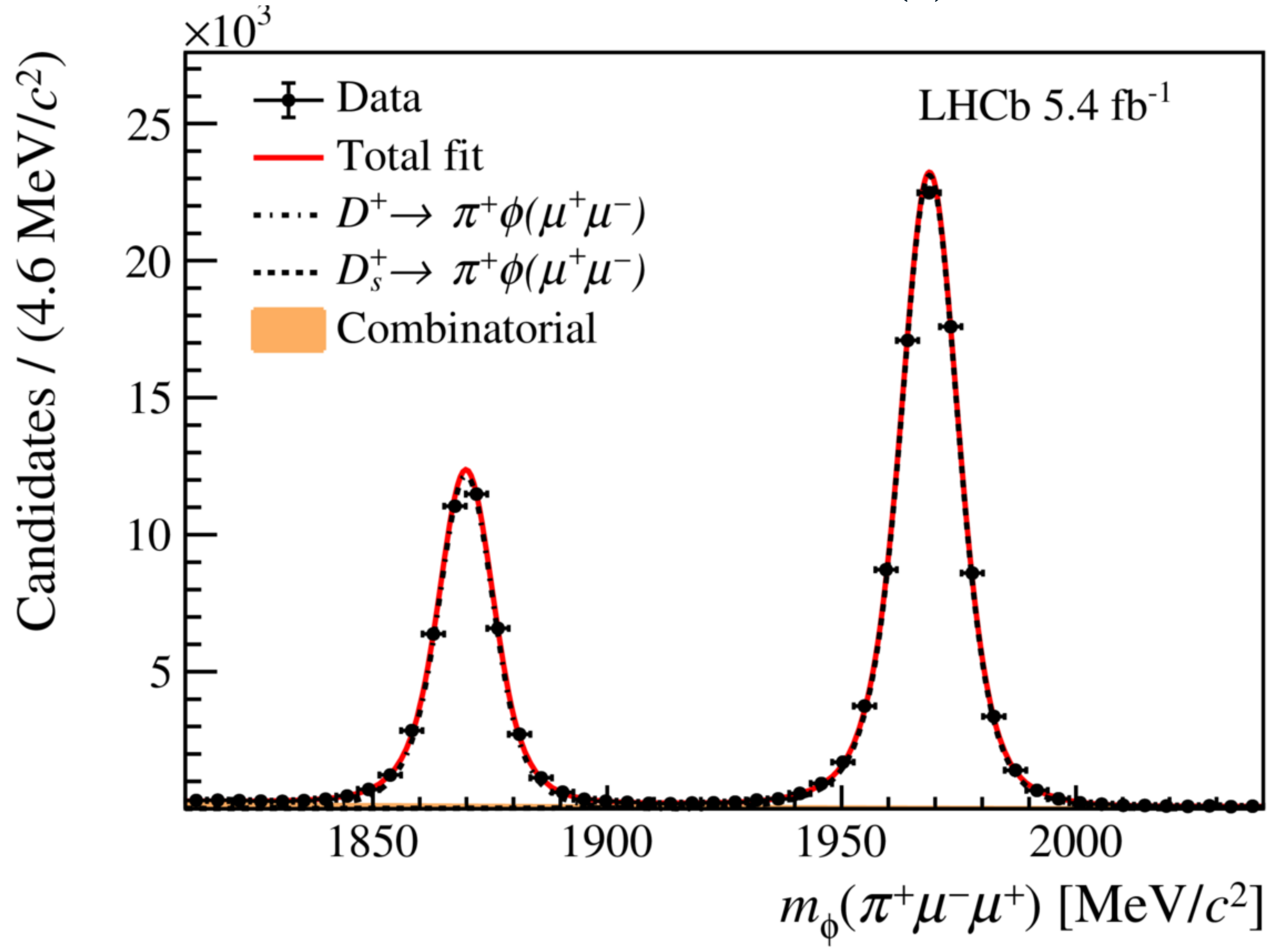

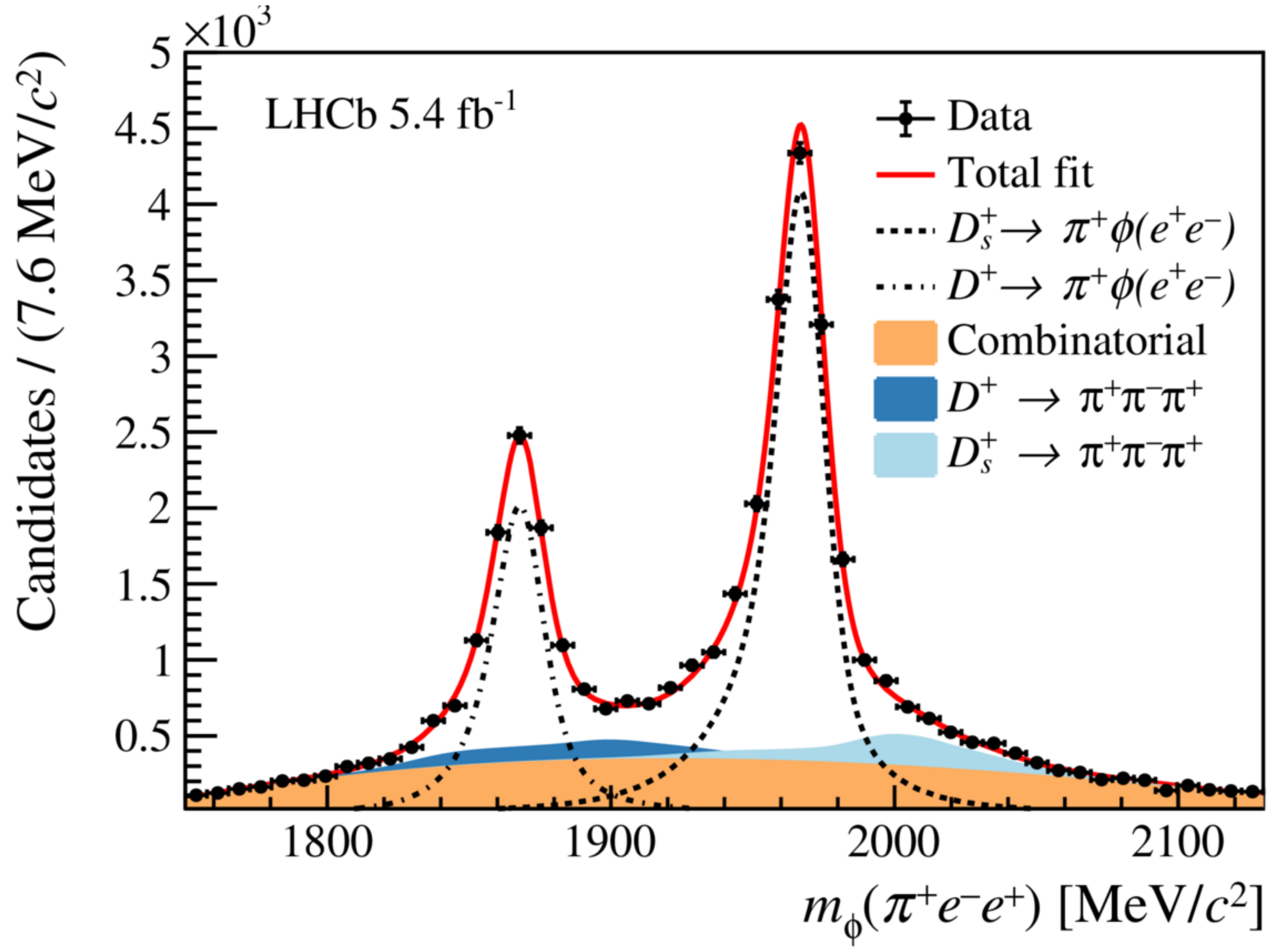

$\mathcal{B}(\phi \to \mu^+\mu^-)/\mathcal{B}(\phi \to e^+e^-)$

LHCb-PAPER-2023-038
arXiv 2402.01336

Agreement on the shapes from data-simulation

⇒ validation of the resolution description at low q^2.

Still biggest source of syst. uncertainty due to tight reconstructed D and ϕ mass requirements.

Source	$R^d_{\phi\pi}$ [%]	$R^s_{\phi\pi}$ [%]
Resolution on q^2	4.0	3.9
Event multiplicity	2.7	2.7
Simulation reweighting	1.5	1.2
Combinatorial background shape parametrisation	1.5	1.0
PID	0.8	0.8
Finite size of control samples	0.8	0.6
Trigger	0.3	0.3
Tracking	0.1	0.1
Background from doubly misidentified electrons	1.1	0.1
Total	5.5	5.1

Dilepton mass fits in a narrow $m_\phi(\pi^+ l^- l^+)$

D^+ D_s^+

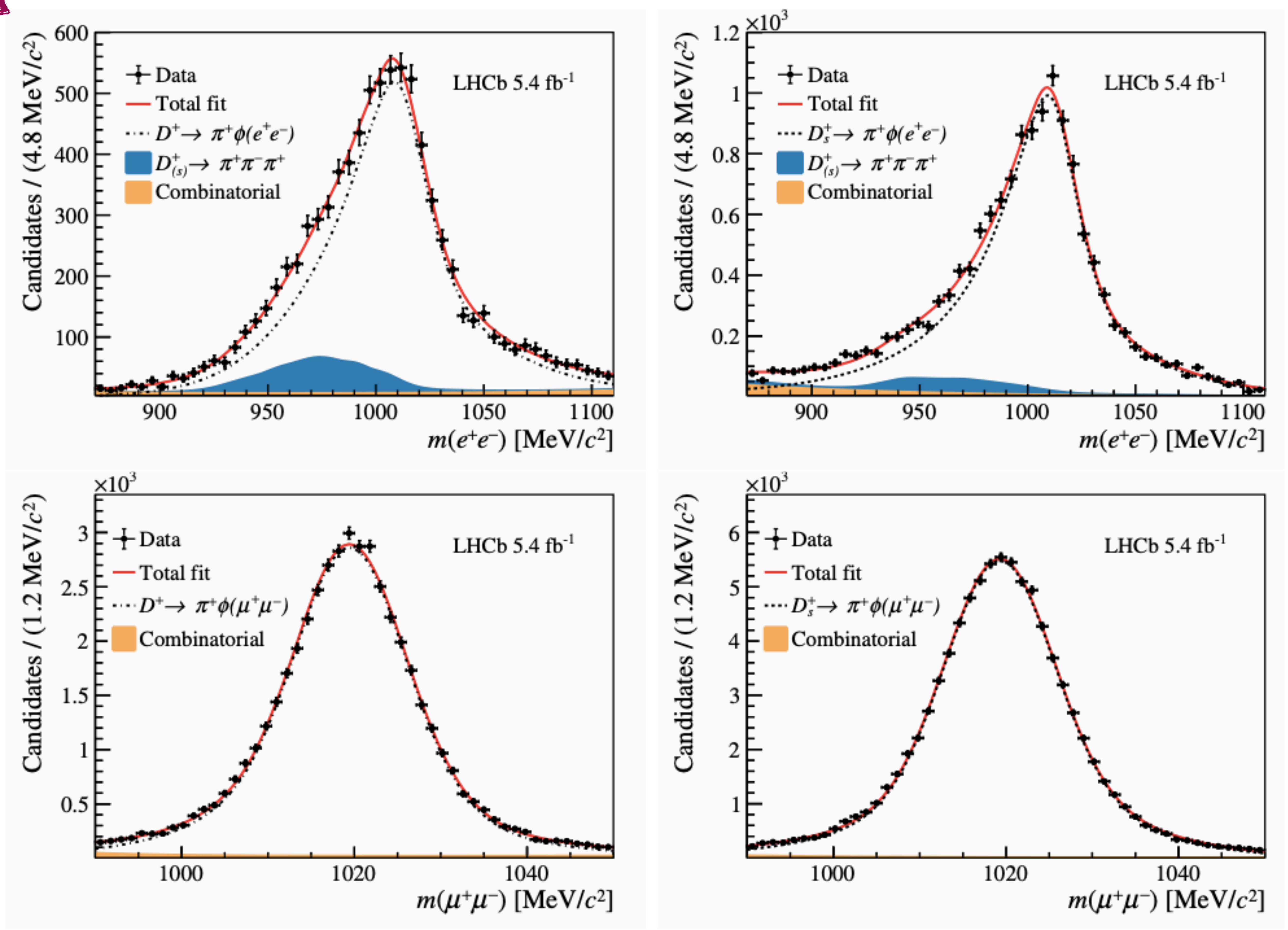

$\mathscr{B}(\phi \to \mu^+\mu^-)/\mathscr{B}(\phi \to e^+e^-)$

LHCb-PAPER-2023-038
arXiv 2402.01336

Final results:

$$R^d_{\phi\pi} = 1.026 \pm 0.020\,(\text{stat}) \ \pm 0.056\,(\text{syst})$$
$$R^s_{\phi\pi} = 1.017 \pm 0.013\,(\text{stat}) \ \pm 0.051\,(\text{syst})$$

Differential measurement of $R^{(d,s)}_{\phi\pi}$:

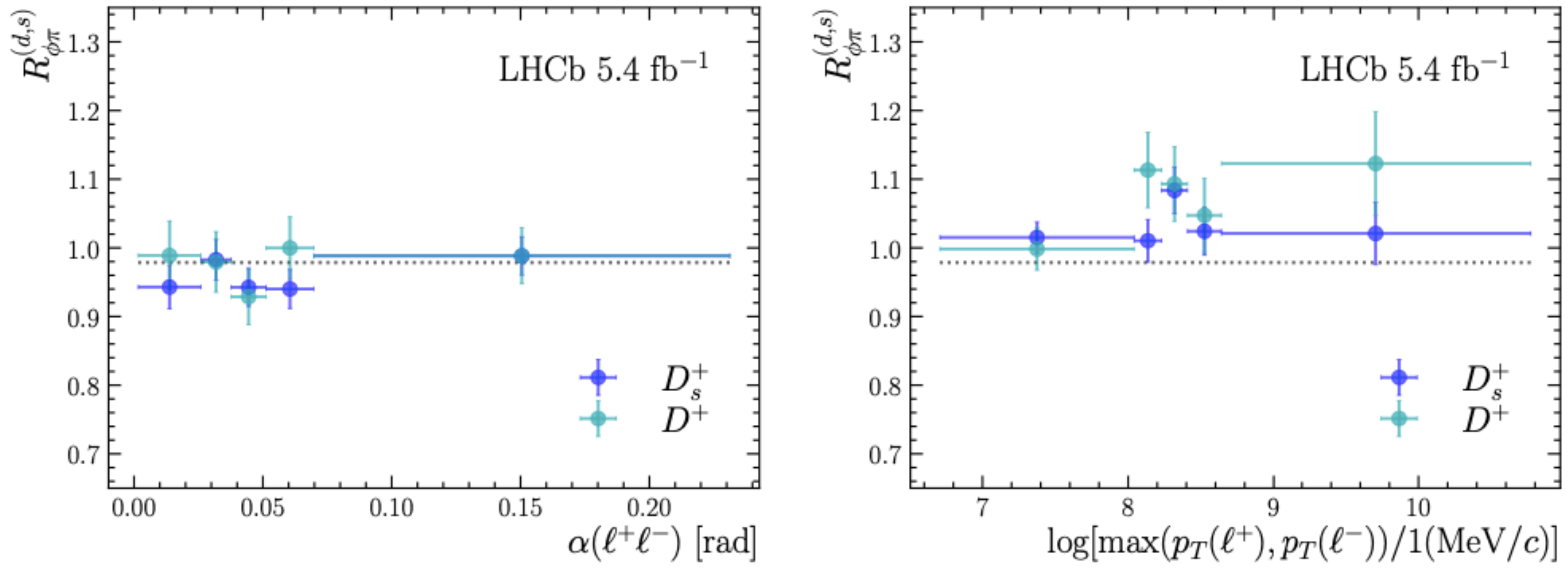

It shows understanding of the portability of the corrections derived at $q^2 \sim m^2(J/\psi)$ to lower values.

Weighted average:

$$R_{\phi\pi} = 1.022 \pm 0.012\,(\text{stat}) \ \pm 0.048\,(\text{syst})$$

Compatible with previous $\mathscr{B}(\phi \to l^+l^-)$ measurements, and with LFU.

Combined with the existing $\phi \to e^+e^-$:

PDG [Exp.Phys.**2022**(2022)083C01]

$$\mathcal{B}(\phi \to \mu^+\mu^-) = (3.045 \pm 0.049\,(\text{stat}) \pm 0.148\,(\text{syst})) \times 10^{-4}$$

Most precise measurement of this branching fraction to date.

Amplitud analysis of the $\Lambda_b^0 \to pK^-\gamma$ decay

LHCb-PAPER-2023-036
In preparation

$\Lambda_b^0 \to pK^-\gamma$

The analysis of $\Lambda_b^0 \to pK^-\gamma$ decays provides information about the composition of the pK^- spectrum with **unique access to the heavier Λ states.**

Removal of peaking backgrounds:

- m(pK) < 2.5 GeV/c² to reduce $\Lambda_b^0 \to pK^-\pi^0$
- Veto 1010 < m(KK) < 1040 MeV/c² to remove $B_s^0 \to \phi(\to K^+K^-)\ \gamma$
- Particle ID on p and K to reduce $B_s^0 \to K^+K^-\ \gamma$ and $B^0 \to K^+\pi^-\ \gamma$
- BDT

Remaining:

- Partially reconstructed $\Lambda_b^0 \to pK^-\pi^0\gamma$
- Combinatorial background

Fit to the three-body invariant mass:

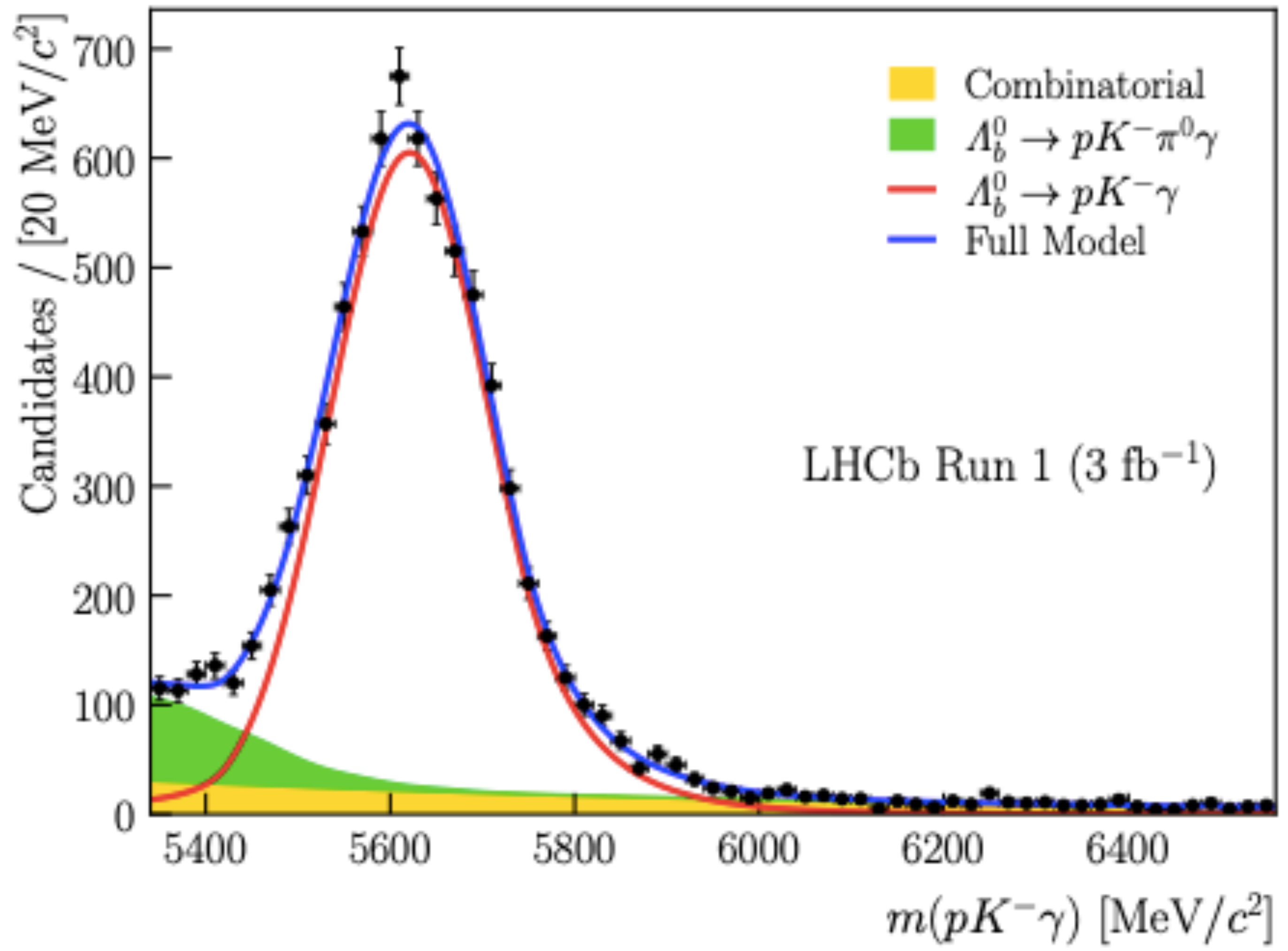

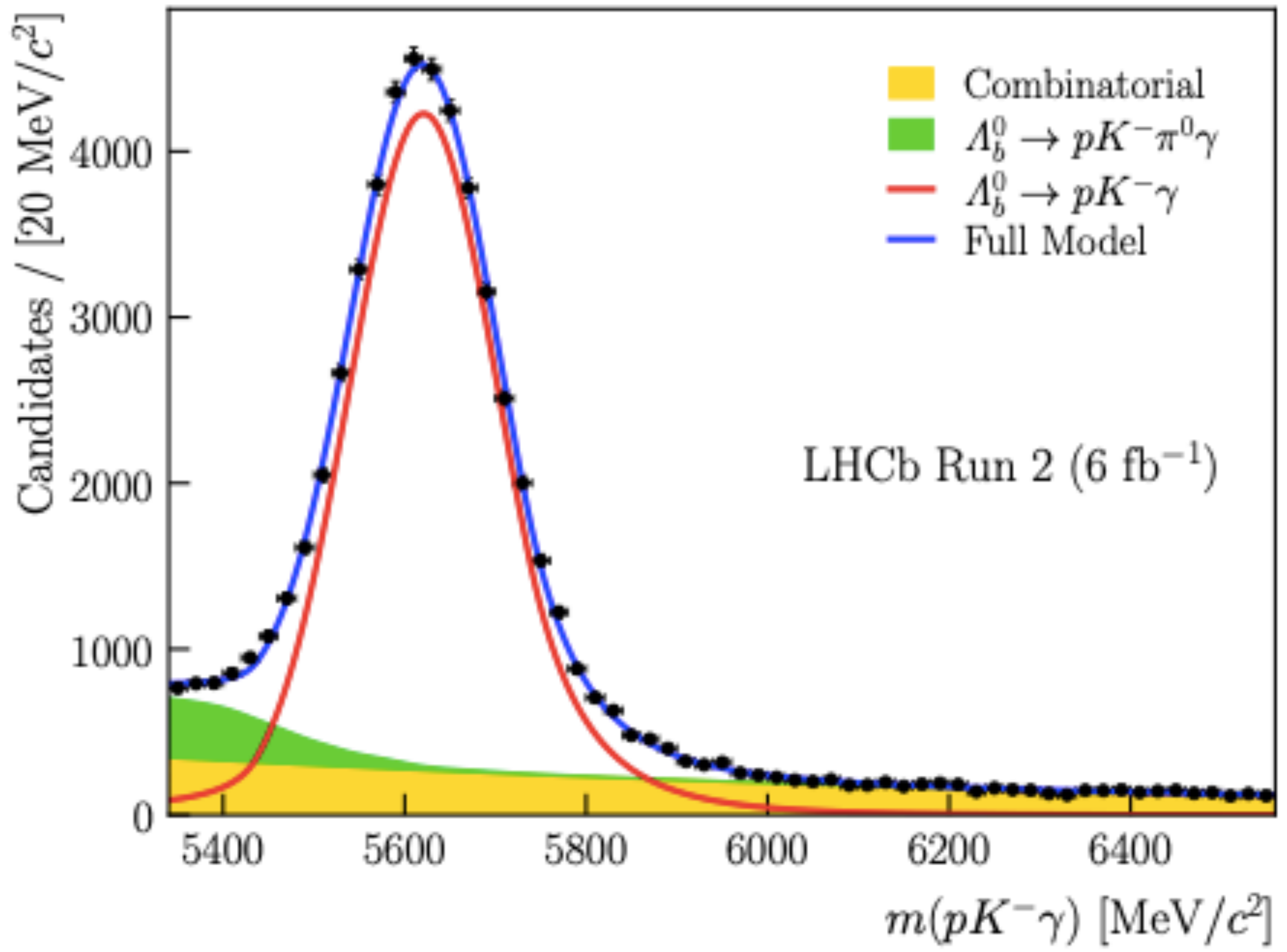

$\Lambda_b^0 \to pK^-\gamma$

LHCb-PAPER-2023-036
In preparation

JHEP **06** (2020) 116
arXiv:2002.02692

Amplitude model for helicity formalism:

$\Lambda_b \to \Lambda^*(\to pK^-)\gamma$ amplitude for a defined set of helicities λ_i

$$\underbrace{d^{J_\Lambda}_{\lambda_p \lambda_\Lambda}(\theta_p)}_{\text{Wigner d}} \times \sum_{L=|J_{\Lambda_b^0}-S|}^{|J_{\Lambda_b^0}+S|} \sum_{S=|J_\Lambda - J_\gamma|}^{|J_\Lambda + J_\gamma|} \left[\underbrace{C_1 C_2 C_3}_{\text{Clebsch-Gordans}} \underbrace{h^\Lambda_{LS}}_{LS\text{ coupling}} \left(\frac{p}{M_{\Lambda_b^0}}\right)^L \left(\frac{q}{M_\Lambda}\right)^l \underbrace{B_L(p) B_l(q) \mathrm{BW}_l(m_{pK})}_{\text{line shape with form factors}} \right]$$

connect p and Λ^* helicity frames (Wigner d); fit parameter (h^Λ_{LS}); orb. ang. mom. barriers ($\left(\frac{p}{M_{\Lambda_b^0}}\right)^L \left(\frac{q}{M_\Lambda}\right)^l$)

Strategy: unbinned maximum likelihood fit to Dalitz plane $(m^2_{p,k}, m^2_{p,\gamma})$ →

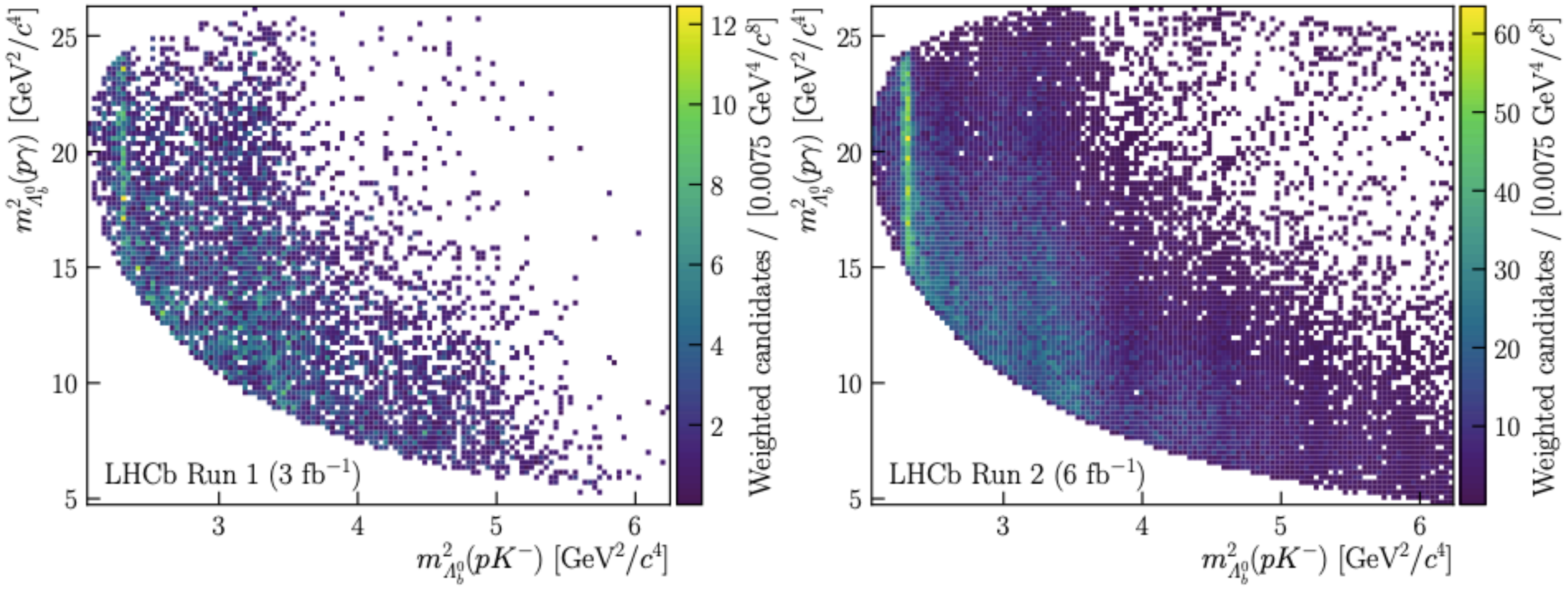

$\Lambda_b^0 \to pK^-\gamma$

1-dimensional projections of the **best fit model**:

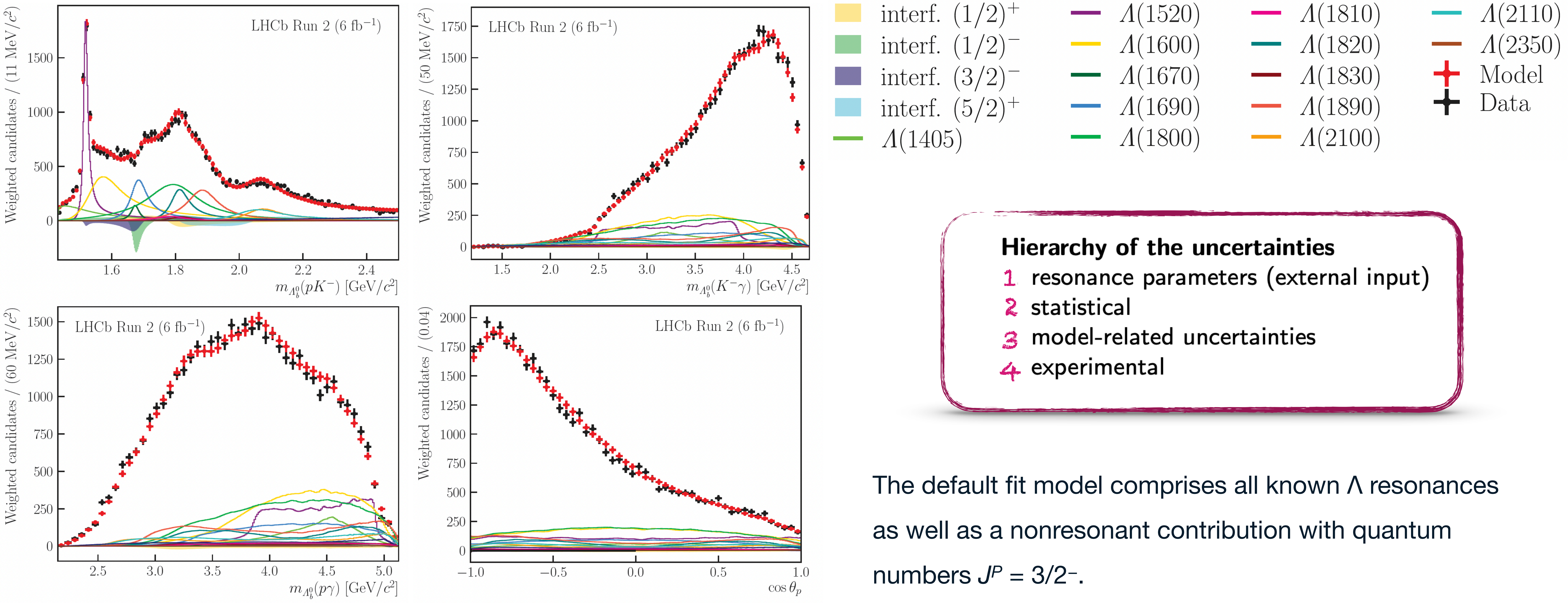

Hierarchy of the uncertainties

1. resonance parameters (external input)
2. statistical
3. model-related uncertainties
4. experimental

The default fit model comprises all known Λ resonances as well as a nonresonant contribution with quantum numbers $J^P = 3/2^-$.

$\theta_p \equiv$ proton helicity angle

Same done for Run 1.

$\Lambda_b^0 \to pK^-\gamma$

LHCb-PAPER-2023-036
In preparation

The results are given in terms of fit and interference fractions between the different components contributing to the final state.

Only Λ resonances decaying to pK^- are found to be relevant, where the largest contributions stem from

$\Lambda(1520)$, $\Lambda(1600)$, $\Lambda(1800)$, and $\Lambda(1890)$ states

The largest interference term involves the

$\Lambda(1405)$ and $\Lambda(1800)$ baryons

First $\Lambda_b^0 \to pK^-\gamma$ amplitude analysis, based on the helicity formalism.

Final results for the (interference) fit fractions:

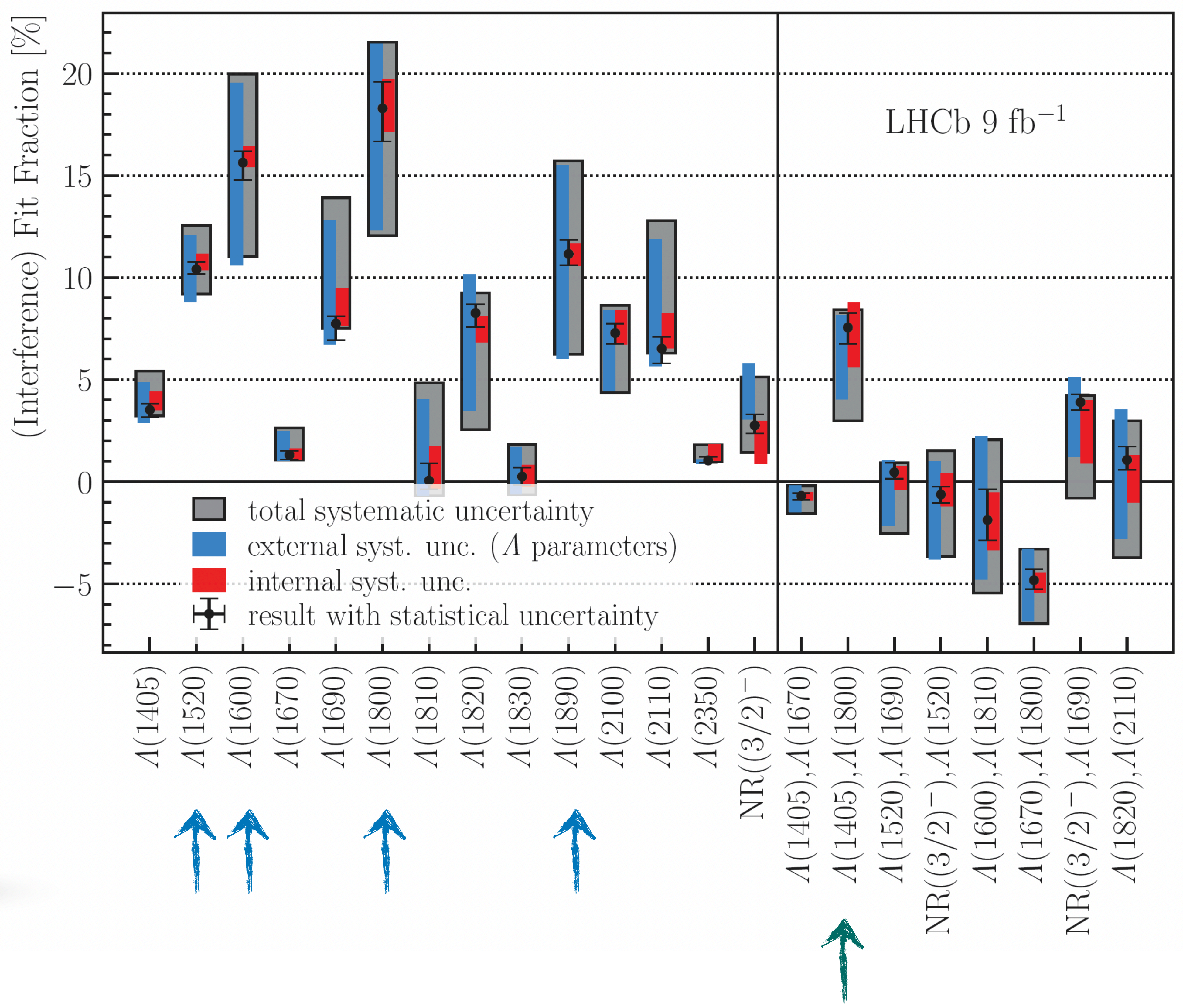

Search for the $B_s^0 \to \mu^+\mu^-\gamma$ decay

LHCb-PAPER-2023-045
In preparation

$B_s^0 \to \mu^+\mu^-\gamma$

LHCb-PAPER-2023-045
In preparation

Phys.Rev.**D97**,053007(2018)
Physics Letters **B 521** (2001)
JHEP **12** (2021) 008

$B_s^0 \to \mu^+\mu^-\gamma$ vs. $B_s^0 \to \mu^+\mu^-$

- (+) Sensitive to a larger set of Wilson coefficients ($\mathcal{C}_7$, $\mathcal{C}_9$, $\mathcal{C}_{10}$) than $B_s^0 \to \mu^+\mu^-$ ($\mathcal{C}_{10}$).
  The photon lifts the helicity suppression making $\mathcal{B}(B_s^0 \to \mu^+\mu^-) \sim \mathcal{B}(B_s^0 \to \mu^+\mu^-\gamma)$.

- (−) Larger theoretical uncertainties due to the form factors of the $B_s^0 \to \gamma$ transition.
  Worse mass resolution due to the photon reconstruction.

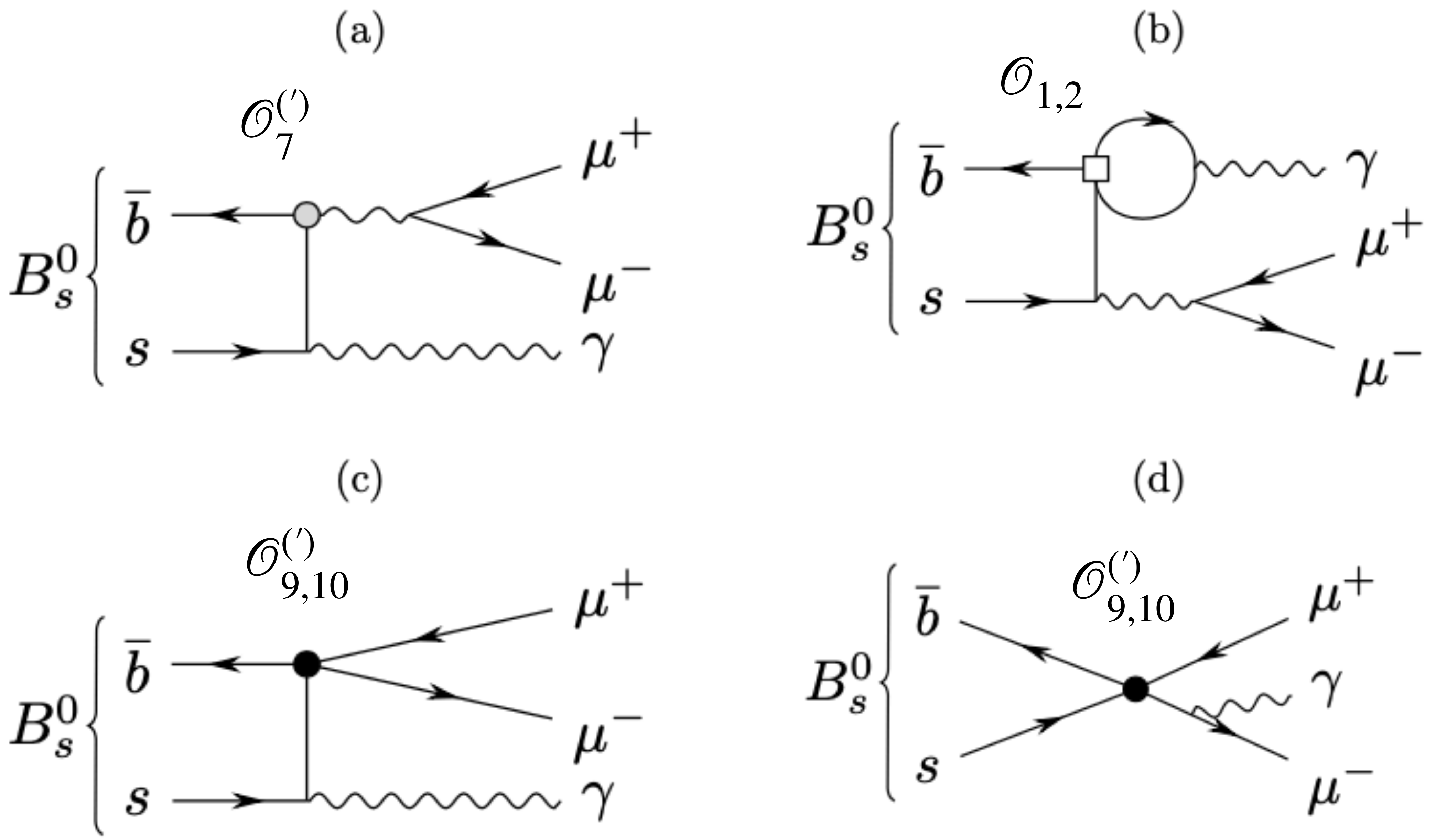

Theory prediction: JHEP **11** (2017) 184

$\mathcal{B}(B_s^0 \to \mu^+\mu^-\gamma) = (8.3 \pm 1.3) \times 10^{-9}$ for $q^2 < 8.64\ \mathrm{GeV}^2/c^4$

$\mathcal{B}(B_s^0 \to \mu^+\mu^-\gamma) = (8.9 \pm 1.0) \times 10^{-10}$ for $q^2 > 15.84\ \mathrm{GeV}^2/c^4$

$q^2 \equiv m^2(\mu^+\mu^-)$

- ○ Electromagnetic-dipole operators
- ● Four-fermion operators
- □ Any four-quark operator

$B_s^0 \to \mu^+\mu^-\gamma$

LHCb-PAPER-2023-045
In preparation

Strategy: Three q^2 regions:

- Bin I: low-q^2
- Bin II: middle-q^2
- Bin III: high-q^2

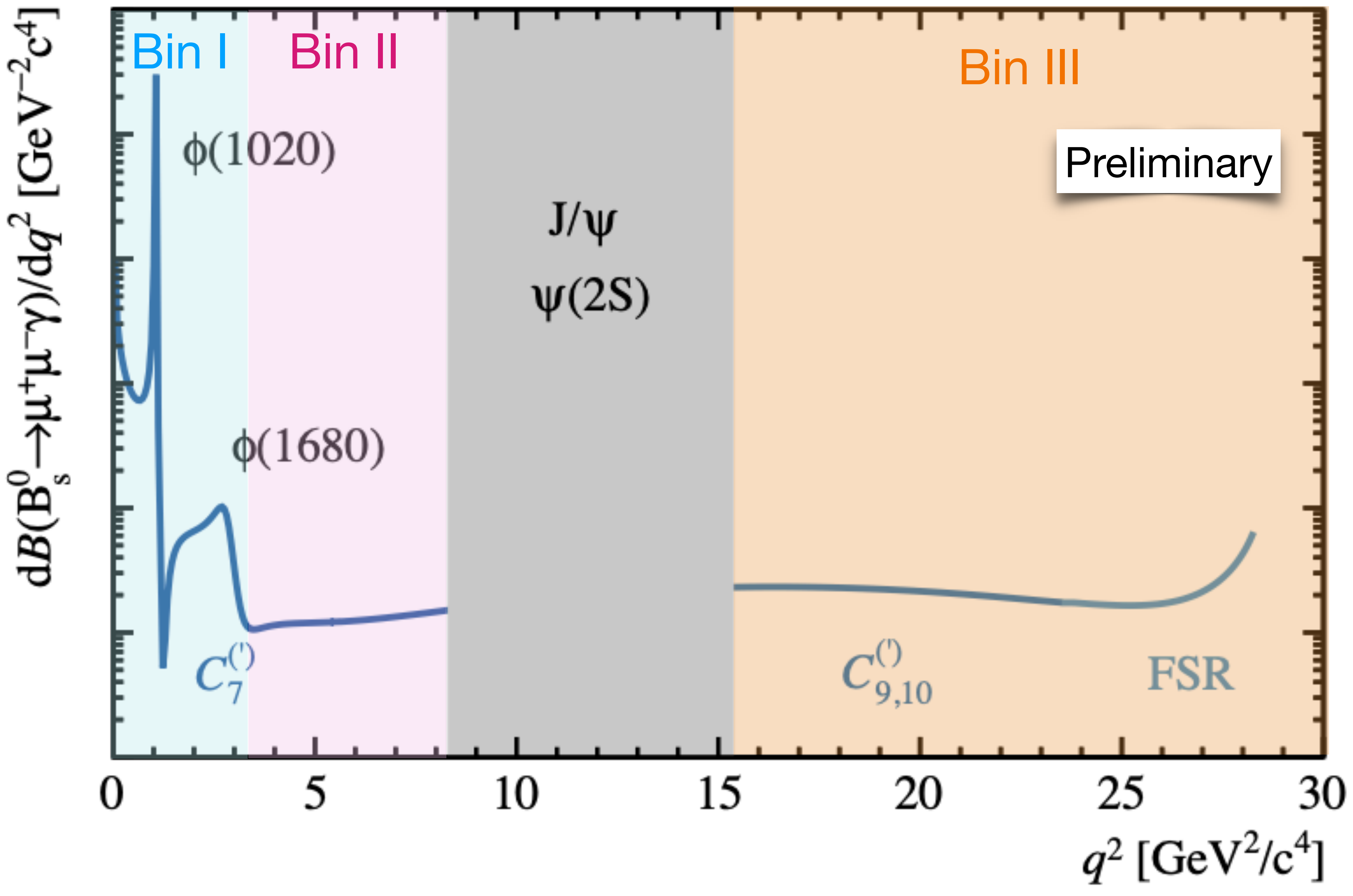

Phys.Rev.**D70**(2004)114028

CERN-THESIS-2020-303

FSR = final state radiation

Additionally, Bin I is also studied with a veto on the ϕ-resonance mass:

$m(\mu^+\mu^-) = [989.6, 1073.4]$MeV/c²

Bin I ϕ-veto: low-q^2 without ϕ region

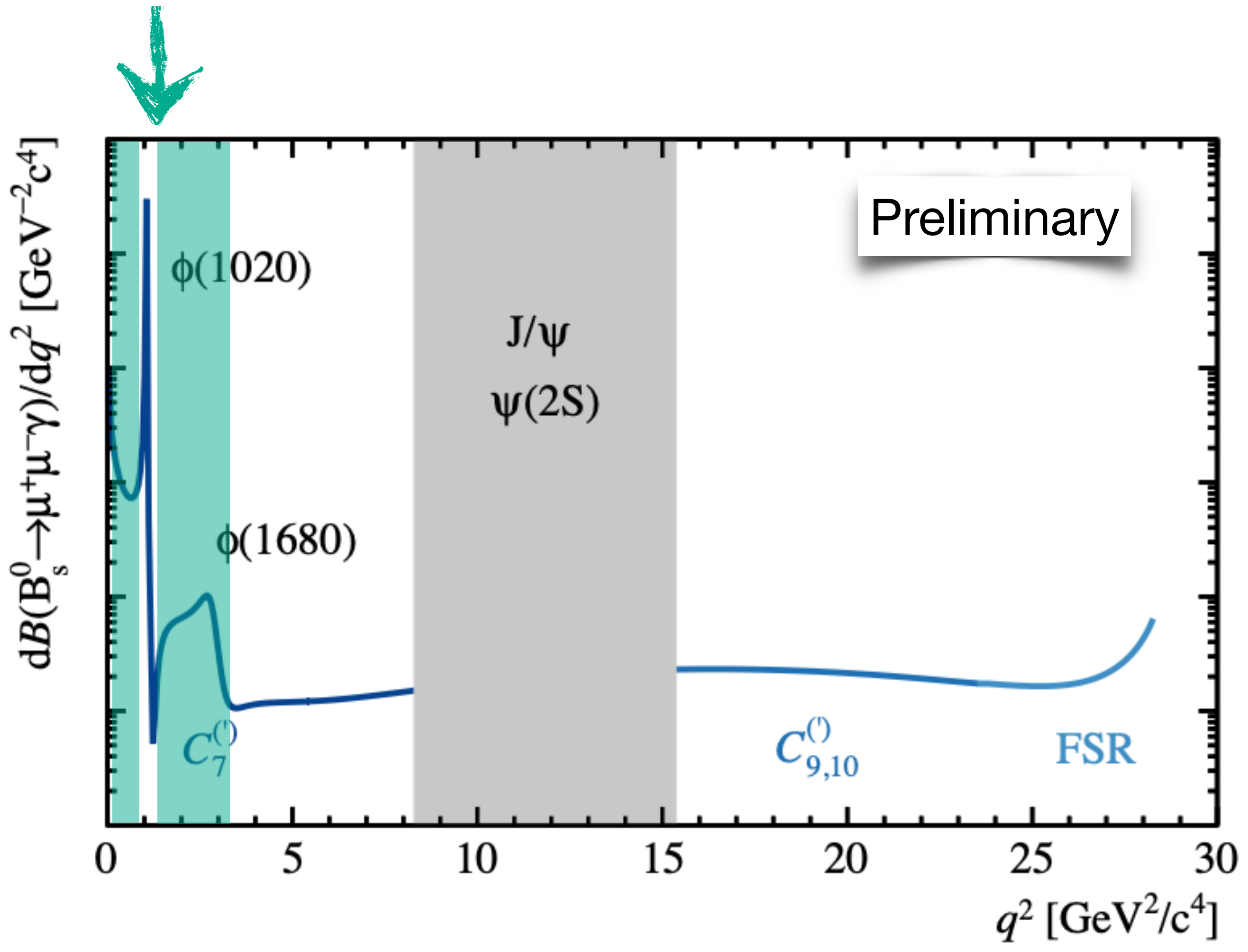

q^2 bin	I	II	III
q^2 [GeV$^2/c^4$]	$[4\,m_\mu^2, 2.89]$	$[2.89, 8.29]$	$[15.37, m_{B_s^0}^2]$
$m(\mu^+\mu^-)$ [GeV$/c^2$]	$[2\,m_\mu, 1.70]$	$[1.70, 2.88]$	$[3.92, m_{B_s^0}]$
$10^{10}\times\mathcal{B}(B_s^0\to\mu^+\mu^-\gamma)$ [8]	82 ± 15	2.54 ± 0.34	9.1 ± 1.1
Fraction of $B_s^0\to\mu^+\mu^-\gamma$	87%	2.7%	9.8%

$B_s^0 \to \mu^+\mu^-\gamma$

LHCb-PAPER-2023-045
In preparation

Control channel:

- To check the agreement between data and simulation.
- Similar kinematics: three body decay and low-p_T photons
- Chosen channel: $B_s^0 \to \phi(\to K^+K^-)\,\gamma$

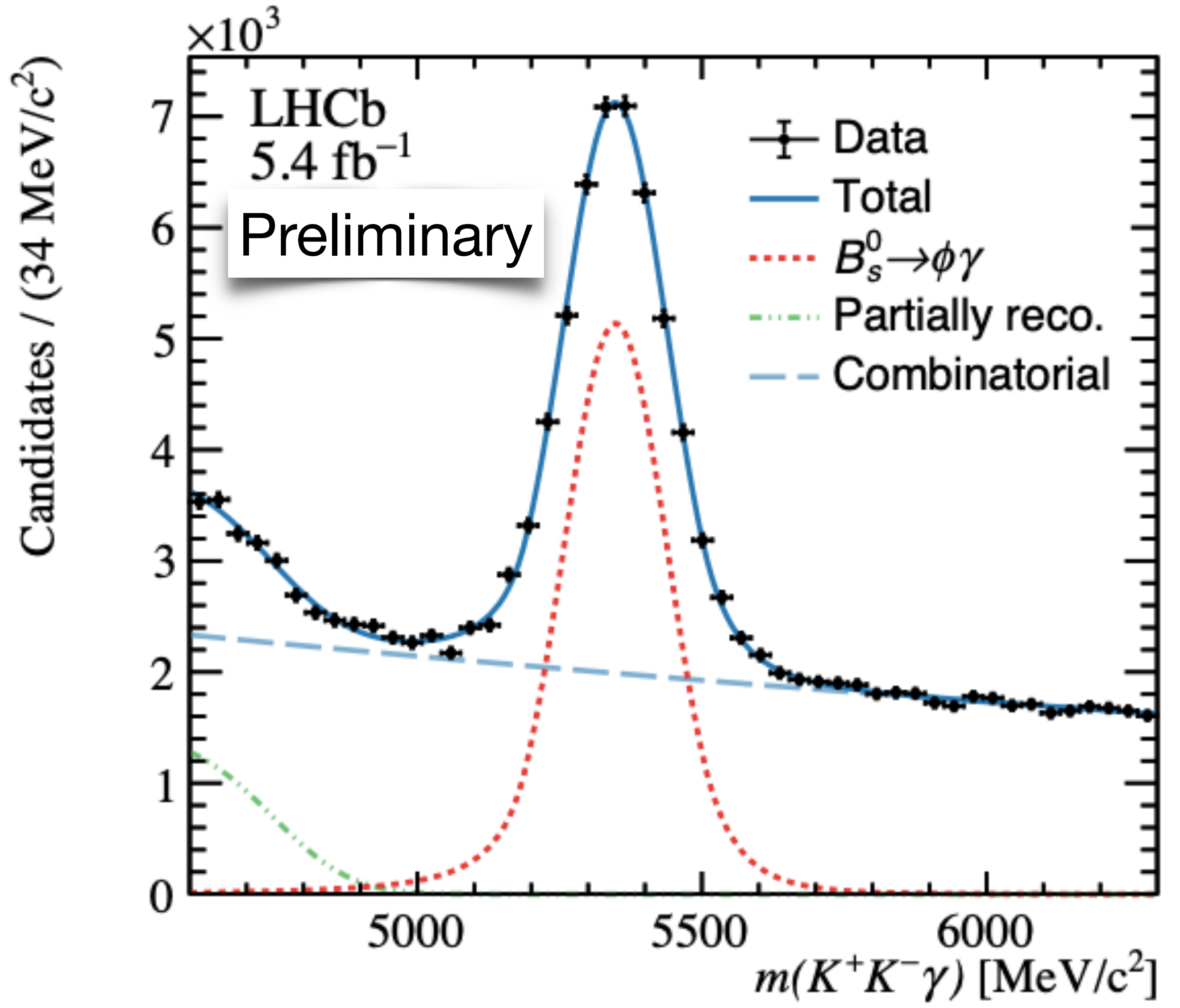

Normalisation channel:

- A well know decay channel
- High statistics.
- Similar final state to the signal: allows uncertainties cancelations.
- Chosen channel: $B_s^0 \to J/\psi(\to \mu^+\mu^-)\,\eta(\to \gamma\gamma)$

$$\mathcal{B}(B_s^0 \to \mu^+\mu^-\gamma) = \frac{\mathcal{B}_{\text{norm}}}{N_{\text{norm}}} \times \frac{\epsilon_{\text{norm}}}{\epsilon_{\text{sig}}} \times N_{\text{sig}}$$

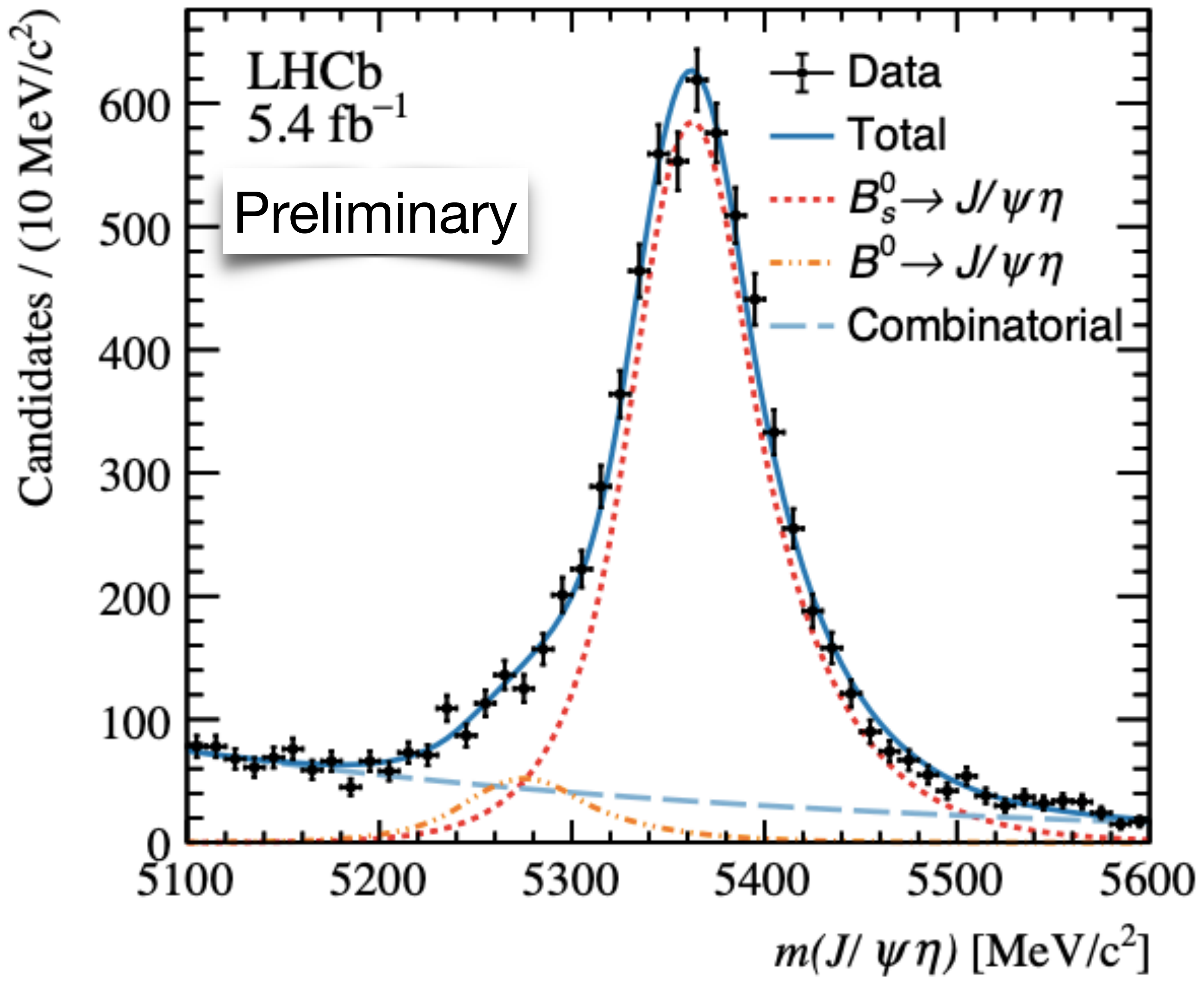

$B_s^0 \to \mu^+\mu^-\gamma$

LHCb-PAPER-2023-045
In preparation

Final fits

The measured $\mathscr{B}(B_s^0 \to \mu^+\mu^-\gamma)$ is not statistically significant in any of the q² regions.

They are consistent with the background-only hypothesis at < 1σ level.

Preliminary

$$
\begin{aligned}
\mathcal{B}(B_s^0 \to \mu^+\mu^-\gamma)_{\rm I} &= (1.34 \pm 1.60 \pm 0.28) \times 10^{-8}, \\
\mathcal{B}(B_s^0 \to \mu^+\mu^-\gamma)_{\rm II} &= (0.76 \pm 3.55 \pm 0.30) \times 10^{-8}, \\
\mathcal{B}(B_s^0 \to \mu^+\mu^-\gamma)_{\rm III} &= (-2.55 \pm 2.25 \pm 0.41) \times 10^{-8}, \\
\mathcal{B}(B_s^0 \to \mu^+\mu^-\gamma)_{\rm I,\ \phi\ veto} &= (0.72 \pm 1.56 \pm 0.29) \times 10^{-8}.
\end{aligned}
$$

stat.±syst.

Dominated by statistical uncertainty.

Candidates mass distribution fit, for each q² region:

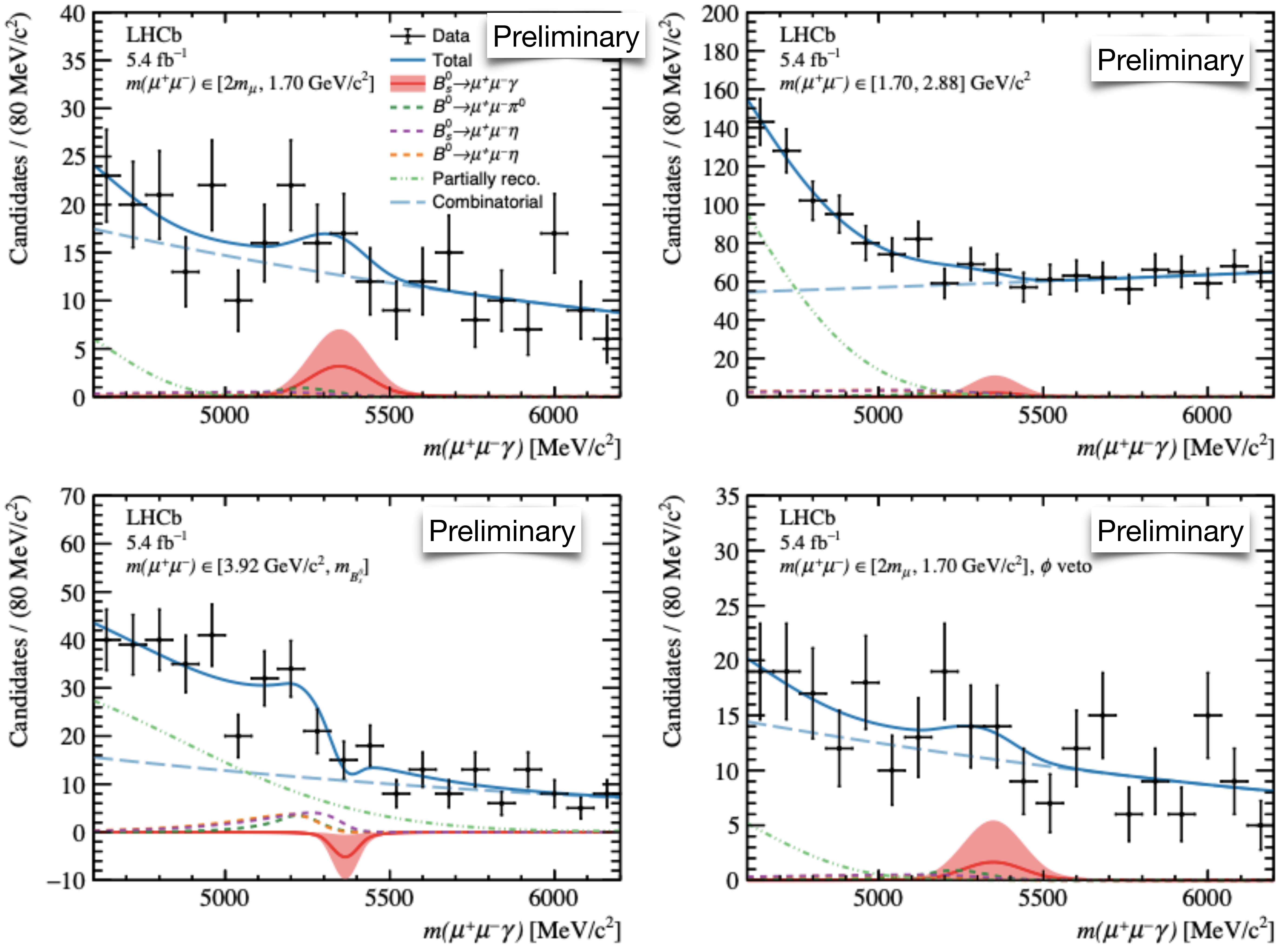

$B_s^0 \to \mu^+\mu^-\gamma$

LHCb-PAPER-2023-045
In preparation

Limits

As no significant excess is observed, upper limits are set on $\mathscr{B}(B_s^0 \to \mu^+\mu^-\gamma)$ using the CLs method.

Upper limits on the branching fraction:

Preliminary

$$\mathcal{B}(B_s^0 \to \mu^+\mu^-\gamma)_{\rm I} < 3.6\,(4.2) \times 10^{-8},$$
$$\mathcal{B}(B_s^0 \to \mu^+\mu^-\gamma)_{\rm II} < 6.5\,(7.7) \times 10^{-8},$$
$$\mathcal{B}(B_s^0 \to \mu^+\mu^-\gamma)_{\rm III} < 3.4\,(4.2) \times 10^{-8},$$
$$\mathcal{B}(B_s^0 \to \mu^+\mu^-\gamma)_{\rm I,\,\phi\ veto} < 2.9\,(3.4) \times 10^{-8},$$
$$\mathcal{B}(B_s^0 \to \mu^+\mu^-\gamma)_{\rm comb.} < 2.5\,(2.8) \times 10^{-8},$$

at 90% (95%) CL.

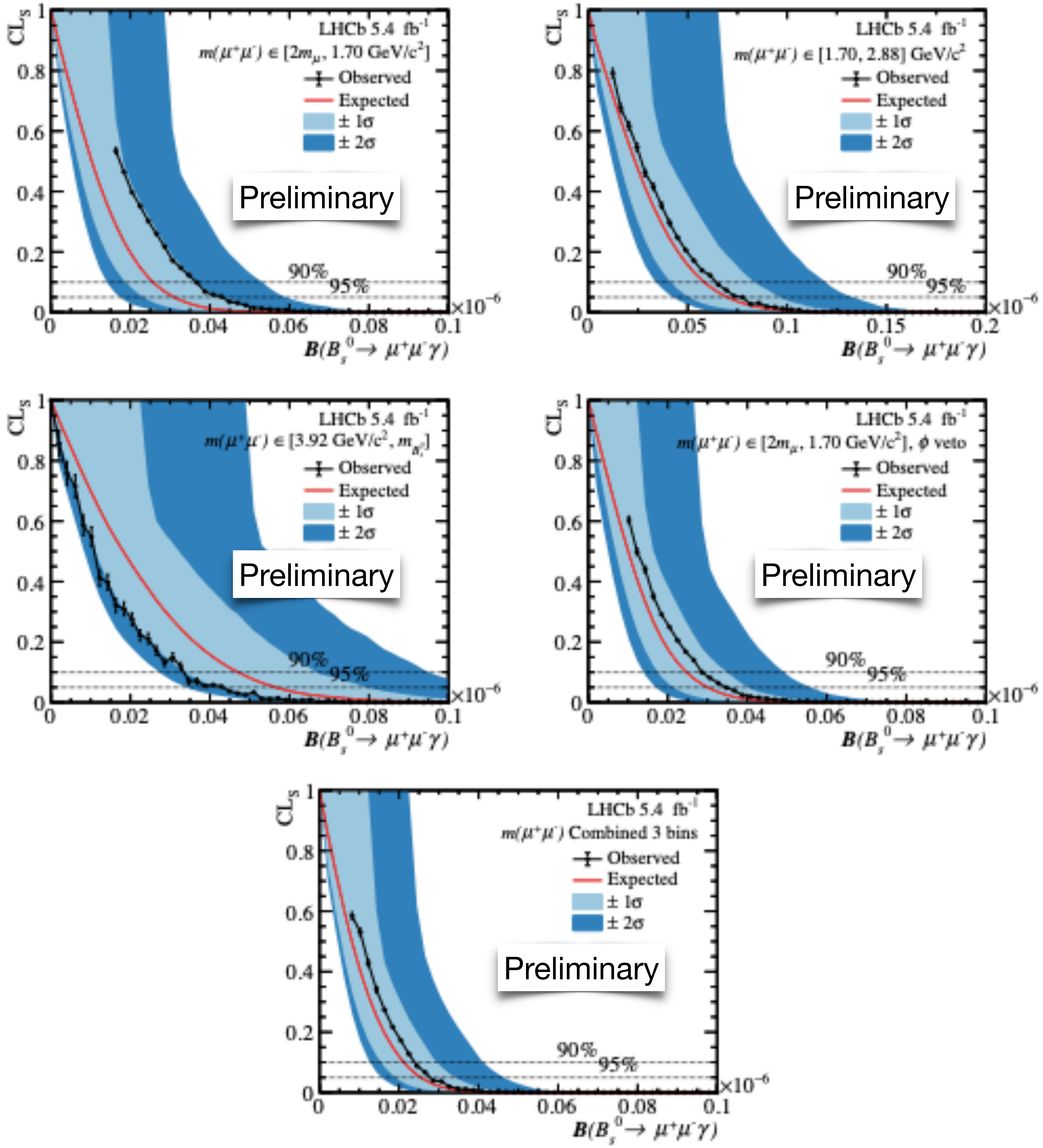

First direct search of $B_s^0 \to \mu^+\mu^-\gamma$, and first search at low q².

$B_s^0 \to \mu^+\mu^-\gamma$

Experimental upper limits in the theoretical context:

- Different approaches to $B_s^0 \to \gamma$ FF's calculation:
  - Different estimates of the $\mathscr{B}$.
- Experimental results are dominated by stat. uncertainties:
  - Run 3 data might be sensitive to different models.
- Indirect method reaches lower ULs.
  - Direct method is sensitive to the full q² spectrum.

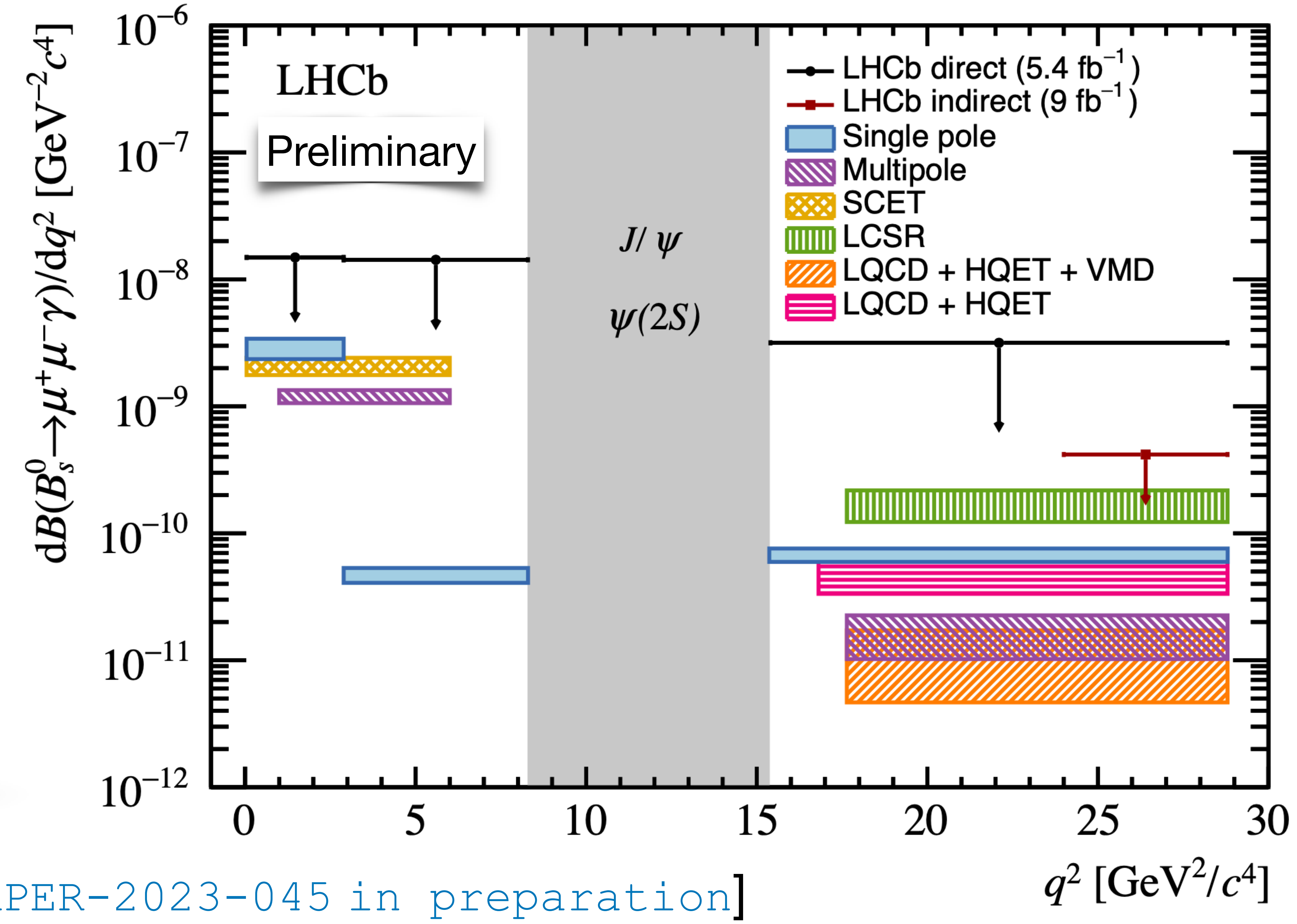

- Direct search $B_s^0 \to \mu^+\mu^-\gamma$, these results, at 95% CL. [LHCb-PAPER-2023-045 in preparation]
- Indirect search from $B_s^0 \to \mu^+\mu^-$ decay at LHCb, limit at 95% CL [Phys.Rev.D105(2022)1]
- Single-pole parametrisation [JHEP11(2017)184]
- Multipole parametrisation [Phys.Rev.D97(2018)053007]
- Soft-collinear effective theory [JHEP148(2020)12]
- Light-cone sum rules [JHEP8(2021)12]
- Lattice QCD with heavy quark effective theory, assuming vector meson dominance [JHEP10(2023)102, JHEP7(2023)112]
- Lattice QCD with heavy quark effective theory extrapolation [arXiv:2402.03262]

Measurement of the D^* longitudinal polarisation in $B^0 \to D^{*-}\tau^+\nu_\tau$ decays

LHCb-PAPER-2023-020
arXiv 2311.05224

$B^0 \to D^{*-}\tau^+\nu_\tau$

LHCb-PAPER-2023-020
arXiv 2311.05224

The studies of the kinematic and angular distributions, such as the **longitudinal D^* polarisation fraction ($F_L^{D^*}$)**, are sensitive to possible NP scenarios

[Phys.Rev.D85(2012)094025, Phys.Rev.D94(2016)094028]:

- Enhanced by new scalar operators
- Suppressed by new tensor operators

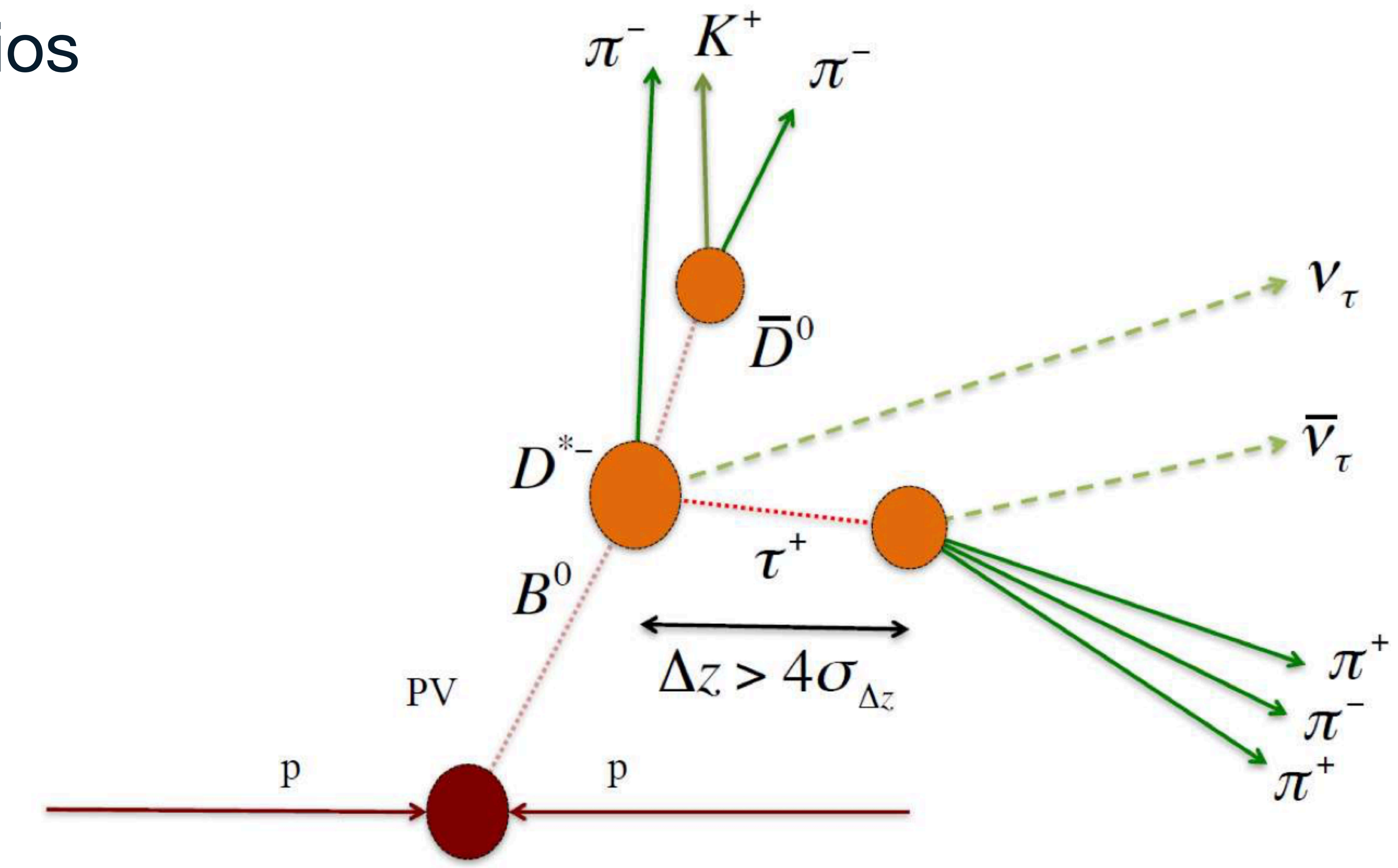

The only measurement, by Belle:

$$F_L^{D^*} = 0.60 \pm 0.08 \pm 0.04$$ [arXiv.1903.03102]

SM predictions:

$$F_L^{D^*} = 0.441 \pm 0.006$$ [Phys.Rev.D98(2018)095018]

$$F_L^{D^*} = 0.457 \pm 0.010$$ [Eur.Phys.J.C79(2019)]

$$F_L^{D^*} = 0.467 \pm 0.009$$ [Eur.Phys.J.C80(2020)]

$$F_L^{D^*} = 0.422 \pm 0.010$$ [arXiv.2310.03680]

Signal simulation: weights are assigned to the events such that the decay kinematics follow the CLN parametrisation of the form factors.

Nuc.Phys.**B530**(1998)153-181

$B^0 \to D^{*-}\tau^+\nu_\tau$

LHCb-PAPER-2023-020
arXiv 2311.05224

Angular distribution

The $a_{\theta_D}(q^2)$ and $c_{\theta_D}(q^2)$ coefficients encapsulate the hadronic effects and the couplings.

arXiv:1907.02257

$$\frac{d^2\Gamma}{dq^2 d\cos\theta_D} = a_{\theta_D}(q^2) + c_{\theta_D}(q^2)\cos^2\theta_D$$

Simulation distributions in two q² regions:

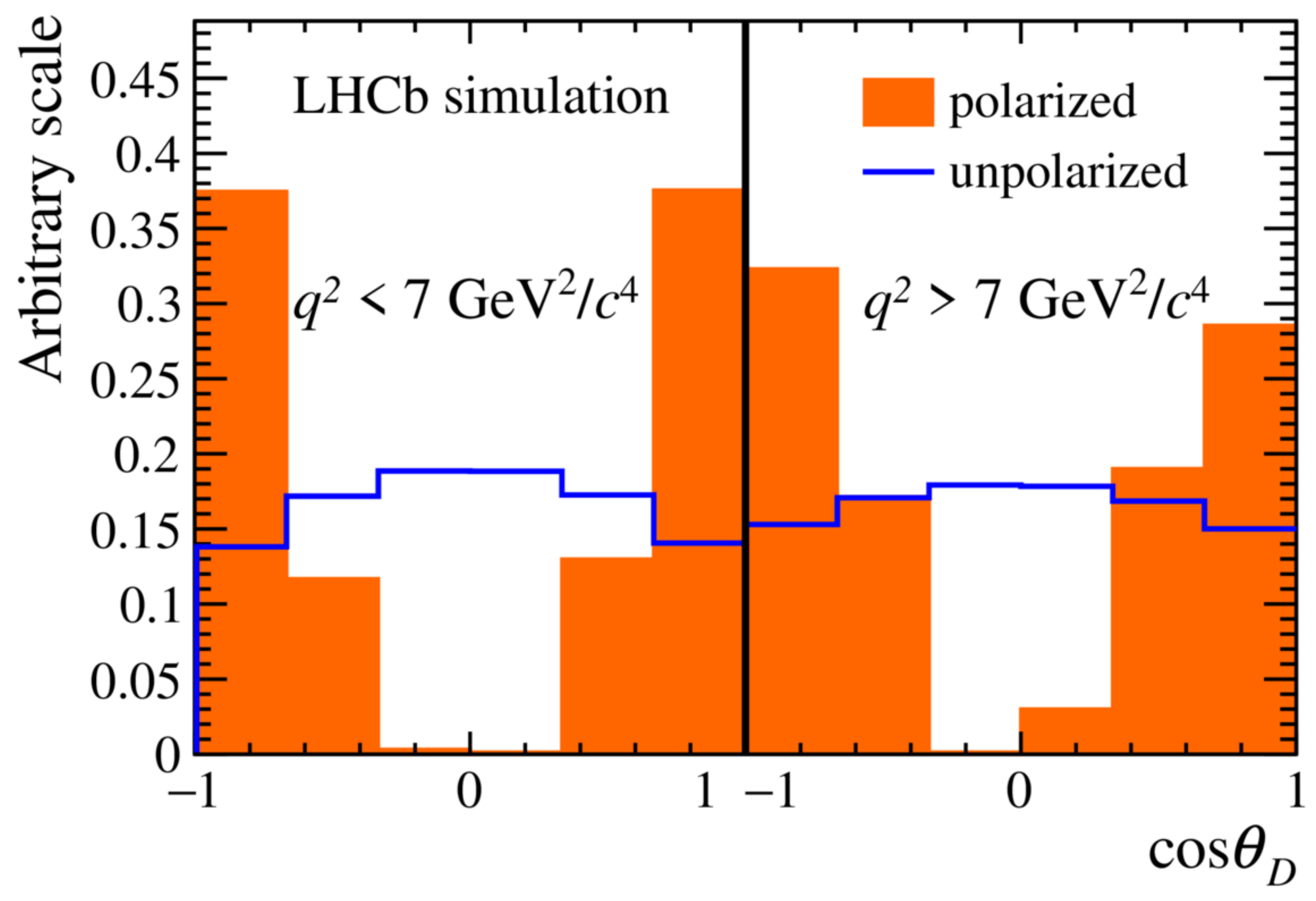

The $F_L^{D^*}$ is calculated from the $a_{\theta_D}(q^2)$ and $c_{\theta_D}(q^2)$ parameters extracted from a binned maximum-likelihood fit to data. The fit uses four-dimensional templates in terms of:

$$F_L^{D^*} = \frac{a_{\theta_D}(q^2) + c_{\theta_D}(q^2)}{3a_{\theta_D}(q^2) + c_{\theta_D}(q^2)}$$

- $\cos\theta_D$ and q^2.
- t_τ: decay-time of the τ lepton, taking into account the corrections due to the missing neutrino.
- Anti-D_s^+ BDT output: BDT response, trained to suppress the
  - background due to the $B \to D^{*-}D_s^0(X)$ decay.

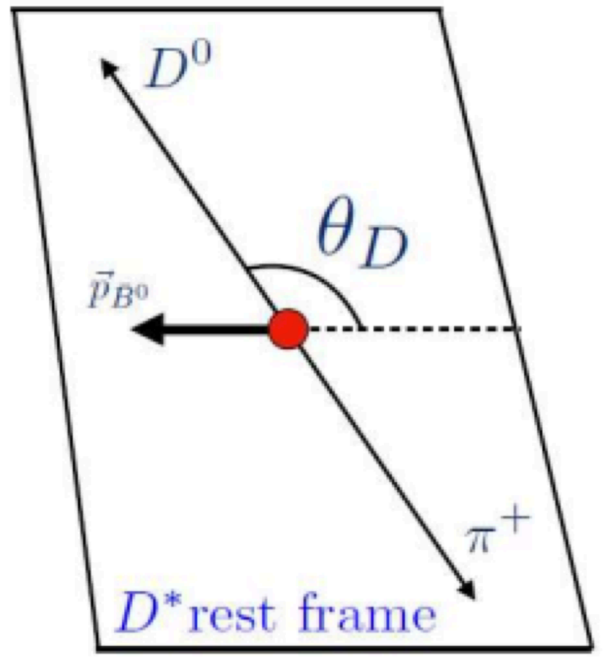

$B^0 \to D^{*-}\tau^+\nu_\tau$

LHCb-PAPER-2023-020
arXiv 2311.05224

Final results

$F_L^{D*} = 0.51 \pm 0.07 \pm 0.03$ at $q^2 < 7\ \mathrm{GeV}^2/c^4$

$F_L^{D*} = 0.35 \pm 0.08 \pm 0.02$ at $q^2 > 7\ \mathrm{GeV}^2/c^4$

The average value over the whole q² range is:

$F_L^{D*} = 0.43 \pm 0.06 \pm 0.03$

First measurement of the longitudinal D^* polarisation fraction by LHCb.

Compatible with Belle measurement and with each the SM prediction (slide 27). As well as with the SM prediction per q^2 region: G.Martinelli, S.Simula, L.Vittorio [arXiv.2310.03680]

$F_L^{D*} = 0.495 \pm 0.017$ at $q^2 < 7\ \mathrm{GeV}^2/c^4$

$F_L^{D*} = 0.383 \pm 0.006$ at $q^2 > 7\ \mathrm{GeV}^2/c^4$

Fit variables in Run 1 and Run 2:

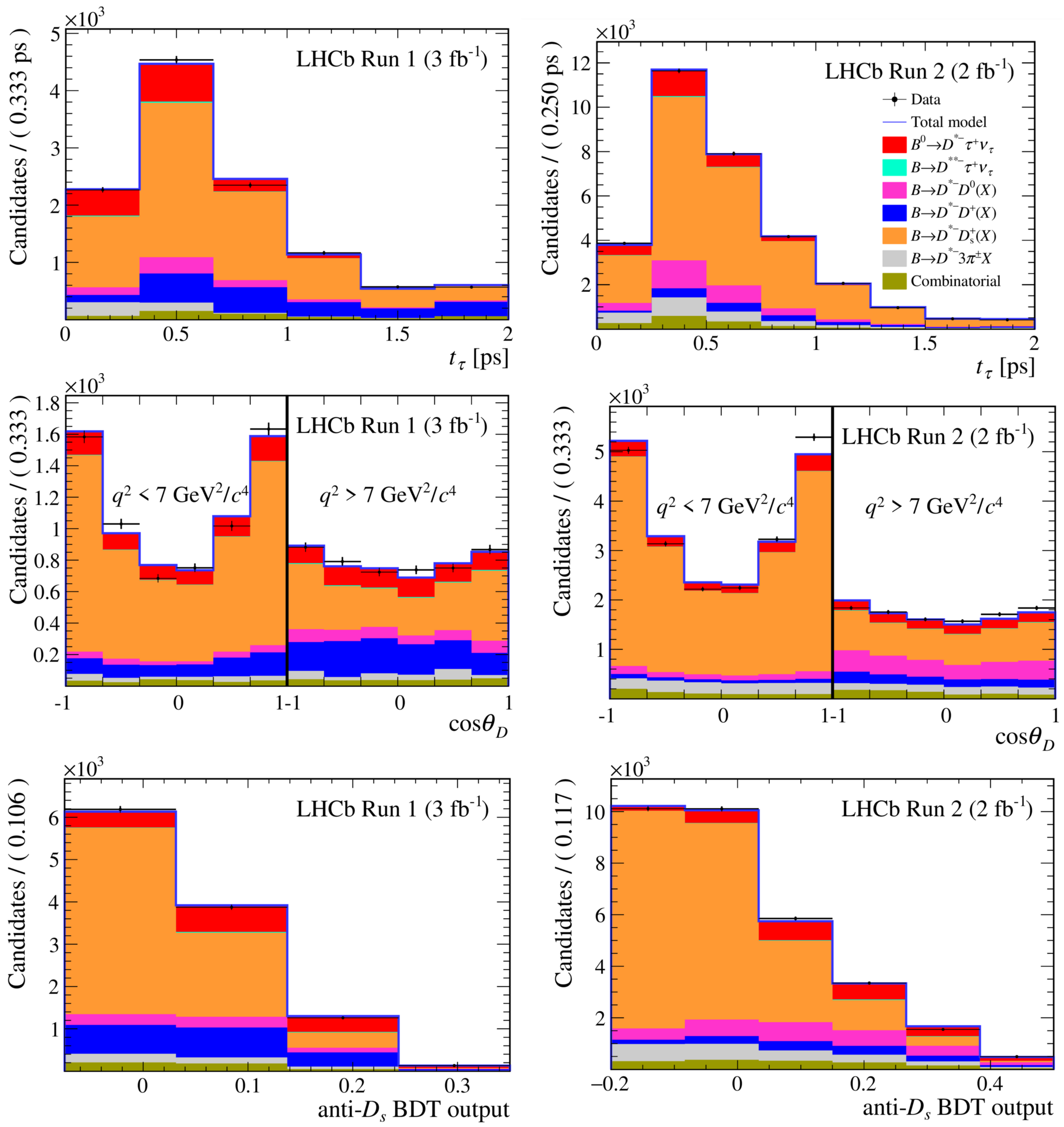

Conclusions

- **Rare** and **semileptonic** *b*-hadron decays are excellent opportunities to check the SM and look for NP.

- **LHCb** is the optimal detector to study *b*-hadron decays. Latest results:

  - $B^0 \to K^{*0}\mu^+\mu^-$ new analysis method to determine hadronic contributions. — LHCb-PAPER-2023-033, arXiv 2312.09115
  - $\mathcal{B}(\phi \to \mu^+\mu^-)/\mathcal{B}(\phi \to e^+e^-)$ first LFU control mode at low q^2. — LHCb-PAPER-2023-038, arXiv 2402.01336
  - $\Lambda_b^0 \to pK^-\gamma$ first amplitude analysis, based on the helicity formalism. — LHCb-PAPER-2023-036, In preparation
  - $B_s^0 \to \mu^+\mu^-\gamma$ first direct search, and first low q^2 search. — LHCb-PAPER-2023-045, In preparation
  - $B^0 \to D^{*-}\tau^+\nu_\tau$ first measurement of D* polarisation by LHCb. — LHCb-PAPER-2023-020, arXiv 2311.05224

Backup

$B^0 \to K^{*0}\mu^+\mu^-$

LHCb-PAPER-2023-033
arXiv 2312.09115

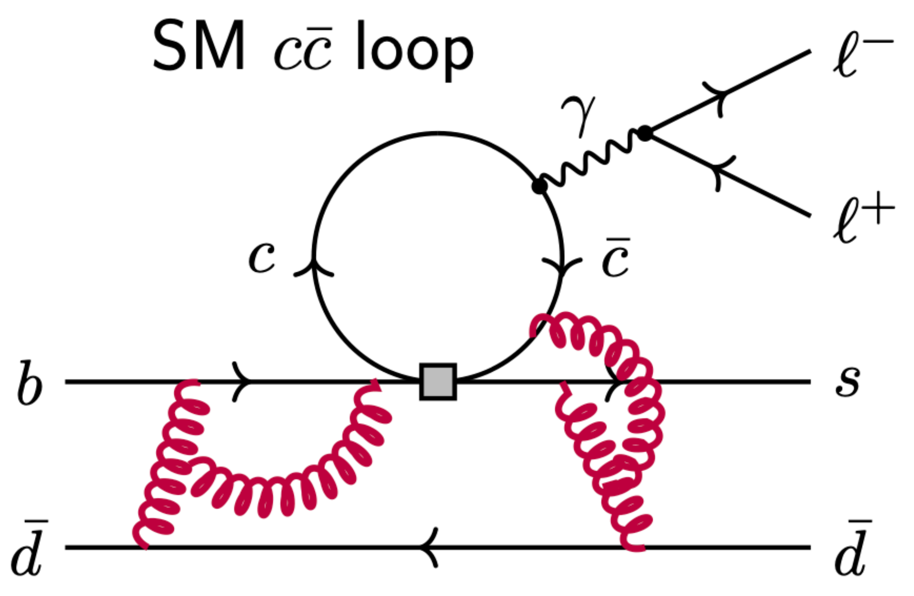

Long-distance hadronic contribution **"charm-loop"** : difficult to calculate reliably from first principles. It can mimic NP.

$$\mathcal{C}_9^{\text{eff}} = \mathcal{C}_9^{\text{SM}} + \mathcal{C}_9^{c\bar{c}}$$

Add information to constrain charm-loop parameters:

Experimental measurements on $B^0 \to \psi_n K^{*0}$

$$\underset{q^2 \to M^2_{\psi_n}}{\text{Res}} \frac{\mathcal{H}_\lambda(q^2)}{\mathcal{F}_\lambda(q^2)} = \frac{M_{\psi_n} f^*_{\psi_n} \mathcal{A}_\lambda^{\psi_n}}{M_B^2 \, \mathcal{F}_\lambda(M^2_{\psi_n})}$$

[BCvDV 2018]

Theory predictions at q² < 0, reliable for q² << 3m$_c$²

[GRvDV 2022]

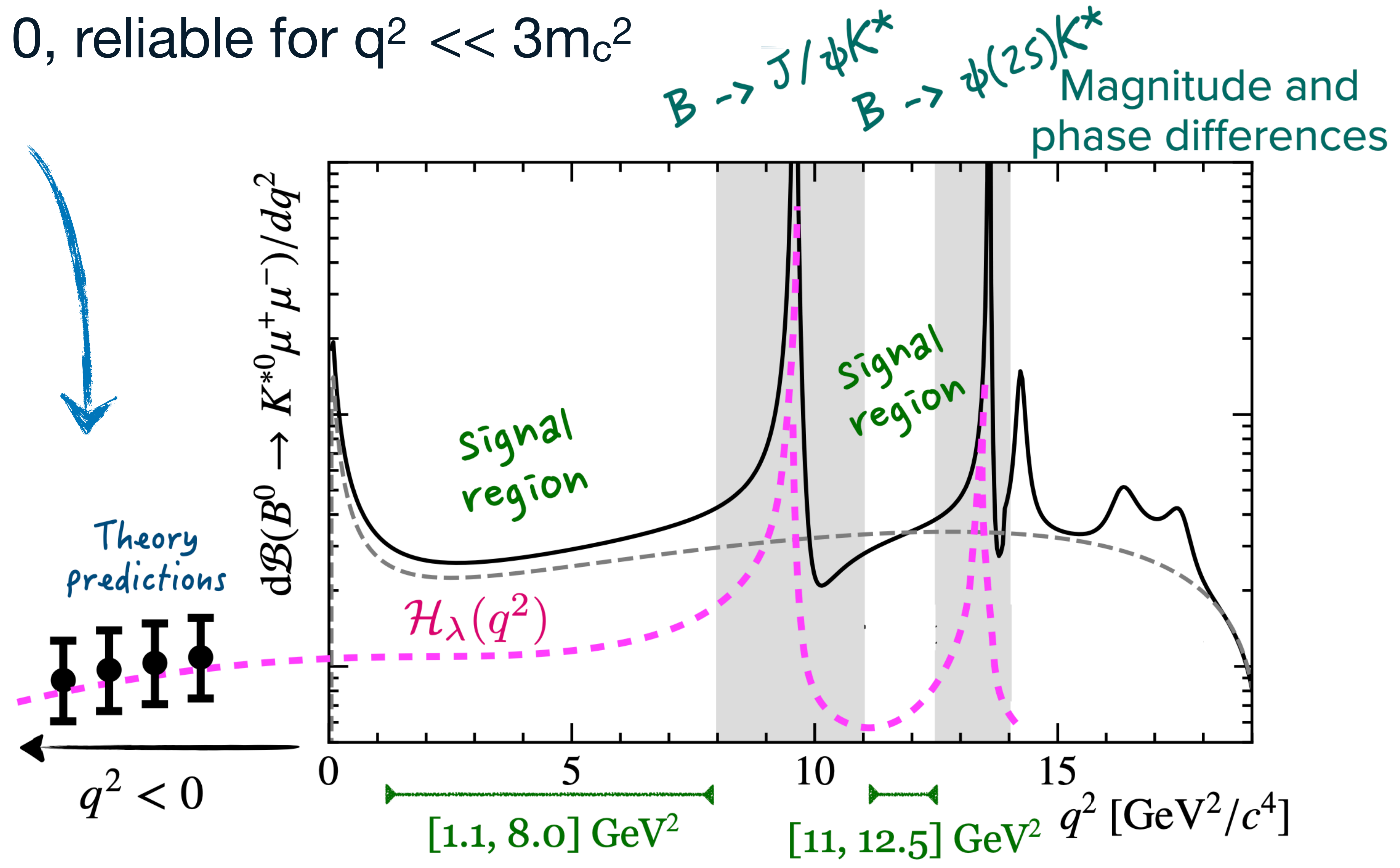

[PRD76(2007)031102]
[PRD88(2013)074026]
[PRD90(2014)112009]
[PRD88(2013)052002]
[EPJC72(2012)2118]

$B^0 \to K^{*0}\mu^+\mu^-$

LHCb-PAPER-2023-033
arXiv 2312.09115

Systematics due to the amplitude model

Largest systematic for $\mathcal{C}_9$, $\mathcal{C}_{10}$ comes from BR external inputs

Systematics related to exp. effects are in common with binned BR/angular analyses

Total syst. negligible w.r.t. statistical uncertainty

	$\mathcal{C}_9$	$\mathcal{C}_{10}$	$\mathcal{C}'_9$	$\mathcal{C}'_{10}$
Amplitude model				
S-wave form factors	< 0.01	< 0.01	< 0.01	< 0.01
S-wave non-local hadronic	0.02	0.02	0.14	0.04
S-wave k^2 model	< 0.01	< 0.01	0.05	0.03
Subtotal	0.02	0.02	0.15	0.05
External inputs on BR				
$\mathcal{B}(B^0 \to J/\psi K^+\pi^-)$	0.05	0.08	0.02	0.01
$f^{B^0\to J/\psi K\pi}_{\pm 100\text{MeV}}$	0.03	0.03	0.01	< 0.01
Others (R_ε)	0.03	0.04	0.03	0.01
Subtotal	0.07	0.09	0.04	0.01
Background model				
Chebyshev polynomial order	0.01	0.01	0.01	< 0.01
Combinatorial shape in k^2	0.02	< 0.01	0.02	< 0.01
Background factorisation	0.01	0.01	0.01	0.01
Peaking background	0.01	< 0.01	0.02	0.01
Subtotal	0.03	0.02	0.03	0.01
Experimental effects				
Acceptance parametrisation	< 0.01	< 0.01	< 0.01	< 0.01
Statistical uncertainty on acceptance	0.02	< 0.01	0.02	< 0.01
Subtotal	0.02	< 0.01	0.02	< 0.01
Total systematic uncertainty	0.08	0.10	0.16	0.05
Statistical uncertainty ($q^2 < 0$ constr.)	0.40	0.28	0.40	0.24

$B^0 \to K^{*0}\mu^+\mu^-$

LHCb-PAPER-2023-033
arXiv 2312.09115

Fit projections: 2568 ± 60 signal decays

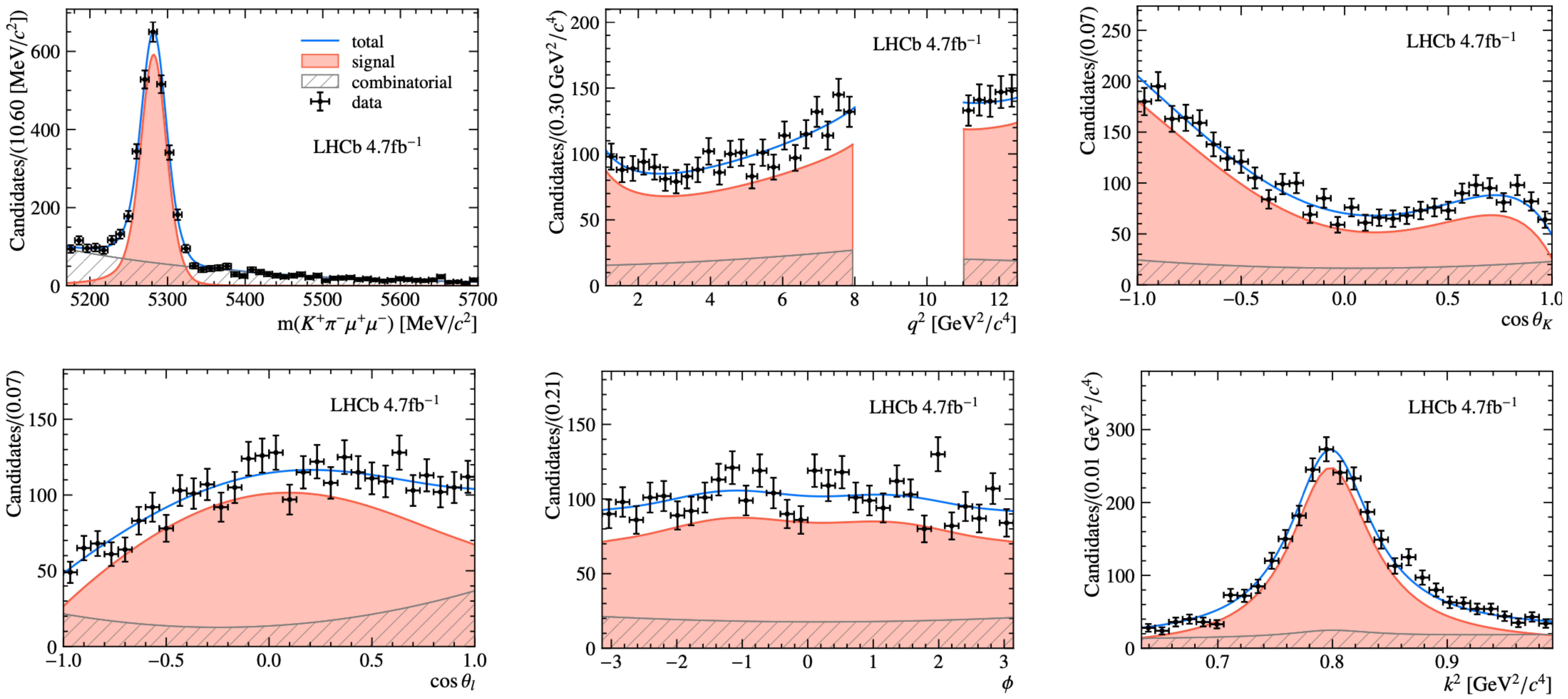

$B^0 \to K^{*0}\mu^+\mu^-$

LHCb-PAPER-2023-033
arXiv 2312.09115

Decay rate:

- K^{*0} meson has spin-1 (P-wave)
  - reconstructed through $K^{*0} \to K^+\pi^-$
  - 3 polarisations: $\lambda = \perp, \parallel, 0$
    ↳ rich angular structure

$\vec{\Omega} = \{\cos\theta_K, \cos\theta_\ell, \phi\}$

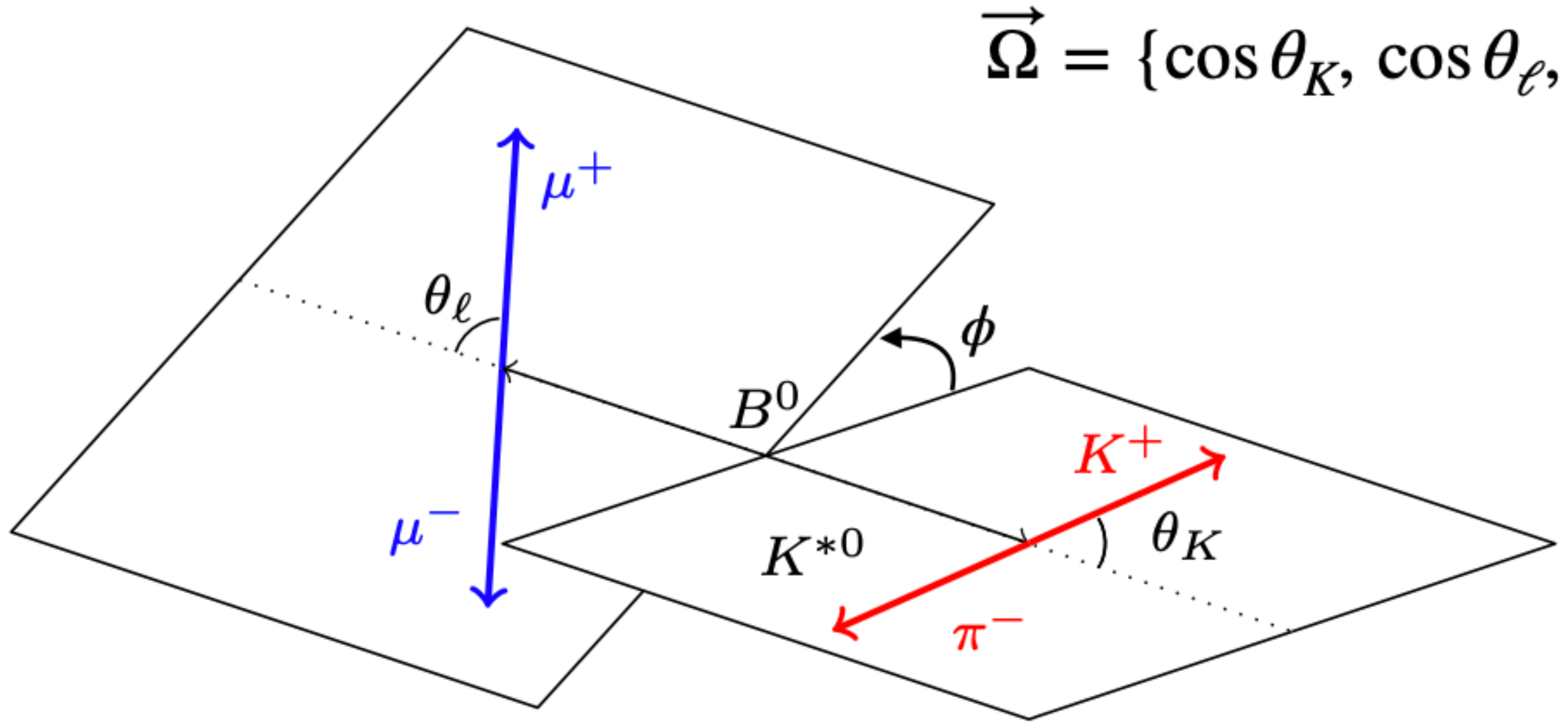

$$\frac{\mathrm{d}^5\Gamma[B^0 \to K^{*0}\mu^+\mu^-]}{\mathrm{d}q^2\,\mathrm{d}k^2\,\mathrm{d}\vec{\Omega}} = \frac{9}{32\pi}\sum_i I_i(q^2,k^2) f_i(\vec{\Omega})$$

Angular coeffs   Angular terms (11)

bilinear combination of decay amplitudes [*] ↓

$$I_i \propto (\mathcal{A}_{\lambda_1}\mathcal{A}^*_{\lambda_2})$$

difference w.r.t. binned approach ⟷

$$< S_i >= \frac{\int_a^b I_i(q^2)\mathrm{d}q^2}{\int_a^b \frac{\mathrm{d}\Gamma}{\mathrm{d}q^2}\mathrm{d}q^2}$$

$\mathcal{B}(\phi \to \mu^+\mu^-)/\mathcal{B}(\phi \to e^+e^-)$

LHCb-PAPER-2023-038
arXiv 2402.01336

Tight cuts around the D^+ mass at trigger level

$\Downarrow$

Variations of effs. as a function of the ϕ-constrained D^+ mass

$\Downarrow$

Backgrounds shapes get warped in *el.* channel

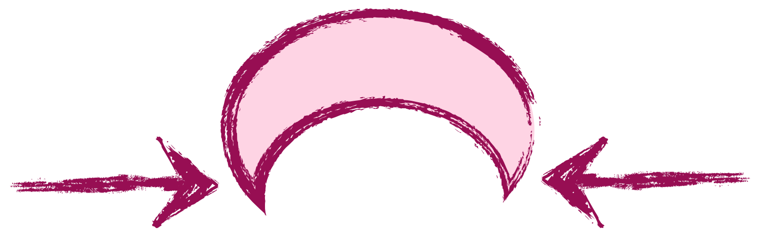

$\Downarrow$

Validations of the shapes in control samples

Combinatorial background modelled with a third order Chebychev polynomial. Control channel:

- of candidates with leptons of same charge
- where BDT classifier requirement is inverted

Reconstructed ϕ-constrained D-mass:

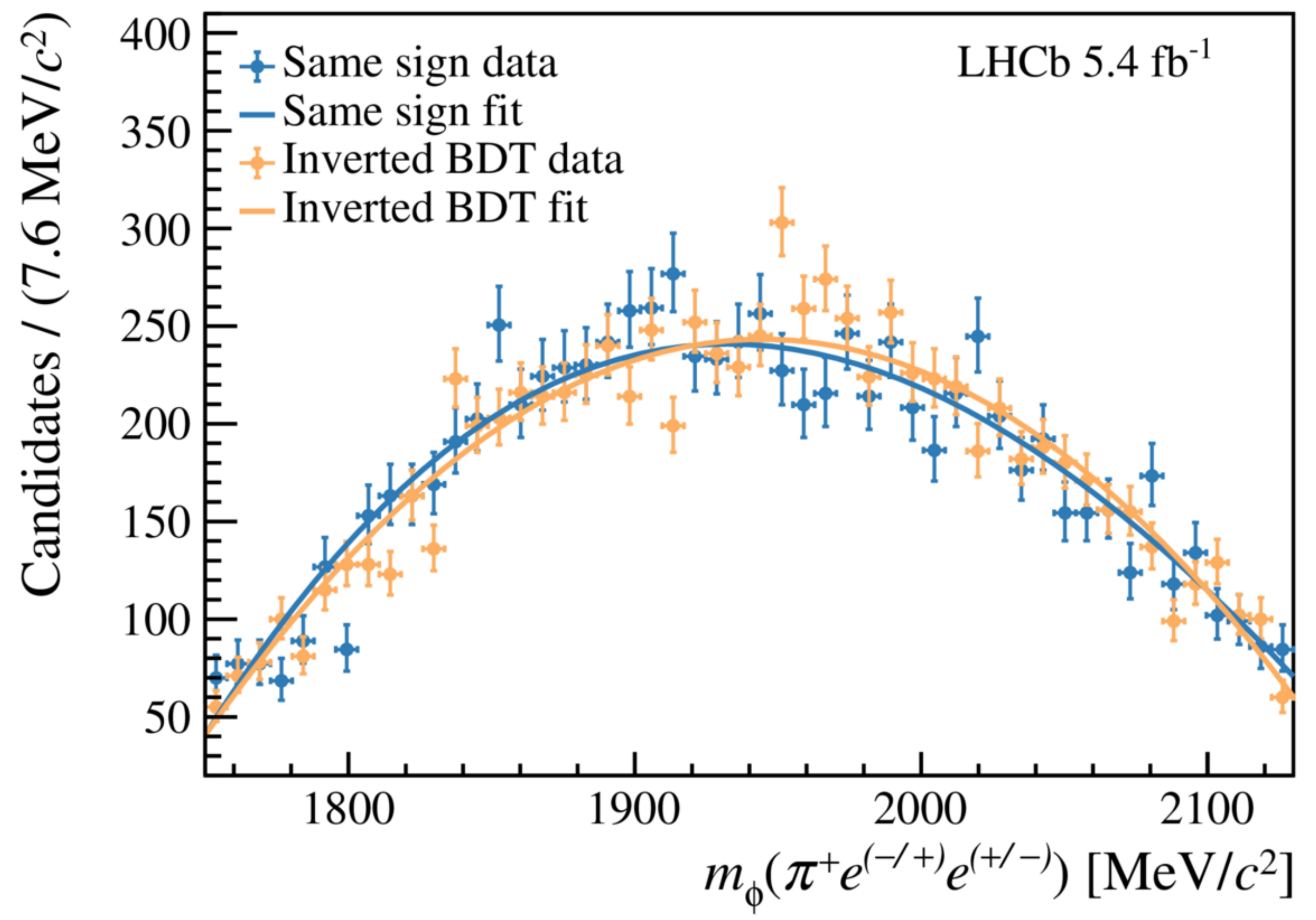

Dominant peaking background is $D^+_{(s)} \to \pi^+\pi^-\pi^+$ with two misID pions. Size and shape are obtained by reversing the electron identification requirements in data.

Reconstructed $D^+_{(s)}$ mass bkg.:

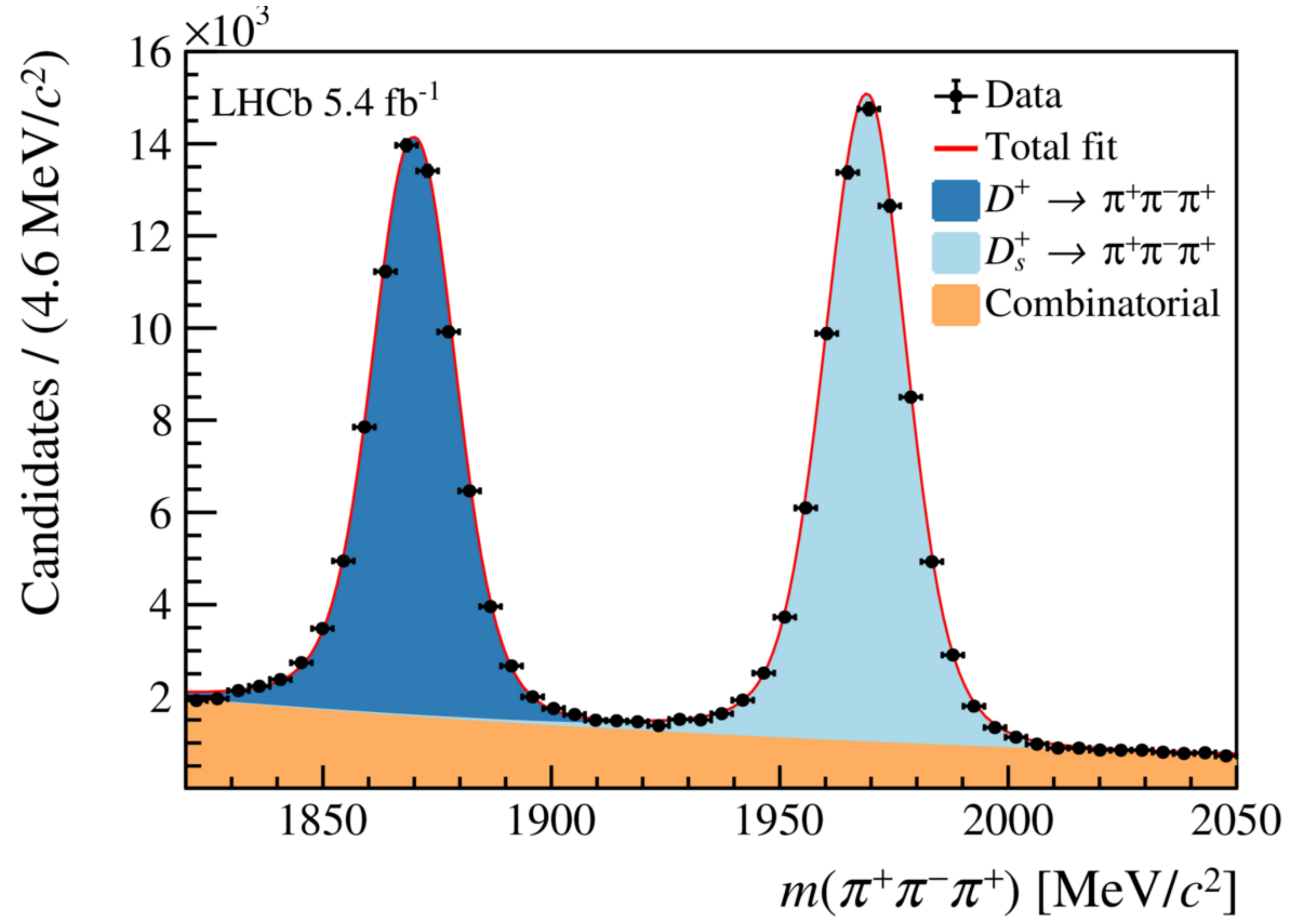

$\mathcal{B}(\phi \to \mu^+\mu^-)/\mathcal{B}(\phi \to e^+e^-)$

LHCb-PAPER-2023-038
arXiv 2402.01336

Alternative procedure to the **estimation of the doubly misID bkg.** :

The expected $D^+_{(s)} \to \pi^+\pi^-\pi^+$ contamination is obtained from a fit to the $\pi^+\pi^-\pi^+$ invariant-mass distribution for signal candidates selected in the signal PID region, such that no translation across PID regions is needed.

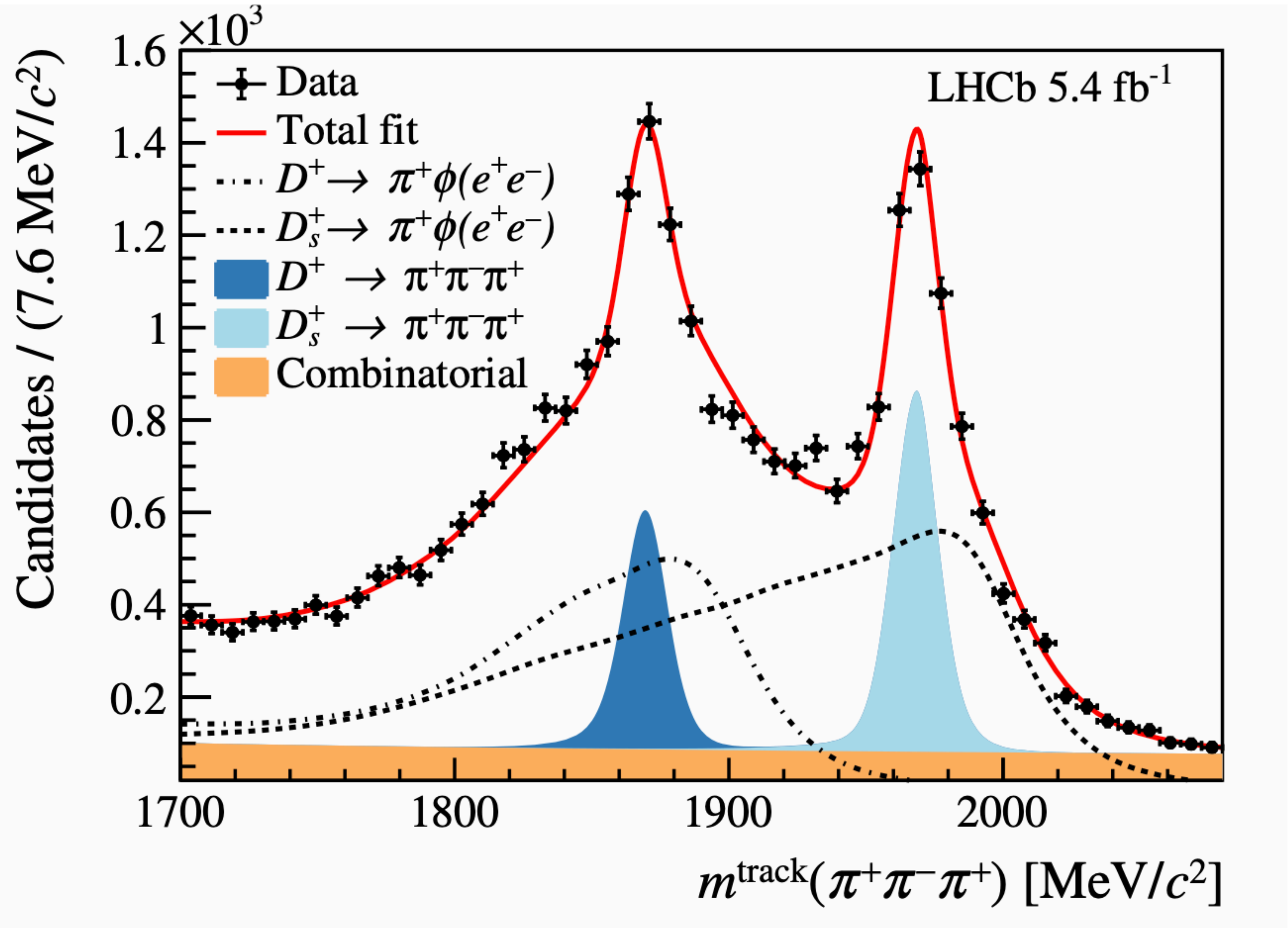

The difference between this and the nominal result is taken as a systematic uncertainty.

$\mathcal{B}(\phi \to \mu^+\mu^-)/\mathcal{B}(\phi \to e^+e^-)$

LHCb-PAPER-2023-038
arXiv 2402.01336

Ratio of efficiency-corrected $D^+_{(s)} \to \pi^+\phi$ and $B^+ \to K^+J/\psi(\to e^+e^-)$ yields as a function of the (left) transverse momentum recovered with the bremmstrahlung recovery algorithm and (right) its fraction with respect to the total transverse momentum of the electron.

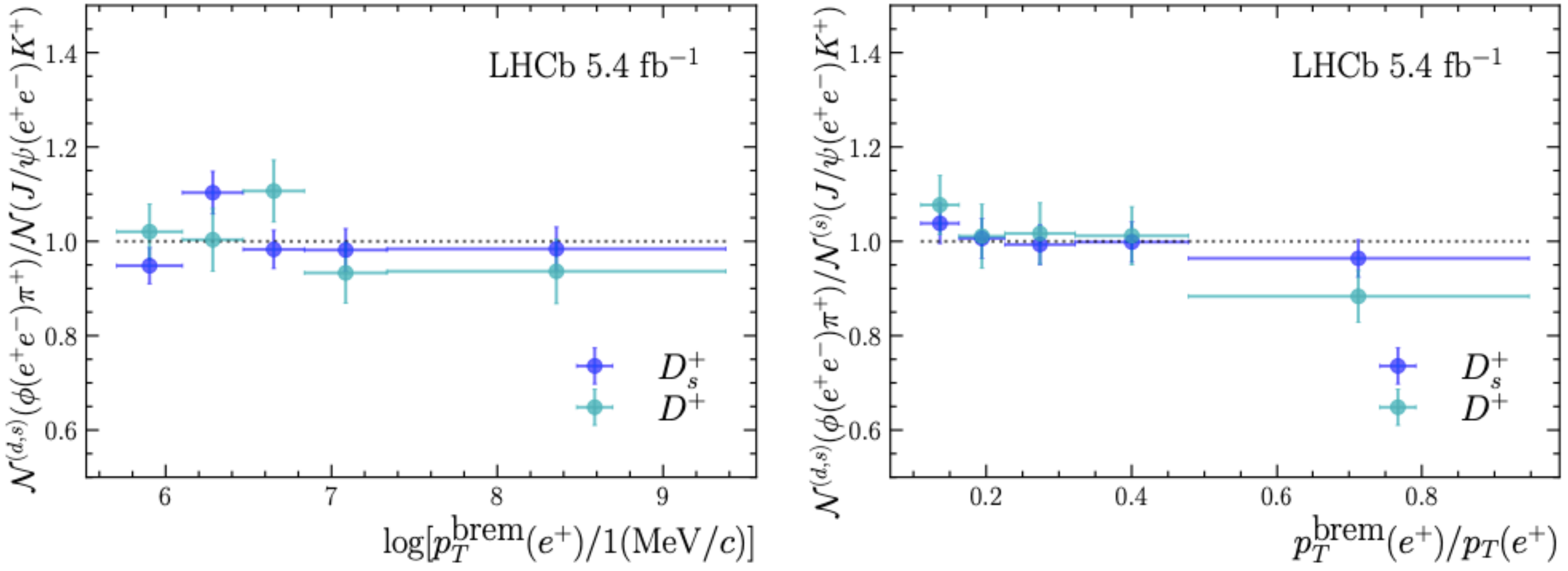

The flatness of these distributions indicates that the bremsstrahlung recovery algorithm is well reproduced in simulation at low q^2. The normalisation of these distributions is arbitrary and the uncertainties displayed are statistical only.

$\Lambda_b^0 \to pK^-\gamma$

LHCb-PAPER-2023-036
In preparation

Observable	Amplitude model				Acceptance model			Mass fit model		
	$\sigma^{\Lambda}_{\text{BW}}$	$\sigma^{\Lambda}_{\text{radius}}$	$\sigma_{\text{amp.}}$	$\sigma_{\text{res.}}$	σ_{finite}	$\sigma_{\text{acc.}}$	$\sigma_{\text{kin.}}$	σ_{pK}	$\sigma_{p\gamma}$	$\sigma_{\text{comb.}}$
$\Lambda(1405)$	$^{+1.2}_{-0.7}$	$^{+0.0}_{-0.0}$	$^{+0.9}_{+0.2}$	$^{+0.0}_{-0.4}$	$^{+0.2}_{-0.2}$	$^{+0.2}_{-0.2}$	$^{+0.0}_{-0.0}$	$^{+0.0}_{-0.1}$	$^{+0.1}_{-0.0}$	$^{+0.0}_{-0.0}$
$\Lambda(1520)$	$^{+1.0}_{-1.3}$	$^{+1.1}_{-1.1}$	$^{+0.3}_{+0.0}$	$^{+0.0}_{-0.1}$	$^{+0.2}_{-0.2}$	$^{+0.2}_{-0.2}$	$^{+0.1}_{-0.1}$	$^{+0.3}_{-0.0}$	$^{+0.1}_{-0.0}$	$^{+0.0}_{-0.1}$
$\Lambda(1600)$	$^{+3.6}_{-4.5}$	$^{+1.8}_{-1.8}$	$^{+0.5}_{+0.0}$	$^{+0.3}_{-0.2}$	$^{+0.3}_{-0.3}$	$^{+0.2}_{-0.2}$	$^{+0.1}_{-0.1}$	$^{+0.0}_{-0.1}$	$^{+0.1}_{-0.0}$	$^{+0.0}_{-0.0}$
$\Lambda(1670)$	$^{+1.1}_{-0.3}$	$^{+0.2}_{-0.2}$	$^{+0.2}_{-0.2}$	$^{+0.2}_{-0.2}$	$^{+0.1}_{-0.1}$	$^{+0.0}_{-0.0}$	$^{+0.0}_{-0.0}$	$^{+0.0}_{-0.0}$	$^{+0.0}_{-0.0}$	$^{+0.0}_{-0.0}$
$\Lambda(1690)$	$^{+4.1}_{-0.3}$	$^{+2.0}_{-2.0}$	$^{+1.5}_{+0.2}$	$^{+0.6}_{-0.5}$	$^{+0.2}_{-0.2}$	$^{+0.1}_{-0.1}$	$^{+0.0}_{-0.0}$	$^{+0.1}_{-0.0}$	$^{+0.0}_{-0.1}$	$^{+0.0}_{-0.0}$
$\Lambda(1800)$	$^{+3.0}_{-5.9}$	$^{+1.1}_{-1.1}$	$^{+0.1}_{-0.8}$	$^{+0.8}_{-1.5}$	$^{+0.3}_{-0.3}$	$^{+0.1}_{-0.1}$	$^{+0.1}_{-0.1}$	$^{+0.0}_{-0.0}$	$^{+0.6}_{-0.0}$	$^{+0.4}_{-0.0}$
$\Lambda(1810)$	$^{+3.7}_{-0.7}$	$^{+1.1}_{-1.1}$	$^{+1.5}_{+0.1}$	$^{+0.5}_{-1.4}$	$^{+0.2}_{-0.2}$	$^{+0.1}_{-0.1}$	$^{+0.0}_{-0.0}$	$^{+0.1}_{-0.0}$	$^{+0.2}_{-0.0}$	$^{+0.0}_{-0.0}$
$\Lambda(1820)$	$^{+1.8}_{-4.9}$	$^{+0.2}_{-0.2}$	$^{-0.0}_{-0.9}$	$^{+0.3}_{-0.4}$	$^{+0.3}_{-0.3}$	$^{+0.1}_{-0.1}$	$^{+0.0}_{-0.0}$	$^{+0.0}_{-0.3}$	$^{+0.1}_{-0.0}$	$^{+0.0}_{-0.1}$
$\Lambda(1830)$	$^{+1.3}_{-0.9}$	$^{+0.6}_{-0.6}$	$^{+0.3}_{-0.4}$	$^{+0.3}_{-0.5}$	$^{+0.1}_{-0.1}$	$^{+0.1}_{-0.1}$	$^{+0.0}_{-0.0}$	$^{+0.2}_{-0.0}$	$^{+0.1}_{-0.0}$	$^{+0.0}_{-0.0}$
$\Lambda(1890)$	$^{+4.2}_{-5.1}$	$^{+0.8}_{-0.8}$	$^{+0.4}_{-0.4}$	$^{+0.1}_{-0.4}$	$^{+0.2}_{-0.2}$	$^{+0.1}_{-0.1}$	$^{+0.0}_{-0.0}$	$^{+0.1}_{-0.0}$	$^{+0.1}_{-0.0}$	$^{+0.0}_{-0.0}$
$\Lambda(2100)$	$^{+1.0}_{-2.6}$	$^{+0.8}_{-0.8}$	$^{+0.9}_{-0.7}$	$^{+0.2}_{-0.2}$	$^{+0.1}_{-0.1}$	$^{+0.0}_{-0.0}$	$^{+0.0}_{-0.0}$	$^{+0.0}_{-0.0}$	$^{+0.1}_{-0.0}$	$^{+0.1}_{-0.0}$
$\Lambda(2110)$	$^{+5.0}_{-0.6}$	$^{+1.5}_{-1.5}$	$^{+1.5}_{-0.1}$	$^{+0.3}_{-0.2}$	$^{+0.1}_{-0.1}$	$^{+0.1}_{-0.1}$	$^{+0.0}_{-0.0}$	$^{+0.0}_{-0.2}$	$^{+0.0}_{-0.0}$	$^{+0.2}_{-0.0}$
$\Lambda(2350)$	$^{+0.0}_{-0.1}$	$^{+0.0}_{-0.0}$	$^{+0.6}_{-0.2}$	$^{+0.0}_{-0.0}$	$^{+0.0}_{-0.0}$	$^{+0.0}_{-0.0}$	$^{+0.0}_{-0.0}$	$^{+0.1}_{-0.0}$	$^{+0.1}_{-0.0}$	$^{+0.1}_{-0.0}$
$\text{NR}(\frac{3}{2}^-)$	$^{+2.9}_{+0.3}$	$^{+0.4}_{-0.4}$	$^{+1.0}_{-2.4}$	$^{+0.0}_{-0.6}$	$^{+0.1}_{-0.1}$	$^{+0.1}_{-0.1}$	$^{+0.0}_{-0.0}$	$^{+0.0}_{-0.1}$	$^{+0.0}_{-0.3}$	$^{+0.0}_{-0.0}$
$\Lambda(1405), \Lambda(1670)$	$^{+0.4}_{-0.7}$	$^{+0.3}_{-0.3}$	$^{+0.2}_{-0.0}$	$^{+0.1}_{-0.1}$	$^{+0.1}_{-0.1}$	$^{+0.0}_{-0.0}$	$^{+0.0}_{-0.0}$	$^{+0.0}_{-0.0}$	$^{+0.0}_{-0.0}$	$^{+0.0}_{-0.1}$
$\Lambda(1405), \Lambda(1800)$	$^{+0.5}_{-3.6}$	$^{+0.3}_{-0.3}$	$^{+0.1}_{-1.9}$	$^{+1.7}_{-0.4}$	$^{+0.2}_{-0.2}$	$^{+0.2}_{-0.2}$	$^{+0.0}_{-0.0}$	$^{+0.0}_{-0.0}$	$^{+0.0}_{-0.3}$	$^{+0.1}_{-0.0}$
$\Lambda(1520), \Lambda(1690)$	$^{+0.3}_{-2.3}$	$^{+0.9}_{-0.9}$	$^{-0.1}_{-0.7}$	$^{+0.5}_{-0.4}$	$^{+0.1}_{-0.1}$	$^{+0.0}_{-0.0}$	$^{+0.0}_{-0.0}$	$^{+0.0}_{-0.1}$	$^{+0.0}_{-0.0}$	$^{+0.0}_{-0.0}$
$\Lambda(1520), \text{NR}(\frac{3}{2}^-)$	$^{+1.2}_{-2.4}$	$^{+1.5}_{-1.5}$	$^{+0.5}_{-0.5}$	$^{+0.8}_{-0.4}$	$^{+0.1}_{-0.1}$	$^{+0.1}_{-0.1}$	$^{+0.0}_{-0.0}$	$^{+0.0}_{-0.0}$	$^{+0.0}_{-0.1}$	$^{+0.0}_{-0.0}$
$\Lambda(1600), \Lambda(1810)$	$^{+4.1}_{-2.8}$	$^{+0.6}_{-0.6}$	$^{+1.5}_{-0.7}$	$^{+0.9}_{-0.4}$	$^{+0.3}_{-0.3}$	$^{+0.2}_{-0.2}$	$^{+0.0}_{-0.0}$	$^{+0.0}_{-0.0}$	$^{+0.0}_{-0.4}$	$^{+0.0}_{-0.4}$
$\Lambda(1670), \Lambda(1800)$	$^{+1.5}_{-1.9}$	$^{+0.4}_{-0.4}$	$^{+0.3}_{-0.2}$	$^{+0.4}_{-0.4}$	$^{+0.1}_{-0.1}$	$^{+0.1}_{-0.1}$	$^{+0.0}_{-0.0}$	$^{+0.0}_{-0.0}$	$^{+0.0}_{-0.0}$	$^{+0.0}_{-0.1}$
$\Lambda(1690), \text{NR}(\frac{3}{2}^-)$	$^{+0.9}_{-2.2}$	$^{+1.1}_{-1.1}$	$^{+0.2}_{-2.7}$	$^{+0.2}_{-0.5}$	$^{+0.1}_{-0.1}$	$^{+0.1}_{-0.1}$	$^{+0.0}_{-0.0}$	$^{+0.0}_{-0.0}$	$^{+0.0}_{-0.1}$	$^{+0.0}_{-0.0}$
$\Lambda(1820), \Lambda(2110)$	$^{+2.4}_{-3.1}$	$^{+1.6}_{-1.6}$	$^{+0.5}_{-1.6}$	$^{+0.3}_{-0.5}$	$^{+0.2}_{-0.2}$	$^{+0.1}_{-0.1}$	$^{+0.0}_{-0.0}$	$^{+0.2}_{-0.0}$	$^{+0.0}_{-0.3}$	$^{+0.0}_{-0.2}$

Table 2: Systematic uncertainties on the fit fractions (top part of the table) and interference fit fractions (bottom part of the table). The values are given in %. The subscripts "BW", "radius", "amp.", and "res." refer to the systematic uncertainty due to fixing the resonance mass and width, fixing the radius of the hadrons, the choice of amplitude model, and the neglected resolution in the amplitude fit, respectively. The subscripts "finite", "acc.", and "kin." refer to the systematic uncertainties due to the finite simulation sample used to determine the acceptance model, the choice of acceptance model, and the kinematic reweighting respectively. The subscripts "pK", "$p\gamma$", and "comb." refer to the systematic uncertainty due to calculating the *sWeights* in bins of the proton-kaon invariant mass, the proton-gamma invariant mass, and the choice of model for the combinatorial background in the three-body invariant mass fit respectively.

$\Lambda_b^0 \to pK^-\gamma$

LHCb-PAPER-2023-036
In preparation

Observable	Value	σ_{stat}	$\sigma_{\text{syst}}^{\text{internal}}$	$\sigma_{\text{syst}}^{\text{external}}$	σ_{syst}
$\Lambda(1405)$	3.5	$^{+0.3}_{-0.4}$	$^{+0.9}_{-0.0}$	$^{+1.3}_{-0.6}$	$^{+1.9}_{-0.3}$
$\Lambda(1520)$	10.4	$^{+0.4}_{-0.2}$	$^{+0.7}_{-0.0}$	$^{+1.7}_{-1.6}$	$^{+2.2}_{-1.2}$
$\Lambda(1600)$	15.6	$^{+0.6}_{-0.9}$	$^{+0.8}_{-0.2}$	$^{+3.9}_{-5.0}$	$^{+4.3}_{-4.6}$
$\Lambda(1670)$	1.3	$^{+0.2}_{-0.2}$	$^{+0.3}_{-0.2}$	$^{+1.2}_{-0.3}$	$^{+1.3}_{-0.2}$
$\Lambda(1690)$	7.7	$^{+0.4}_{-0.8}$	$^{+1.8}_{-0.1}$	$^{+5.1}_{-1.0}$	$^{+6.2}_{-0.2}$
$\Lambda(1800)$	18.3	$^{+1.3}_{-1.6}$	$^{+1.4}_{-1.1}$	$^{+3.2}_{-6.0}$	$^{+3.2}_{-6.2}$
$\Lambda(1810)$	0.1	$^{+0.9}_{-0.4}$	$^{+1.7}_{-0.4}$	$^{+4.0}_{-0.7}$	$^{+4.8}_{-0.7}$
$\Lambda(1820)$	8.3	$^{+0.4}_{-0.7}$	$^{-0.2}_{-1.4}$	$^{+1.9}_{-4.8}$	$^{+1.0}_{-5.7}$
$\Lambda(1830)$	0.3	$^{+0.4}_{-0.4}$	$^{+0.6}_{-0.5}$	$^{+1.5}_{-0.9}$	$^{+1.6}_{-0.9}$
$\Lambda(1890)$	11.2	$^{+0.7}_{-0.6}$	$^{+0.5}_{-0.6}$	$^{+4.3}_{-5.1}$	$^{+4.6}_{-4.9}$
$\Lambda(2100)$	7.3	$^{+0.5}_{-0.5}$	$^{+1.1}_{-0.6}$	$^{+1.1}_{-2.8}$	$^{+1.4}_{-2.9}$
$\Lambda(2110)$	6.5	$^{+0.6}_{-0.7}$	$^{+1.7}_{-0.0}$	$^{+5.4}_{-0.9}$	$^{+6.3}_{-0.2}$
$\Lambda(2350)$	1.0	$^{+0.2}_{-0.1}$	$^{+0.8}_{-0.0}$	$^{+0.0}_{-0.2}$	$^{+0.8}_{-0.1}$
$\text{NR}(3/2^-)$	2.8	$^{+0.5}_{-0.4}$	$^{+0.2}_{-1.9}$	$^{+3.0}_{+0.3}$	$^{+2.4}_{-1.3}$

$\Lambda(1405), \Lambda(1670)$	−0.7	$^{+0.1}_{-0.2}$	$^{+0.2}_{-0.2}$	$^{+0.5}_{-0.8}$	$^{+0.5}_{-0.9}$
$\Lambda(1405), \Lambda(1800)$	7.6	$^{+0.7}_{-0.8}$	$^{+1.2}_{-2.0}$	$^{+0.6}_{-3.5}$	$^{+0.9}_{-4.6}$
$\Lambda(1520), \Lambda(1690)$	0.5	$^{+0.5}_{-0.3}$	$^{+0.3}_{-0.9}$	$^{+0.6}_{-2.6}$	$^{+0.5}_{-3.0}$
$\Lambda(1520), \text{NR}(3/2^-)$	−0.6	$^{+0.4}_{-0.4}$	$^{+1.0}_{-0.6}$	$^{+1.6}_{-3.2}$	$^{+2.1}_{-3.0}$
$\Lambda(1600), \Lambda(1810)$	−1.9	$^{+1.5}_{-1.0}$	$^{+1.3}_{-1.5}$	$^{+4.1}_{-2.9}$	$^{+3.9}_{-3.6}$
$\Lambda(1670), \Lambda(1800)$	−4.8	$^{+0.5}_{-0.4}$	$^{+0.4}_{-0.6}$	$^{+1.5}_{-2.0}$	$^{+1.5}_{-2.1}$
$\Lambda(1690), \text{NR}(3/2^-)$	3.9	$^{+0.4}_{-0.4}$	$^{+0.1}_{-3.0}$	$^{+1.2}_{-2.7}$	$^{+0.3}_{-4.7}$
$\Lambda(1820), \Lambda(2110)$	1.1	$^{+0.7}_{-0.5}$	$^{+0.2}_{-2.1}$	$^{+2.5}_{-3.9}$	$^{+1.9}_{-4.8}$

$\Lambda_b^0 \to pK^-\gamma$

LHCb-PAPER-2023-036
In preparation

Five alternative models:

1. removing the nonresonant component and instead floating mass and width of the $\Lambda(2100)$ and $\Lambda(2110)$ states using Gaussian constraints (this is the second best model);
2. using an exponential function instead of a constant for the lineshape of the nonresonant component;
3. employing a sub-threshold Breit–Wigner for the lineshape of the $\Lambda(1405)$ state instead of the Flatté shape;
4. adding a second nonresonant component with constant lineshape and $J^P = \frac{5}{2}^+$;
5. adding a second nonresonant component with constant lineshape and $J^P = \frac{1}{2}^+$.

Alternatives to quantify systematics:

1. modelling the combinatorial background using a polynomial instead of an exponential function;
2. modelling the partially reconstructed background using an Argus function [46] instead of a kernel density estimator obtained from simulation samples;
3. letting the signal tail parameters vary in the fit to data using a Gaussian constraint instead of fixing them;
4. calculating the *sWeights* in bins of $m_{\Lambda_b^0}(pK^-)$ and $m_{\Lambda_b^0}(p\gamma)$ to account for possible correlations between the Dalitz variables and the three-body invariant mass.

$B_s^0 \to \mu^+\mu^-\gamma$

LHCb-PAPER-2023-045
In preparation

Two complementary methods

Indirect no photon reconstruction, probing this decay as a background of the $B_s^0 \to \mu^+\mu^-$ process:

$\mathscr{B}(B_s^0 \to \mu^+\mu^-\gamma) < 2.0 \times 10^{-9}$ at 95% C.L. for $m(\mu\mu) > 4.9\ \mathrm{GeV}/c^2$

Only sensitive to high q²

Phys.Rev.D105(2022)012010

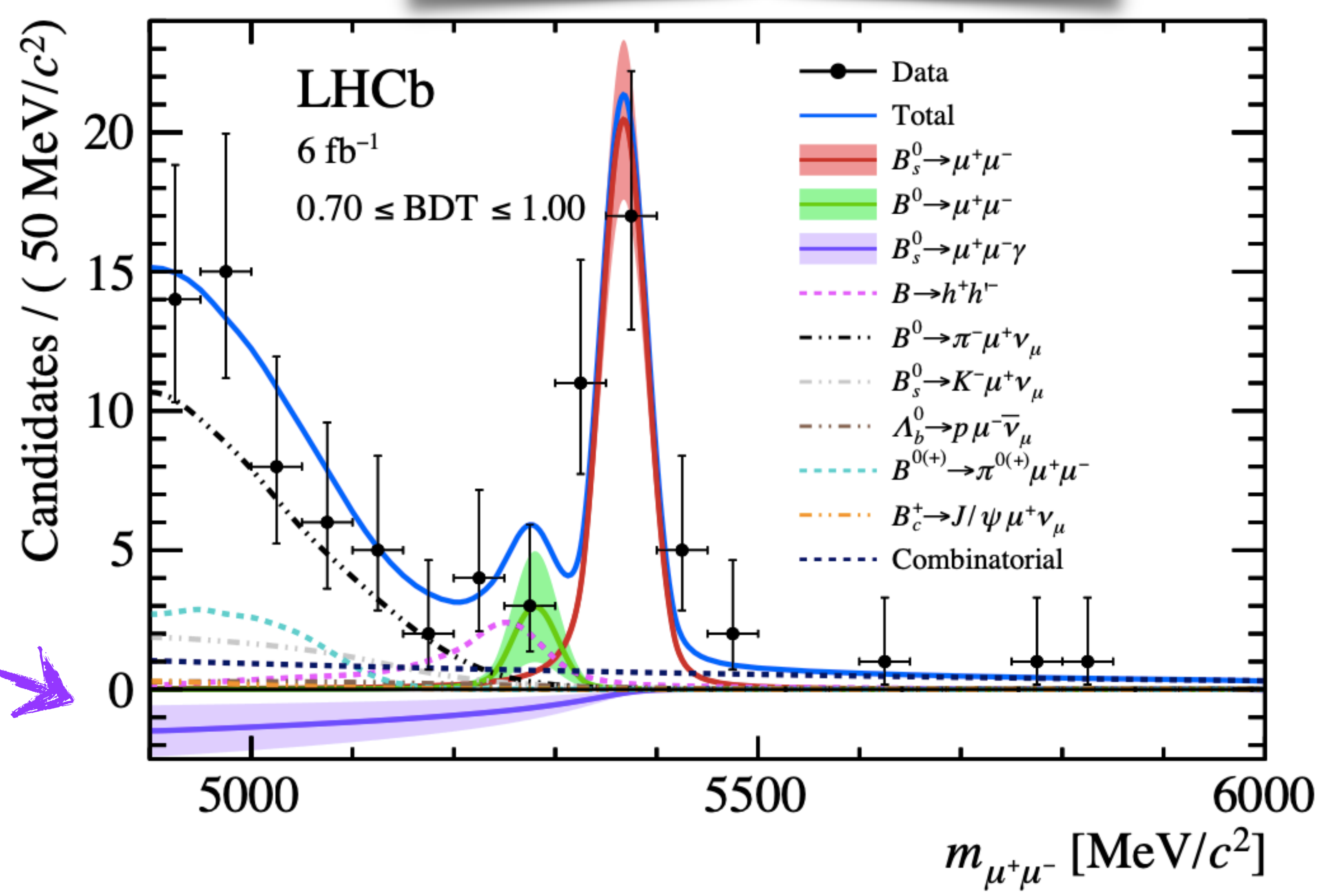

Direct with photon reconstruction, presented today.

- ⊕ Sensitive to low-q² region, therefore, to larger set of Wilson coefficients ($\mathcal{C}_7$, $\mathcal{C}_9$, $\mathcal{C}_{10}$).
- ⊖ Photon reconstruction worsen the resolution.

Search by BABAR:
$\mathscr{B}(B^0 \to \mu^+\mu^-\gamma) < 1.6 \times 10^{-7}$
Phys.Rev.**D77**(2008)011104

Signal simulation: as theory input the differential branching ratio computed in D.Melikhov N.Nikitin [Phys.Rev.D70(2004)114028]. The implementation of this result is detailed in N.Nikitin, A. Popov, D.V.Savrina [LHCb-INT-2011-011]. + PHOTOS ON for final state radiation.

$B_s^0 \to \mu^+\mu^-\gamma$

LHCb-PAPER-2023-045
In preparation

Selection: after basic preselection and trigger, candidates must pass a requirement in two MLP classifiers:

First MLP

Aim: reduce the combinatorial background using geometrical and kinematic variables.

Trained in data mass side-bands and background, and signal simulation.

Second MLP

Aim: reduce other backgrounds, exploiting the fact that the signal objects are isolated.

Trained with samples after passing the first MLP.

Optimised cut for each q² bin.

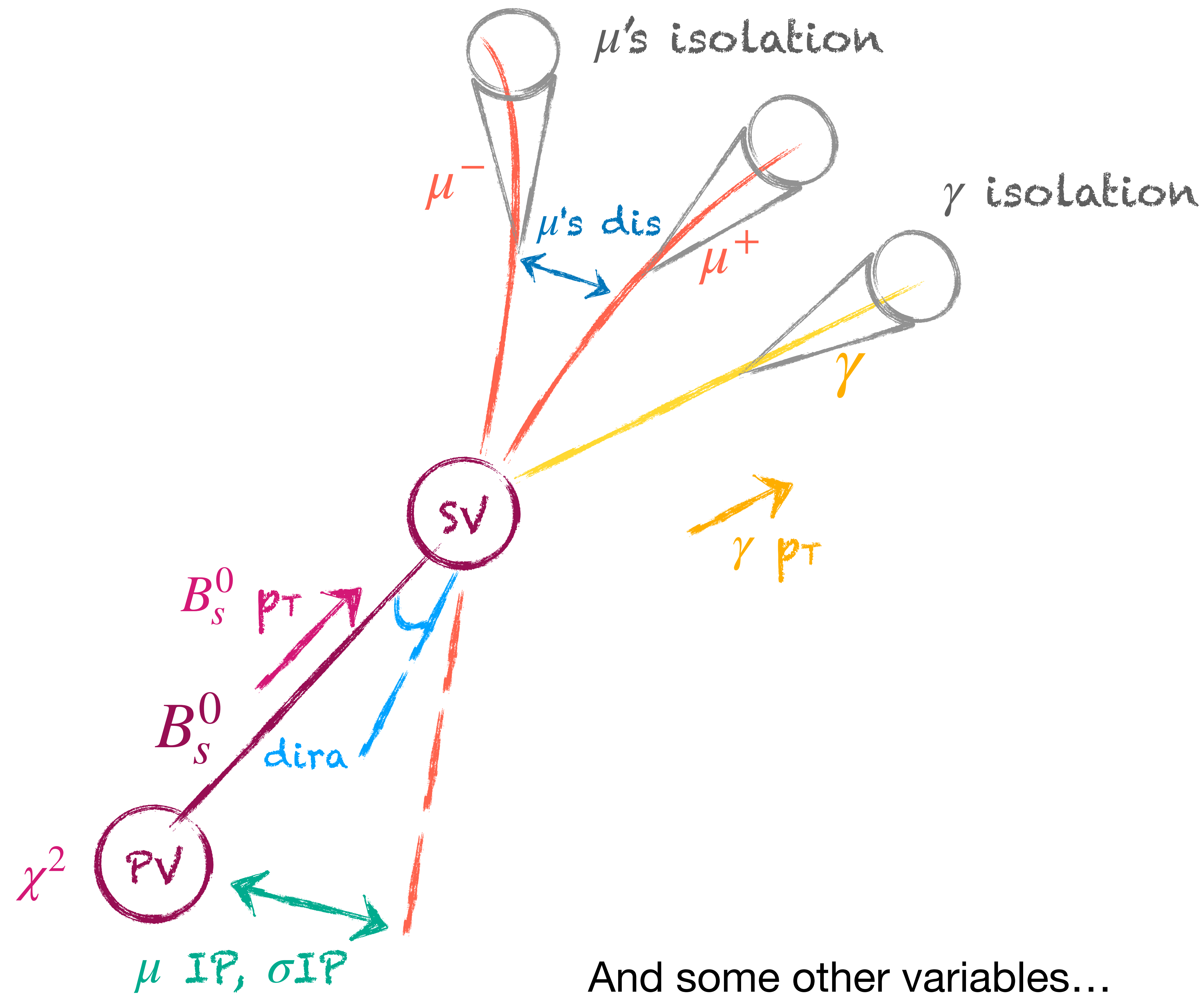

And some other variables…

$B_s^0 \to \mu^+\mu^-\gamma$

LHCb-PAPER-2023-045
In preparation

Background: studied with simulation

Double misID

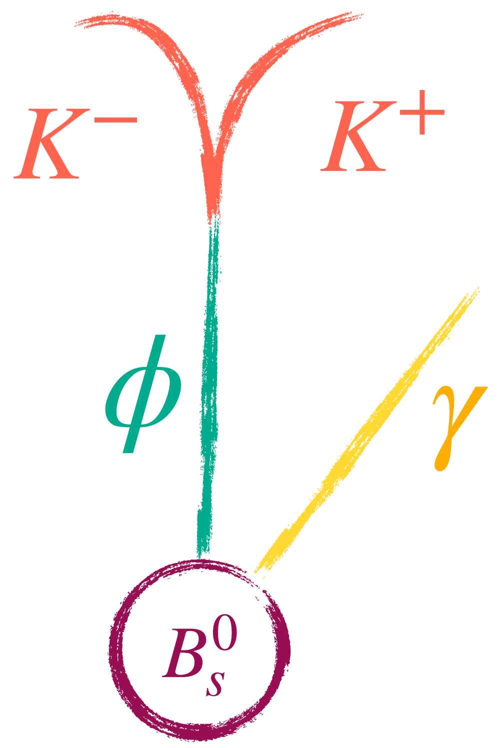

Double misidentification of kaons or pions as muons. Such as:

$B_s^0 \to \phi(\to KK)\gamma$

$B^0 \to K^{*0}(\to \pi K)\gamma$

Probability of ~10^{-4} of double misID

$B^0 \to \mu\mu\pi^0$

If one γ is not reconstructed or both γ's are merge and reconstructed in one.

Low contribution but peaking very close to the signal.

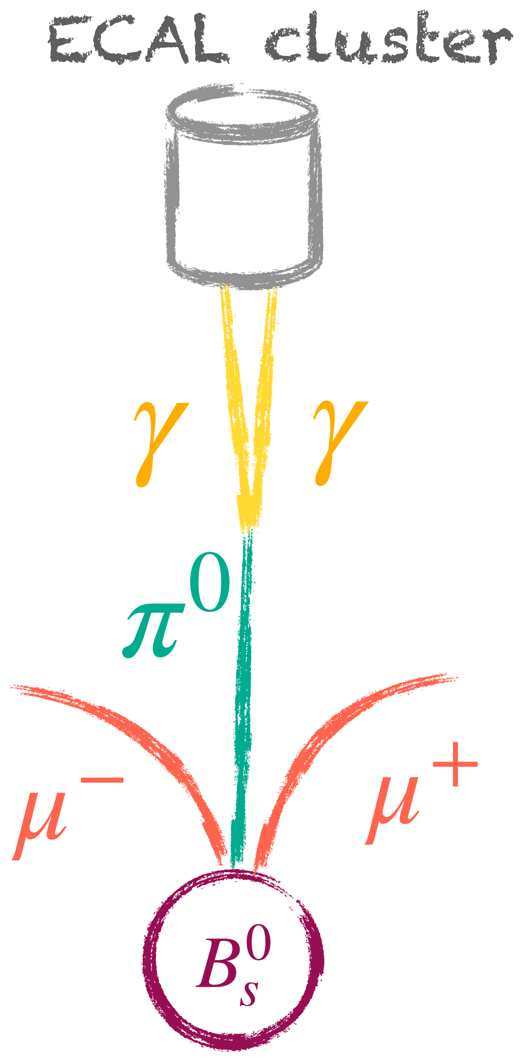

Partially reconstructed

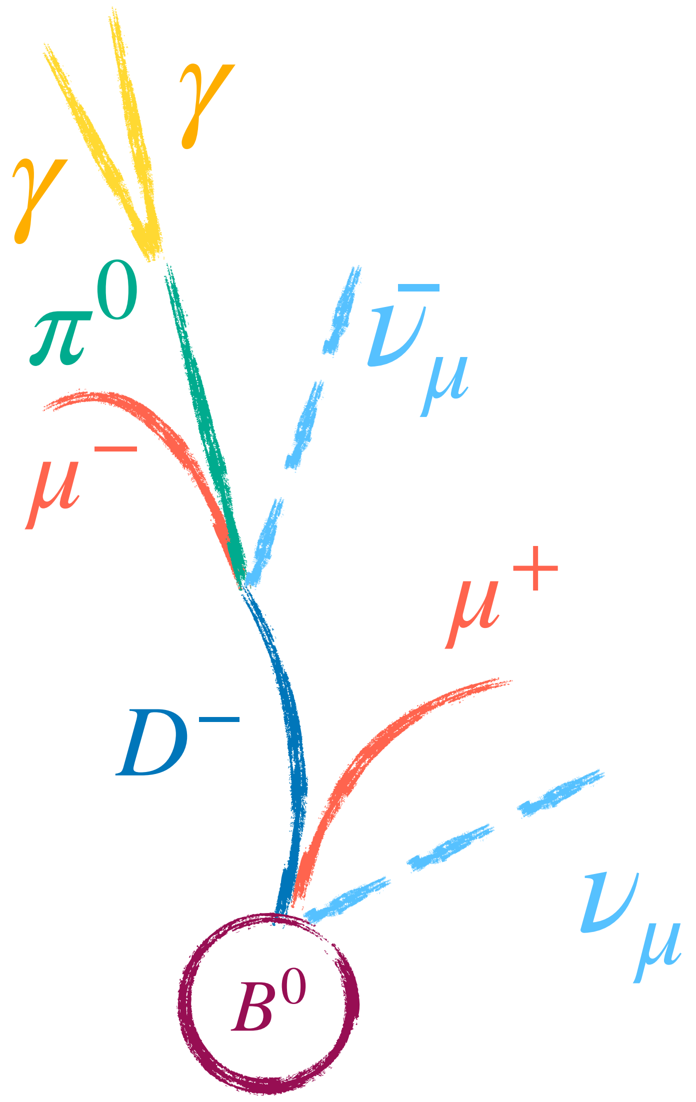

When one particle of the final state is not reconstructed (neutrinos, or by an inefficiency).

A broad peak outside the mass region is expected.

$B_{(s)}^0 \to \mu\mu\eta$

By same reasons than $B^0 \to \mu\mu\pi^0$.

Main peaking background in the signal region, but broader than $B^0 \to \mu\mu\pi^0$.

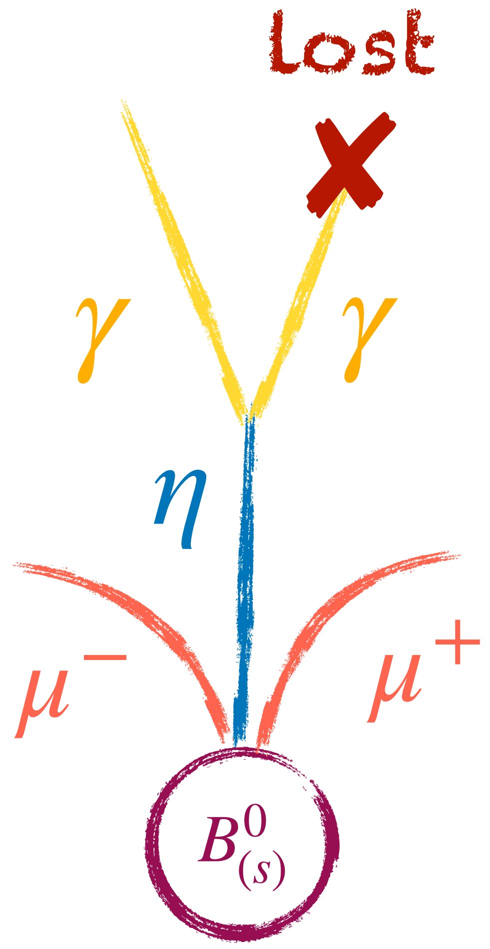

Other backgrounds were studied and estimated negligible: $B^0 \to \mu\mu\gamma$, $B^0 \to \pi^+\pi^-\pi^0$, $B^{*0} \to B^0\gamma$, $\Lambda_b \to pK\gamma$, etc.

$B^0 \to D^{*-}\tau^+\nu_\tau$

LHCb-PAPER-2023-020
arXiv 2311.05224

Control variables fits:

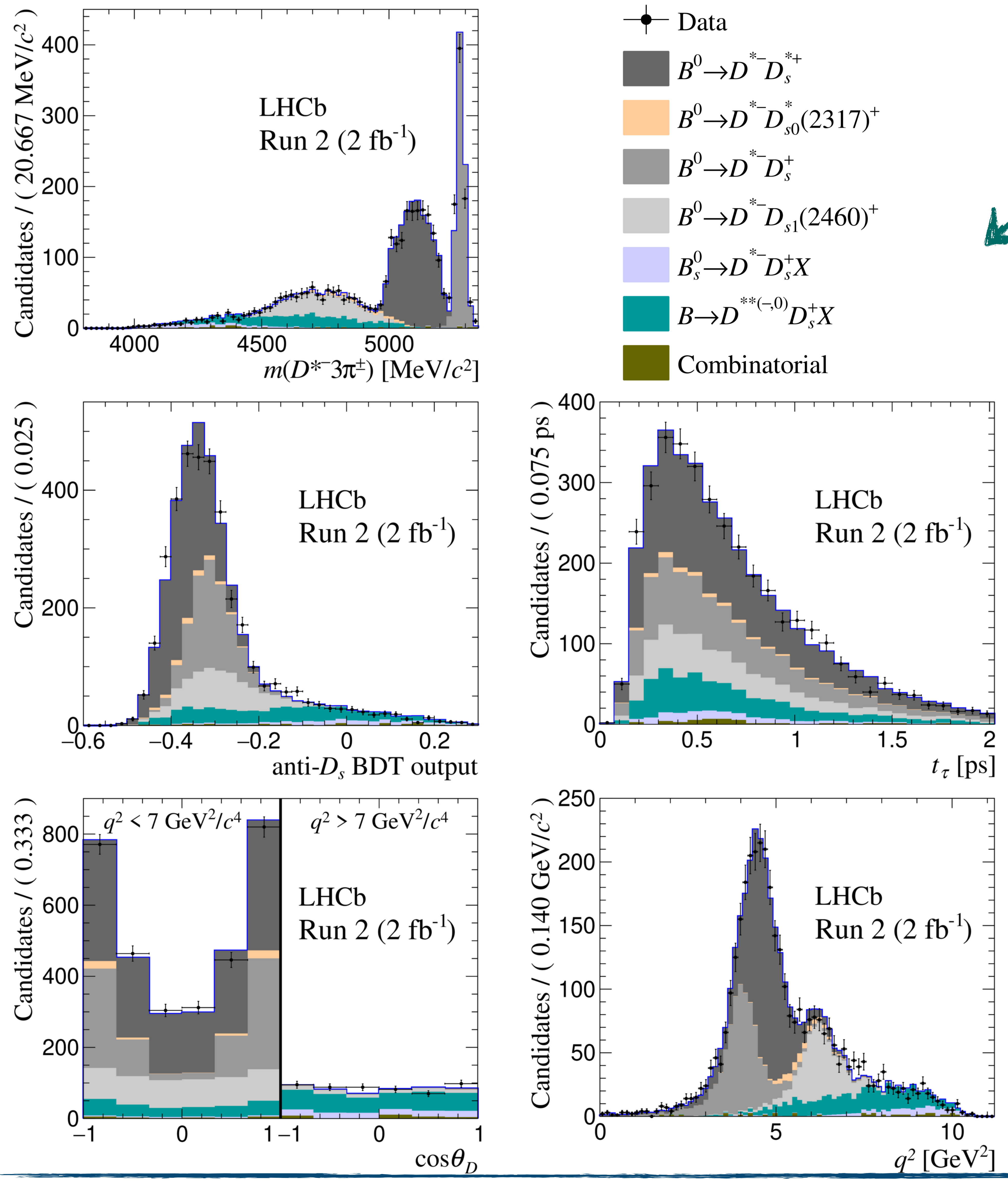

Control sample $B \to D^{*-}D^+(X)$ and $B \to D^{*-}D^0(X)$ used to extract weights and correct the imperfect simulation.

Data-simulation distributions:

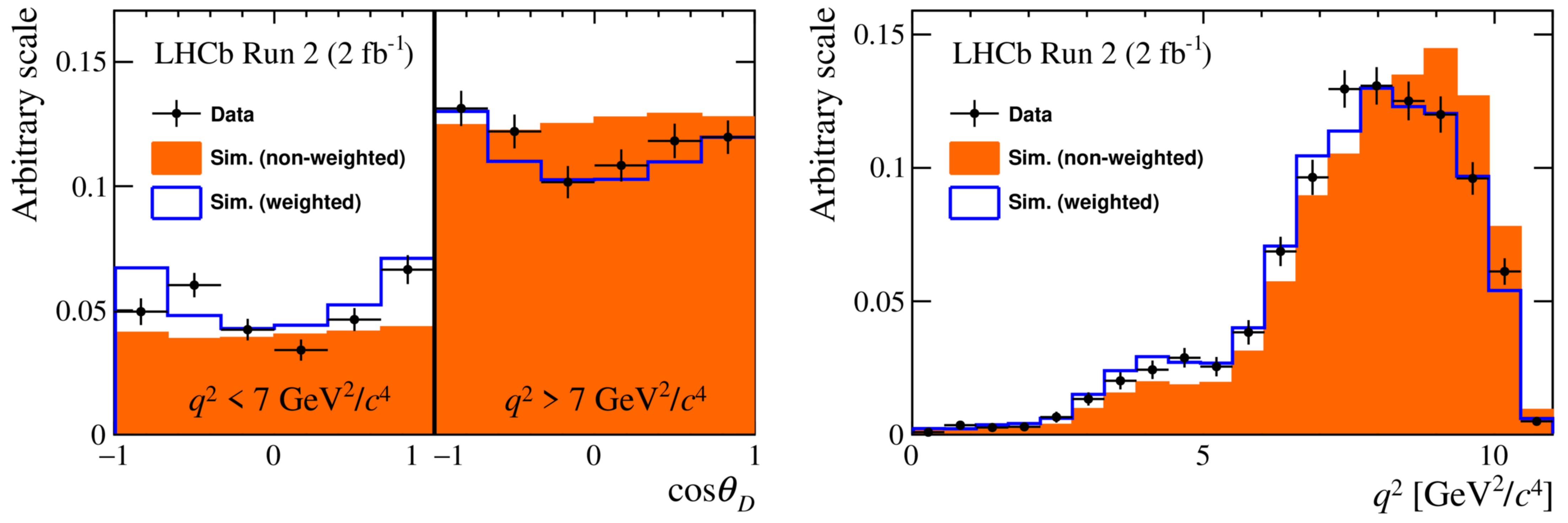

- $N^{\text{unpol}}_{\text{low } q^2}$ and $N^{\text{unpol}}_{\text{high } q^2}$: parameters accounting for the number of unpolarized signal events in the low- and high-q^2 regions, respectively.
- $f^{\text{pol}}_{\text{low } q^2}$ and $f^{\text{pol}}_{\text{high } q^2}$: parameters accounting for the fraction of signal polarized events with respect to the number of unpolarized signal events in the low- and high-q^2 regions, respectively.
- $N_{B^0\to D^{*-}D^+(X)}$: parameter accounting for the number of $B^0\to D^{*-}D^+(X)$ events.
- $f^{\text{v1v2}}_{B^0\to D^{*-}D^0(X)}$: free parameter accounting for the fraction of $B^0\to D^{*-}D^0(X)$ events where at least one pion comes from a different vertex than the D^0 vertex, with respect to $N^{\text{same}}_{B^0\to D^{*-}D^0(X)}$.
- $N_{B^0\to D^{*-}D_s^{*+}}$: parameter accounting for the yield of the $B^0\to D^{*-}D_s^{*+}$ mode.

To ensure the stability of the fit some parameters are constrained or fixed:

- $f_{\tau^+\to\pi^+\pi^-\pi^+\pi^0\nu_\tau}$: fraction of $\tau^+\to\pi^+\pi^-\pi^+\pi^0\nu_\tau$ signal events with respect to the $\tau^+\to\pi^+\pi^-\pi^+\nu_\tau$ mode. This parameter is fixed taking into account the different branching ratios and efficiencies of the two modes.
- $f_{B^0\to D^{**-}\tau^+\nu_\tau}$: fraction of $B^0\to D^{**-}\tau^+\nu_\tau$ decays with respect to the $B^0\to D^{*-}\tau^+\nu_\tau$ signal. This parameter is fixed in the fit to the expected value determined from simulation after correcting the branching fractions used in the generation.[4]
- $f_{B^0\to D^{*-}D'^+_{s1}}$, $f_{B^0\to D^{*-}D_s^+}$, $f_{B^{0,\pm}\to D^*D_s^+X}$, $f_{B_s^0\to D^{*-}D_s^+(X)}$ and $f_{B^0\to D^{*-}D^{*+}_{s0}}$: set of parameters representing the fraction of the relevant decay mode of interest with respect to the $B^0\to D^{*-}D_s^{*+}$ decay. These parameters are constrained to the results of the fit described in Section 5 after correcting for efficiency.
- $N^{\text{same}}_{B^0\to D^{*-}D^0(X)}$: number of $B^0\to D^{*-}D^0(X)$ events where the three pions in the final state come from the same vertex. This parameter is Gaussian-constrained to the number of exclusive $D^0\to K^-\pi^+\pi^-\pi^+$ events recovered by the isolation tool after correcting for the data-simulation differences.
- $N_{B^0\to D^{*-}\pi^+\pi^-\pi^+X}$: number of prompt $B^0\to D^{*-}\pi^+\pi^-\pi^+X$ events. The central value is determined from the observed ratio between exclusive $B^0\to D^{*-}\pi^+\pi^-\pi^+$ and the inclusive $B^0\to D^{*-}\pi^+\pi^-\pi^+X$ decays, corrected for data-simulation differences.
- $N_{\text{B1-B2}}$: number of combinatorial backgrounds where the D^* and the three pions come from different b-hadrons. Its value is fixed to the value observed in the wrong-sign sample satisfying the non-isolation and the higher B-mass requirements.
- $N_{\text{fake } D^0}$ & $N_{\text{fake } D^*}$: number of combinatorial background events where a fake D^0 or D^* is reconstructed, respectively. Their value is fixed to the values obtained from a fit to $m(K\pi)$ and $m(K\pi\pi)-m(K\pi)$.

The fit is performed within the SM framework with these free parameters

The fitted parameters values are

Fractions of polarized signal events:

low- q2: 0.361±0.074 (stat)

high-q2: 0.013±0.081 (stat)

Table 3: Fit results for the Run 1 and Run 2 datasets.

Parameter	Run 1	Run 2
$N^{\text{unpol}}_{\text{low } q^2}$	360 ± 55	758 ± 62
$N^{\text{unpol}}_{\text{high } q^2}$	532 ± 70	827 ± 109
$f^{\text{pol}}_{\text{low } q^2}$	0.36 ± 0.07	
$f^{\text{pol}}_{\text{high } q^2}$	0.01 ± 0.08	
$f_{\tau^+\to\pi^+\pi^-\pi^+\pi^0\nu_\tau}$	0.28	
$f_{B^0\to D^{**-}\tau^+\nu_\tau}$	0.044	
$N_{B^0\to D^{*-}D_s^{*+}}$	2087 ± 77	7475 ± 170
$f_{B^0\to D^{*-}D'^+_{s1}}$	0.38 ± 0.05	0.37 ± 0.04
$f_{B^0\to D^{*-}D_s^+}$	0.51 ± 0.03	0.60 ± 0.03
$f_{B^{0,\pm}\to D^*D_s^+X}$	0.83 ± 0.06	0.48 ± 0.05
$f_{B_s^0\to D^{*-}D_s^+(X)}$	0.17 ± 0.03	0.10 ± 0.02
$f_{B^0\to D^{*-}D^{*+}_{s0}}$	0.11 ± 0.02	0.02 ± 0.03
$N^{\text{same}}_{B^0\to D^{*-}D^0(X)}$	448 ± 22	1039 ± 52
$f^{\text{v1v2}}_{B^0\to D^{*-}D^0(X)}$	0.39 ± 0.18	2.26 ± 0.28
$N_{B^0\to D^{*-}D^+(X)}$	1747 ± 118	1740 ± 182
$N_{B^0\to D^{*-}\pi^+\pi^-\pi^+X}$	408 ± 21	2190 ± 33
$N_{\text{B1-B2}}$	197	216
$N_{\text{fake } D^0}$	110	457
$N_{\text{fake } D^*}$	133	533

The extracted $F_L^{D^*}$, $a_{\theta_D}(q^2)$ and $c_{\theta_D}(q^2)$ values are

Table 4: Values of $a_{\theta_D}(q^2)$, $c_{\theta_D}(q^2)$ and $F_L^{D^*}$ from the fit.

Parameter	$q^2 < 7\,\text{GeV}^2/c^4$	$q^2 > 7\,\text{GeV}^2/c^4$	whole q^2 range
$a_{\theta_D}(q^2)$	0.12 ± 0.02	0.15 ± 0.03	0.14 ± 0.03
$c_{\theta_D}(q^2)$	0.13 ± 0.05	0.01 ± 0.02	0.07 ± 0.06
$F_L^{D^*}$	0.51 ± 0.07	0.35 ± 0.08	0.43 ± 0.06

$B^0 \to D^{*-}\tau^+\nu_\tau$

LHCb-PAPER-2023-020
arXiv 2311.05224

Lattice FFs	$R(D^*)$	$P_\tau(D^*)$	$F_{L,\tau}$	$F_{L,\ell}$	$A_{FB,\ell}$
FNAL/MILC [15]	0.275(8)	-0.529(7)	0.418(9)	0.450(19)	0.261(14)
HPQCD [16]	0.266(12)	-0.543(18)	0.399(23)	0.435(42)	0.265(30)
JLQCD [17]	0.247(8)	-0.509(11)	0.448(16)	0.516(29)	0.220(21)
Average [15]-[17] (PDG scale factor)	0.262(9) (1.8)	-0.525(7) (1.3)	0.422(10) (1.4)	0.465(22) (1.5)	0.251(13) (1.2)
Combined [15]-[17]	0.259(5)	-0.521(6)	0.425(7)	0.473(14)	0.252(10)
Experimental value	0.284(12) [36]	$-0.38 \pm 0.51^{+0.21}_{-0.16}$ [38]	0.49(8) [39, 40]	0.520(6) [13, 14]	0.232(10) [13, 14]

Lattice FFs	low-q^2 bin ($q^2 < 7$ GeV$^2/c^4$)	high-q^2 bin ($q^2 > 7$ GeV$^2/c^4$)
FNAL/MILC [15]	0.486(15)	0.381(5)
HPQCD [16]	0.459(38)	0.367(14)
JLQCD [17]	0.534(25)	0.398(10)
Average [15]-[17] (PDG scale factor)	0.495(17) (1.4)	0.383(6) (1.4)
Combined [15]-[17]	0.498(12)	0.384(4)
Experimental value [40]	0.51(7)(3)	0.35(8)(2)

G.Martinelli, S.Simula, L.Vittorio
[arXiv.2310.03680]